THE UNIVERSITY OF MICHIGAN
FEB 15 1966
PHOENIX LIBRARY

REACTOR MATERIALS

Phoz (Dep)

A Quarterly Technical Progress Review

Prepared for DIVISION OF TECHNICAL INFORMATION, USAEC, by
R. W. DAYTON, E. M. SIMONS, and ASSOCIATES, BATTELLE MEMORIAL INSTITUTE

Winter 1965-1966

● VOLUME 8

● NUMBER 4

DEPOSITED BY THE
UNITED STATES OF AMERICA

TECHNICAL PROGRESS REVIEWS

To meet the needs of industry for concise summaries of current atomic developments, the Atomic Energy Commission is publishing this series, Technical Progress Reviews. Issued quarterly, each of the reviews digests and evaluates the latest findings in a specific area of nuclear technology and science.

The five journals published in this series are:

Isotopes and Radiation Technology, P. S. Baker, A. F. Rupp, and associates, Oak Ridge National Laboratory

Nuclear Safety, Wm. B. Cottrell, W. H. Jordan, and associates, Oak Ridge National Laboratory

Power Reactor Technology, Argonne National Laboratory

Reactor Fuel Processing, Stephen Lawroski and associates, Chemical Engineering Division, Argonne National Laboratory

Reactor Materials, R. W. Dayton, E. M. Simons, and associates, Battelle Memorial Institute

Each journal may be purchased from the Superintendent of Documents, U. S. Government Printing Office, Washington, D. C., 20402. *Isotopes and Radiation Technology* at $2.00 per year for subscription or $0.55 for individual issues; the other four journals at $2.50 per year and $0.70 per issue. See back cover for remittance instructions and foreign postage requirements.

The views expressed in this publication do not necessarily represent those of the United States Atomic Energy Commission, its divisions or offices, or of any Commission advisory committee or contractor.

Availability of Reports Cited in This Review

Unclassified AEC reports are available for inspection at AEC depository libraries and are sold by the Clearinghouse for Federal Scientific and Technical Information, National Bureau of Standards, U. S. Department of Commerce, 5285 Port Royal Road, Springfield, Va., 22151. Some of the reports cited are not available owing to their preliminary nature; however, the information contained in them will eventually be made available in formal progress or topical reports.

Unclassified reports issued by other Government agencies or private organizations should be requested from the originator.

Unclassified British and Canadian reports may be inspected at AEC depository libraries. British reports are sold by the British Information Service, 45 Rockefeller Plaza, New York, N. Y.; Canadian reports (AECL series) are sold by the Scientific Document Distribution Office, Atomic Energy of Canada, Ltd., Chalk River, Ontario, Canada.

Classified U. S. and foreign reports identified in this journal as Classified may be purchased by properly cleared Access Permit Holders from the Division of Technical Information Extension, U. S. Atomic Energy Commission, P. O. Box 1001, Oak Ridge, Tenn., 37831. Such reports may be inspected at classified AEC depository libraries.

REACTOR MATERIALS

A REVIEW OF RECENT DEVELOPMENTS

Prepared for DIVISION OF TECHNICAL INFORMATION, USAEC,
by R. W. DAYTON, E. M. SIMONS, and ASSOCIATES,
BATTELLE MEMORIAL INSTITUTE

WINTER 1965–1966

VOLUME 8

NUMBER 4

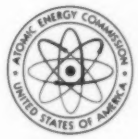

Foreword

Reactor Materials is one of a series of quarterly technical progress reviews broadly covering the field of nuclear science and technology. Under the auspices of the AEC Division of Technical Information, *Reactor Materials* is prepared by Battelle personnel from worldwide literature. It covers properties, behavior, and fabrication processes of materials applicable to nuclear reactor components and associated equipment.

The reader will recognize that the scope of this Review is too broad to permit detailed coverage of every topic. Rather, the authors and editors attempt to combine the highlights of significant new developments into an informative summary of current research for both management and the technical specialist. As a rule, enough of the results are presented to define the research and summarize the findings. For readers desiring more information on any particular topic, a complete set of references is provided at the end of each section.

Each quarter a number of bibliographies, monographs, and books appear on subjects within the scope of *Reactor Materials*. Although the main purpose of this Review is to call attention to findings that are new and significant, such publications are noted in the text because they often represent excellent compilations of available information on important materials topics.

R. W. DAYTON
E. M. SIMONS
R. W. ENDEBROCK
Battelle Memorial Institute

DEPOSITED BY THE
UNITED STATES OF AMERICA

Contents

I Fuel and Fertile Materials 175
Uranium Metal and Alloys 175
Plutonium 178
Thorium 183
Metal–Ceramic Fuels 184
Coated-Particle Fuel Materials 184
Uranium Oxide Fuel Materials 187
Uranium and Thorium Carbides, Nitrides, and Sulfides 189
Basic Studies of Irradiation Effects in Fuel Materials 190
References 193

II Moderator Materials 196
Graphite 196
Beryllium Metal and Alloys 198
Beryllium Oxide 201
Solid Hydrides 201
References 203

III Nuclear Poisons 204
Metallic Poison Materials 204
Dispersion and Nonmetallic Poison Materials 204
References 205

IV Cladding and Structural Materials . 206
Corrosion 206
Selected Mechanical Properties of Cladding and Structural Materials . . 212
Selected Metallurgical Aspects of Cladding and Structural Materials 215
Diffusion Studies 218
Ceramic Technology 219
Radiation Effects in Nonfuel Materials . 220
References 222

V Special Fabrication Techniques . . 225
Melting, Casting, and Working 225
Cladding 226
Metals Joining 228
Nondestructive Testing 231
References 232

Index, Volume 8 235

Issued quarterly by the U. S. Atomic Energy Commission. Use of funds for printing this publication approved by the Director of the Bureau of the Budget on October 14, 1963.

Section

I

Reactor Materials

Fuel and Fertile Materials

Uranium Metal and Alloys

Unalloyed Uranium

Angerman and Caskey[1] studied swelling of natural uranium in specimens irradiated to burnups of 0.05 to 0.77 at.% at temperatures ranging from 130 to 550°C. Cavities 10 to 200 μ in length were responsible for volume increases up to 50% in specimens irradiated to burnups of over 0.2 at.% at temperatures from 370 to 500°C. The cavities were absent at both lower and higher temperatures. These cavities were believed to form by shear along grain and twin boundaries in a manner similar to that responsible for the intergranular cavities or voids, which form during plastic deformation at temperatures just below the recrystallization temperature. In the case of the irradiated specimens, the necessary stress arises from interaction of crystallites resulting from anisotropic growth. The volume increase caused by precipitation of fission-gas bubbles (0.01 to 0.5 μ in diameter) was only 0.5% for specimens irradiated at 370 to 500°C. Only 50% of the generated fission gas was accounted for by the gas bubbles in these irradiated specimens, although all of the fission gas could be accounted for in specimens irradiated at 400°C and subsequently annealed at 580°C for 100 hr.

Work by Sykes and Greenwood[2] has shown that the 525 and 625°C tensile creep ductility of irradiated uranium is drastically reduced at stresses above about 5000 psi. The transition from low (~0.5% elongation) ductility to relatively high ductility seemed to be governed more by stress than by strain rate or temperature. It is suggested that the effect of stress on ductility may be interpreted in terms of the growth and linking up of bubbles of fission gas.

Buddery et al.[3] describe the development of a uranium-alloy coating designed to protect uranium fuel bars from oxidation in the event of carbon dioxide leakage into a can in a uranium–Magnox type of reactor. Eleven possible elements (copper, manganese, aluminum, iron, nickel, titanium, zirconium, niobium, molybdenum, vanadium, and chromium) were initially selected for alloying. Further selection, by oxidizing cross sections of diffusion couples, revealed the best system to be the one involving aluminum, in particular the intermetallic compound UAl_3. Subsequently, coatings of UAl_3 were prepared on small laboratory test specimens by a pack-aluminizing method and were found to delay the onset of the rapid oxidation occurring with uncoated uranium for about 400 hr in static and about 100 hr in flowing carbon dioxide at 450°C. In addition, the coatings appear to possess suitable mechanical properties, can be applied at a convenient temperature, are compatible with Magnox, do not diffuse into uranium, have an acceptable neutron-capture cross section, and seem unlikely to hinder heat transfer from a fuel element.

In another investigation[4] deposits of magnesium, iron, copper, zirconium, and molybdenum formed on uranium by flame-spraying techniques all failed on thermal testing in CO_2 at 500°C owing to volume changes in the underlying oxide film, the inherent porosity of flame deposits, and differential expansion of the deposit and the uranium base. A short term, 10-hr, protection was found with aluminum deposits when they were annealed to form UAl_3. Such deposits on a uranium core might be used to guard against the undesirable consequences of a fuel-element-can failure.

Readers concerned with the physical metallurgy of uranium should find of interest the published papers on quench-induced texture,[5]

stacking faults,[6] polygonization,[7] annealing-temperature–transition-temperature relations,[8] and aqueous corrosion.[9] A book, *Uranium Technology*, published by the Russians[10] contains data on the chemical and physicochemical properties of uranium and its major compounds, on uranium-ore processing, and on uranium-metal production.

Alpha-Phase Uranium Alloys

The continuous-cooling transformation characteristics of U–Fe–Al alloys were studied in the United Kingdom.[11] The separate and joint effects of a few hundred ppm iron and aluminum on the transformation kinetics of uranium and the structure of the transformed product have been established. High iron content increases the tendency for high cooling rates to depress the beta-to-alpha transformation temperature. It also reduces the minimum grain size and lowers the rate of beta-to-alpha transformation at a given rate of cooling. Iron content and cooling rate both affect the texture produced by beta-to-alpha transformation. The only effect of aluminum is to produce fine precipitates whose morphology is little influenced by beta-to-alpha transformation.

In work performed by Battelle–Northwest,[12] it was found that transmission-electron microscopy can be successfully utilized to study particle-size distributions in dilute alloys of uranium. The data this method yielded agreed well with particle-size distributions determined from replica electron micrography. The high resolution inherent in transmission techniques permits inclusion of particles normally too small to be resolved by replica methods. Other work (Ref. 13) describes the quantitative metallographic methods used for investigating the size distribution of micron and submicron second-phase particles present in dilute uranium-base alloys.

A program was instituted at Nuclear Metals Division of Textron Inc.[14] to develop new, improved uranium-base alloys by the SLIS technique, in which dispersions are achieved with metallic particles rather than oxides. The alloying elements are those which are highly insoluble in the solid state and thus have little tendency to agglomerate at elevated temperatures. Alloys of U–Be, U–C, U–Be–C, and U–Al–Si were prepared by dissolving the alloying elements in liquid uranium and then quenching rapidly by splat cooling. Examination of the as-quenched U–Al–Si alloy at magnifications up to 30,000× failed to show any precipitate particles. However, a similar examination of the U–Be, U–Be–C, and U–C alloys revealed that particles about 0.008 μ in diameter had been precipitated. Following compaction at 600°C, plus extrusion at 500°C, a precipitate was observed in the U–Al–Si alloy; the precipitate had an irregular shape, being about 0.1 to 0.4 μ across. Particle concentrations in the range of 1×10^{12} to $5 \times 10^{12}/cm^3$ were observed in the splat-cooled alloys following compaction and extrusion. Aging of the splat-cooled U–Al–Si alloy for 100 hr at 600°C produced considerable particle agglomeration, whereas similar aging of the U–Be and U–Be–C alloys produced only a moderate growth in particle size. After aging of these alloys, an increase in particle size was usually accompanied by a decrease in particle concentration. However, aging of the U–C alloy increased the number of particles by about $1.7 \times 10^{12}/cm^3$.

The results indicate that the strength of splat-cooled uranium can be increased substantially at 600°C with additions of up to 0.4 wt.% beryllium metal. After aging, little change in the strength of the U–Be alloy at a test temperature of 600°C is apparent. The U–C splat-cooled alloy shows little improvement in strength after aging for 100 hr at 600°C over that of unalloyed uranium at a similar test temperature.

Workers at Nuclear Metals have shown that it is possible to achieve particles less than 0.01 μ in diameter at concentrations of 10^{12} to $10^{13}/cm^3$ by splat cooling. Additional studies should be conducted, in the case of some splat-cooled uranium-base alloys, specifically the U–Be compositions, to determine the irradiation stability of the splat-cooled alloys for comparison with that of adjusted uranium alloys. It is believed that other uranium alloys can be developed in which fine particles achieved by splat cooling would be stable in size at temperatures of 600°C and above. Such alloys probably would involve ternary compositions in which the precipitate would be formed by the two elements added to the uranium.

The metastable phases in the U–Nb system were studied in India.[15] Composition limits of metastable α', α'', and γ°, and changes in parameters a, b, c and angle $\gamma(ab)$ of the alpha-

uranium lattice with increasing niobium additions have been determined.* Figures I-1 and I-2 show the results of the investigation. With increasing niobium content up to about 16 at.%, the parameter a is not affected noticeably, whereas parameter b decreases steadily and parameter c increases steadily. The angle γ abruptly changes from 90° at 10.00 at.% niobium to 91.07° at 11.93 at.% niobium. A study of the effect of cooling rates in producing alternative structures shows that the mode of formation of α', α'', and $\gamma°$ in the U–Nb system is similar to that observed in the U–Mo system. On the basis of the size of the solute atom, a relation is developed for predicting the α'/α'' boundary composition in various uranium binary systems with high solute solubility in the gamma phase.

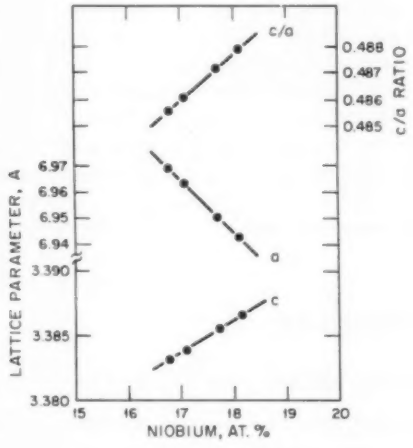

Fig. I-1 Variation of lattice parameters of the $\gamma°$ phase in U–Nb alloys with composition.[15]

In similar work with U–Ru alloys[16] containing up to 9.51 at.% ruthenium, the metastable α' and $\gamma°$ phases produced upon water quenching were investigated. For compositions up to 6.90 at.% ruthenium, only α' phase is produced,

*The phase α' has the alpha-uranium structure with a contracted b parameter as compared with a and c parameters. The phase α'' has parameter distortions similar to α', plus an increase in angle (between the a and b axes), thus resulting in a monoclinic structure. The phase $\gamma°$ is an ordered tetragonal phase based on a block of 2 by 2 by 1 gamma cells; the c/a ratio is less than 0.5.

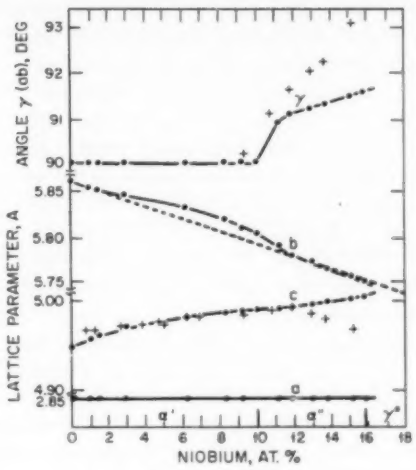

Fig. I-2 Variation[15] *in lattice parameters a, b, c and angle γ in U–Nb alloys water quenched from 900°C. ●, Tangri and Chaudhuri; +, Anagnostidis et al.*

whereas for higher compositions (up to the solubility limit of 10 at.% ruthenium), both the α' and $\gamma°$ phases exist. The absence of the α'' phase, which exists in the U–Mo and U–Nb alloys, may be ascribed to the incompressibility of the b parameter below 5.80 A, possibly due to a variation in the state of ionization of the ruthenium atoms when present in varying amounts in the uranium matrix.

Other interesting publications concerned with alpha-uranium alloys which have come to the reviewer's attention during the past quarter include papers on The Precipitation of Intermetallic Compounds in Adjusted Uranium,[17] Phase Transformations and Equilibrium Structures in Uranium-Rich Niobium Alloys,[18] and The Phase Equilibria in Uranium–Cobalt–Iron Alloys in the Partial System U–UCo_2–UFe_2 (Ref. 19).

Gamma-Phase Uranium Alloys

Investigators at Lawrence Radiation Laboratory[20] report that the U–10 wt.% Mo alloy is highly susceptible to cracking, and hence to ultimate failure, when stressed in air. Tests conducted in various environments show that oxygen is responsible for the cracking. In this alloy the elongation in a stress–strain test is sensitive to strain rate, and the maximum ductility is obtained at a strain rate of about 0.05/min. Tests at both faster and slower strain rates result in a lower elongation. Delayed

failure was observed at a stress as low as 37,500 psi (30% of the yield stress). The critical stress appears to be dependent on carbon content but not on grain size. Attempts to protect the alloy by electrolytic or vapor-deposited coatings were not successful. Small additions of niobium to the binary alloy do not alleviate the cracking problem. The critical stress for a U–8 wt.% Mo–1 wt.% Ti alloy was determined to be 108,000 psi. This value is the highest for all the materials tested that demonstrated the stress cracking.

Other studies[21] on the U–8 wt.% Mo–0.50 wt.% Ti alloy show that it also is subject to stress cracking in air during static or low-strain-rate loading while in the metastable gamma-phase condition. The average critical stress (62,500 psi) is higher than the critical stress observed for the U–10 wt.% Mo alloy. If the alloy is transformed from the gamma phase to the alpha-plus-gamma condition, the stress-cracking brittleness disappears. The long-term effect on the general corrosion resistance of the material by this heat-treatment was not established.

Lawrence Radiation Laboratory[22] conducted dynamic tensile tests on U–10 wt.% Mo alloys in as-cast and wrought conditions. Carbon content was varied from 71 to 800 ppm. Heat-treatment was also varied. Tests were conducted on a universal testing machine at strain rates of 4.8×10^{-5}/sec and 0.057/sec and on a modified Dynapak at strain rates up to 100/sec. Tests were run from 75 to 600°F. Relatively low strain rates were used to determine the susceptibility to stress corrosion, whereas the higher strain rates demonstrated the sensitivity of various mechanical properties to strain-rate effects. The following conclusions are drawn from the data obtained for the specimens tested:

1. Dynamic loading increases the tensile strength and lowers the ductility of U–10 wt.% Mo alloy in both the as-cast and wrought conditions.

2. The U–10 wt.% Mo alloy is sensitive to stress corrosion.

3. Extruded specimens are best suited for room-temperature applications and in cases where notch sensitivity may be a problem.

4. Hot-rolled specimens are superior at relatively high temperatures, i.e., around 600°F. At lower temperatures they are extremely notch sensitive.

5. As-cast specimens do not display as consistent mechanical properties as wrought specimens. As-cast specimens are also less ductile.

The following observations are tentative, owing to the many variables present:

1. Carbon content should be kept low, below 200 ppm. High carbon content tends to reduce both ductility and tensile strength.

2. The heat-treatment period should be kept short. A period of about 1 hr seems to be best. A vacuum of at least 20 μ should be maintained during the heat-treatment period.

The effect of reactor irradiation on the corrosion rate of two U–10 wt.% Mo alloys was studied at elevated temperatures by investigators at Sandia Laboratory.[23] The corrosion rate in commercially bottled CO_2 and N_2 gas increased with temperature and amount of prior hot work. Activated specimens gained weight in the test environments 3.5 times as fast as unirradiated specimens. Because the corrosion products in both environments were UO_2 and U_3O_8, it was concluded that the H_2O impurity in the bottled gas was the principal corrosive agent, and the pure N_2 gas would be a suitable coolant for as-cast, unplated ^{235}U–10 wt.% Mo pulsed-reactor fuel. (M. S. Farkas)

Plutonium

Plutonium Metal and Alloys

Investigators at Los Alamos Scientific Laboratory are continuing studies of the phase relations in several alloy systems of plutonium.[24,25] An intermediate phase in the Pu–Sc system was found to have a maximum solubility range from 34 to 40 at.% scandium at about 650°C. The dimensions of the hexagonal unit cell suggest a double hexagonal closed-packed structure of the alpha-neodymium type. The Pu–Am and Pu–In phase diagrams are shown in Figs. I-3 and I-4, respectively.

The crystal structures and lattice parameters of the five compounds found in the Pu–B system are shown in Table I-1. The composition assigned to the PuB_{100} compound is tentative at this point. Metallographic evidence indicates that PuB_4 melts congruently, whereas all the other borides melt peritectically. A eutectic reaction occurs between PuB_{12} and PuB_{100}.

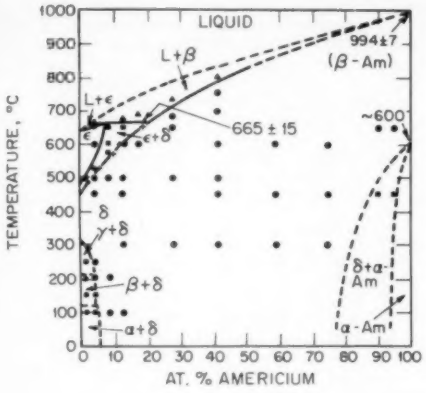

Fig. I-3 The Pu–Am phase diagram.[24] ●, *single-phase alloy;* ■, *two-phase alloy;* ▲, *liquid present; and* +, *X-ray parametric.*

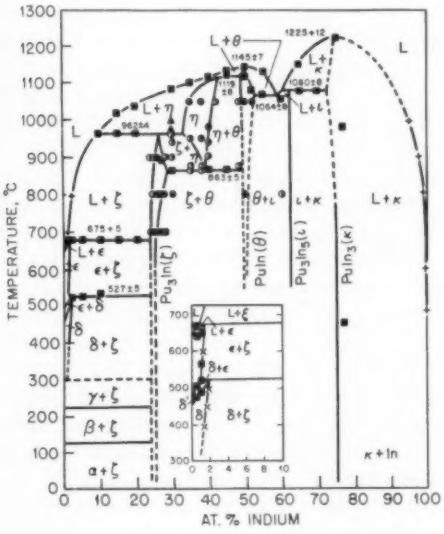

Fig. I-4 The Pu–In phase diagram.[25] ■, *thermal analysis;* ●, *single phase;* ◑, *two phases;* ▲, *liquid present;* ×, *lattice parameter; and* +, *filtration data.*

Studies of the solubility of plutonium in U_2Ti indicate that plutonium can replace at least 50% of the uranium atoms.

Experiments of self-diffusion in gamma plutonium have been conducted in more detail than previously reported. The diffusion data fit the equation

$$D = 2.1 \times 10^{-5} \exp(-16{,}700/RT)$$

The vapor pressure of liquid plutonium in the temperature range 1100 to 1800°K has been determined by the Knudsen effusion method. The least-squares equation that fits the data is

$$\log p \text{ (atm)} = -17{,}420/T(°\text{K}) + 4.913$$

No effects of oxygen on the volatility were found. The heat of vaporization computed from the temperature dependence of the vapor pressure is $\Delta H_{298} = 82.3$ kcal/gram atom.

The solubility[26] of tungsten in liquid plutonium has been measured over the temperature range 700 to 1000°C. Solubility increased from 29 ppm (by weight) tungsten at 700°C to 291 ppm tungsten at 900°C. The data fit the empirical equation

$$\log N_W = 0.3518 - 4.639 \times 10^3 \, T^{-1}$$

where N_W is solubility expressed as the mole fraction of tungsten and T is temperature in degrees Kelvin.

In continued studies of containment of molten-plutonium-alloy fuels, Los Alamos has found[24,25] that carbide layers on tantalum and tantalum alloys seem to improve the resistance to corrosion by liquid Pu–Co–Ce alloys. Gross carbon additions to the capsule material, however, appear to cause a gross degradation of containment properties.

Attempts are being made to protect capsule welds, which are the points most susceptible to attack by liquid fuel, by placing them a sufficient distance above the fuel so that they are never in contact with the fuel. This has required a measurement of the distance that the fuel alloy will creep up the capsule walls. At 700°C a Pu–Co–Ce alloy containing 5 g of plutonium per cubic centimeter reached a height of 4 to 5 in. above the fuel level. At the

Table I-1 PROPERTIES OF PLUTONIUM BORIDES[25]

Compound	Structure	Unit cell dimensions, A
PuB_2	Hexagonal (AlB_2 type)	$a_0 = 3.1857 \pm 0.0002$ $c_0 = 3.9485 \pm 0.0004$
PuB_4	Tetragonal (ThB_4 type)	$a_0 = 7.1018 \pm 0.0003$ $c_0 = 4.0028 \pm 0.0001$
PuB_6	Simple cubic	$a_0 = 4.1134 \pm 0.0003$
PuB_{12}	Face-centered cubic	$a_0 = 7.4843 \pm 0.0003$
"PuB_{100}"	Simple cubic	$a_0 = 23.43 \pm 0.04$

same temperature, fuel containing 62 and 80 g of plutonium per cubic centimeter climbed $3\frac{3}{4}$ and $3\frac{1}{2}$ in. above the fuel level, respectively.

Workers at Rocky Flats Division of The Dow Chemical Co.[27] have investigated the effects of ternary additions of aluminum, cerium, and zinc on the properties and the stability of the delta phase in Pu–Ga alloys. At two of the compositions tested, Pu–0.10 wt.% Al–0.60 wt.% Ga and Pu–0.36 wt.% Ce–0.66 wt.% Ga, the delta phase appeared to be more stable than in the reference Pu–1 wt.% Ga alloy. Tensile properties of the alloys studied are tabulated in Table I-2, and thermal-expansion data are shown in Table I-3.

Argonne National Laboratory has examined a total of seventy-eight U–20 wt.% Pu–10 wt.% Fs alloys irradiated to burnups of 1.2 to 4.2 at.% of the heavy metal over a temperature range[28] of 420 to 900°C. The fuel alloys were sodium bonded to various high-temperature jacketing materials including niobium, Nb–1 wt.% Zr, Nb–33 wt.% Ta–1 wt.% Zr, Nb–4 wt.% V, vanadium, molybdenum, Ta–0.1 wt.% W, Inconel X, Hastelloy X, and type 304 stainless steel. Details of the irradiation and the results are listed in Table I-4.

Table I-2 TENSILE DATA FOR DELTA-STABILIZED TERNARY ALLOYS OF PLUTONIUM[27]

Composition (balance plutonium), wt.%	Yield strength, 1000 psi	Ultimate strength, 1000 psi	Elongation, %
Cast, Rolled 82.5%			
0.15 Al–0.80 Ga	28.0	31.4	6
0.10 Al–0.60 Ga	30.6	33.0	4
0.18 Al–0.33 Ga	24.4	28.0	7
0.13 Zn–0.70 Ga	29.4	32.7	6
0.45 Zn–0.49 Ga	26.5	28.5	6
0.60 Zn–0.28 Ga	25.9	27.5	7
0.36 Ce–0.66 Ga	25.6	27.6	4
0.73 Ce–0.50 Ga	28.6	36.5	3
0.99 Ce–0.25 Ga	46.9	52.6	1
1 Ga	28.4	31.7	7
Cast, Rolled 82.5%, Annealed 12 min at 255°C			
0.15 Al–0.80 Ga	15.2	21.6	23
0.10 Al–0.60 Ga	17.6	24.2	25
0.18 Al–0.33 Ga	14.4	20.6	26
0.13 Zn–0.70 Ga	13.9	20.5	22
0.45 Zn–0.49 Ga	11.3	17.4	18
0.60 Zn–0.28 Ga	9.0	15.8	24
0.36 Ce–0.66 Ga	10.7	17.7	24
0.73 Ce–0.50 Ga	11.8	17.9	26
0.99 Ce–0.25 Ga	17.8	26.1	27
10 Ga	18.2	23.4	19

Table I-3 COEFFICIENTS OF EXPANSION OF AS-CAST DELTA-STABILIZED TERNARY ALLOYS OF PLUTONIUM[27] IN THE TEMPERATURE RANGE 25 TO 100°C

Composition (balance plutonium), wt.%	Coefficient of expansion, 10^{-6}/°C
0.15 Al–0.80 Ga	4.7
0.10 Al–0.60 Ga	5.6
0.18 Al–0.33 Ga	6.0
0.13 Zn–0.70 Ga	5.9
0.45 Zn–0.49 Ga	2.9
0.60 Zn–0.28 Ga	6.0
0.36 Ce–0.66 Ga	2.5
0.73 Ce–0.25 Ga	2.0
0.99 Ce–0.25 Ga	2.4
1 Ga	7.2

The compressive strengths of U–Pu–Ti and U_2Ti were measured[29] at temperatures up to 766°C. Results, shown in Table I-5, indicated that U_2Ti is stronger than the ternary alloys. Also, homogenization strengthened the U_2Ti alloy but did not significantly affect the U–15 wt.% Pu–10 wt.% Ti alloy.

Battelle–Northwest has studied the room-temperature fatigue behavior of a Pu–1 wt.% Ga alloy in several metallurgical conditions.[30] It was found that fatigue strength was relatively unaffected by yield strength. Over a 0.1% yield-strength range of 10,300 to 30,400 psi, fatigue strength varied only from 10,000 to 15,000 psi. The cored, as-cast, and the homogenized, 94% rolled, 300°C annealed materials exhibited the lowest fatigue strengths; whereas the cored, 86% rolled material had the highest fatigue strength. The presence of alpha phase seemed to impart increased resistance to fatigue failure.

Related studies of low-iron Pu–Ga alloys showed that the strength decreased uniformly with temperature in the range −32 to 500°C, whereas ductility generally increased.[31] As the amount of iron impurity increased, the material began to exhibit a hot-short behavior, with loss of strength and ductility. No effects of testing speed on strength or ductility were noted. Strain hardening occurred in homogenized, cold-rolled alloys, whereas the alpha-phase formation in cored, cold-rolled alloys gave strengthening over and above that from strain hardening. Recrystallization of a 94% cold-rolled alloy occurred at 250°C. During

Table 1-4 EFFECTS OF IRRADIATION ON CAST U–20 WT.% Pu–10 WT.% Fs SPECIMENS[28]

Specimen	Melt	Jacket composition, wt.%	Void volume, %	Heavy-metal burnup, at.%	Max. temp., °C		Time av. temp., °C		Condition of specimen*
					Jacket surface	Fuel center	Jacket surface	Fuel center	
17-2	R21-10B	Niobium	13	1.4	655	760	595	690	B
17-6	R21-10C	Niobium	13	1.6	790	920	740	855	B
16-4	R21-10A	Niobium	13	1.7	780	910	715	830	B
18-2	R21-10D	Niobium	13	2.0	680	790	665	770	B
22-5	S2-3-2	Nb–1 Zr	36†	0.7	615	715	555	640	C
22-2	S2-3-1	Nb–1 Zr	36†	0.7	655	760	595	690	C
19-1	R21-19C	Nb–1 Zr	28	1.2	520	595	490	570	B
19-6	R21-20C	Nb–1 Zr	28	1.2	535	615	510	590	B
19-4	R21-21C	Nb–1 Zr	28	1.2	535	615	510	590	B
17-1	R21-15D	Nb–1 Zr	13	1.4	655	760	595	690	B
23-1	S2-3-4	Nb–1 Zr	50	1.4	560	650	535	620	D
23-4	R21-11A	Nb–1 Zr	50	1.4	630	730	560	650	A
20-2	R21-21F	Nb–1 Zr	28	1.5	555	640	540	625	B
20-4	R21-22A	Nb–1 Zr	28	1.5	580	670	550	635	B
20-6	R21-22D	Nb–1 Zr	28	1.5	580	670	550	635	B
16-2	R21-15B	Nb–1 Zr	13	1.6	695	810	630	730	B
17-4	R21-15E	Nb–1 Zr	13	1.6	790	920	740	855	B
16-5	R21-15C	Nb–1 Zr	13	1.7	780	910	715	830	B
18-4	R21-17B	Nb–1 Zr	13	2.0	680	790	665	770	A
18-1	R21-17A	Nb–1 Zr	13	2.0	680	790	665	770	B
21-4	S2-1-1	Nb–1 Zr	25	2.1	520	600	395	490	B
21-1	R21-22B	Nb–1 Zr	25	2.1	520	600	495	580	B
21-2	R21-24B	Nb–1 Zr	25	2.1	520	600	495	580	B
27-4	R21-11E	Nb–1 Zr	Vented	2.1	570	660	520	600	C
27-1	R21-11C	Nb–1 Zr	Vented	2.1	570	660	520	600	A
25-4	R21-7B	Nb–1 Zr	50	2.1	575	670	520	600	B
25-1	R21-7A	Nb–1 Zr	50	2.1	580	670	530	620	C
28-1	R21-11B	Nb–1 Zr	57	2.5	580	670	410	480	B
28-4	R21-11D	Nb–1 Zr	57	2.5	580	670	520	610	C
32-1	R21-3B	Nb–1 Zr‡	23	4.2	590	690	460	535	A
32-2	R21-3C	Nb–1 Zr‡	24	4.2	590	690	460	535	C
32-3	R21-3D	Nb–1 Zr‡	24	4.2	590	690	460	535	A
32-4	R21-3E	Nb–1 Zr‡	22	4.2	615	720	480	560	A
32-5	R21-3F	Nb–1 Zr‡	23	4.2	615	720	480	560	A
32-6	R21-4A	Nb–1 Zr‡	17	4.2	615	720	480	560	A
22-4	S2-2-3	Nb–33 Ta–1 Zr	36†	0.7	615	715	555	640	A
22-1	S2-2-2	Nb–33 Ta–1 Zr	36†	0.7	655	760	595	690	B
23-3	R21-9A	Nb–33 Ta–1 Zr	50	1.4	560	650	535	620	B
23-6	R21-9B	Nb–33 Ta–1 Zr	50	1.4	630	730	560	650	A
27-6	R21-25F	Nb–33 Ta–1 Zr	Vented	2.1	570	660	520	600	A
27-3	R21-25E	Nb–33 Ta–1 Zr	Vented	2.1	570	660	520	600	A
25-6	R21-26D	Nb–33 Ta–1 Zr	50	2.1	575	670	520	600	B
25-3	R21-26C	Nb–33 Ta–1 Zr	50	2.1	590	680	575	670	A
29-1	R21-29E	Nb–4 V	57	3.0	490	560	450	510	A
29-5	R21-3A	Nb–4 V	57	3.0	500	570	460	520	A
29-4	R21-29F	Nb–4 V	57	3.0	500	570	460	520	A
22-6	S2-2-4	Vanadium	50†	0.7	615	715	555	640	G
17-3	R21-17E	Vanadium	13	1.4	655	760	595	690	B
16-3	R21-17D	Vanadium	13	1.6	695	810	630	730	B
18-5	R21-18B	Vanadium	13	2.0	680	790	665	770	G
18-3	R21-17E	Vanadium	13	2.0	680	790	665	770	B
19-3	R21-20E	Molybdenum	30	1.2	520	595	490	570	B
20-1	R21-21B	Molybdenum	30	1.5	555	640	540	625	C
22-3	S2-2-6	Ta–0.1 W	36†	0.7	655	760	595	690	B
19-2	R21-20A	Ta–0.1 W	28	1.2	520	595	490	570	C
19-5	R21-20B	Ta–0.1 W	28	1.2	535	615	510	590	C
23-2	R21-9D	Ta–0.1 W	50	1.4	560	650	535	620	B
23-5	S2-3-3	Ta–0.1 W	50	1.4	630	730	560	650	A
20-3	R21-27B	Ta–0.1 W	28	1.5	555	640	540	625	A

(Table continues on next page.)

Table I-4 (Continued)

Specimen	Melt	Jacket composition, wt.%	Void volume, %	Heavy-metal burnup, at.%	Max. temp., °C: Jacket surface	Max. temp., °C: Fuel center	Time av. temp., °C: Jacket surface	Time av. temp., °C: Fuel center	Condition of specimen*
20-5	R21-27D	Ta–0.1 W	28	1.5	580	670	550	635	B
21-5	R21-H9	Ta–0.1 W	25	2.1	520	600	360	420	C
21-6	S2-2-5	Ta–0.1 W	36‡	2.1	520	600	460	540	B
21-3	R21-24E	Ta–0.1 W	25	2.1	520	600	495	580	B
27-2	R21-25A	Ta–0.1 W	Vented	2.1	570	660	520	600	A
27-5	R21-25B	Ta–0.1 W	Vented	2.1	570	660	520	600	A
25-5	R21-14A	Ta–0.1 W	50	2.1	575	670	520	600	B
25-2	R21-7D	Ta–0.1 W	50	2.1	590	680	530	620	A
16-1	R21-18B	Inconel X V barrier	13	1.6	695	810	630	730	E
17-5	R21-18E	304 S.S. V barrier	13	1.6	790	920	740	855	E
16-6	R21-18C	304 S.S. V barrier	13	1.7	780	910	715	830	E
18-6	R21-18F	304 S.S. V barrier	13	2.0	680	790	665	770	A
28-3	R21-28F	Hastelloy X W lined	57	2.5	590	670	410	480	E
28-2	R21-28B	Hastelloy X W lined	57	2.5	590	670	410	480	F
28-5	R21-28C	Hastelloy X W lined	57	2.5	590	670	520	610	A
28-6	R21-28D	Hastelloy X W lined	57	2.5	590	670	520	610	A
29-3	R21-29D	Hastelloy X W lined	57	3.0	490	560	450	510	A
29-2	R21-29C	Hastelloy X W lined	57	3.0	490	560	450	510	A
29-6	R21-29B	Hastelloy X W lined	57	3.0	500	570	460	520	A

*A, specimen straight and intact.
B, longitudinal split in jacket with protrusion of fuel.
C, longitudinal split in jacket without protrusion of fuel.
D, several small cracks around center section of specimen.
E, fuel penetrated barrier and formed extensive eutectic with jacket.
F, fuel penetrated barrier and formed small hole in jacket.
G, specimen bowed but intact.

†No sodium bond.
‡Jacket thickness, 0.38 mm (0.015 in.).
§Jacket thickness, 0.64 mm (0.025 in.).

Table I-5 ULTIMATE COMPRESSIVE STRENGTH OF U–Ti-BASED ALLOYS[29]

Alloy, wt.%	Heat-treatment	Temp., °C	Ultimate compressive strength, kg/mm²	Mode of failure
U_2Ti	As cast	615	66	Ductile
U_2Ti	As cast	709	41	Ductile
U_2Ti	1050°C, 1 week	554	103	Ductile–brittle
U_2Ti	1050°C, 1 week	710	50	Ductile
U_2Ti	1050°C, 1 week	758	36	Ductile
U–15 Pu–10 Ti	As cast	20	120	Brittle
U–15 Pu–10 Ti	As cast	409	44	Brittle
U–15 Pu–10 Ti	As cast	560	39	Ductile–brittle
U–15 Pu–10 Ti	1050°C, 1 week	560	35	Ductile–brittle
U–15 Pu–10 Ti	1050°C, 1 week	643	15	Ductile
U–15 Pu–10 Ti	1050°C, 1 week	766	6.7	Ductile
U–22.1 Pu–11.8 Ti	As cast	25	141	Brittle
U–22.1 Pu–11.8 Ti	As cast	405	71	Brittle
U–22.1 Pu–11.8 Ti	As cast	516	48	Ductile–brittle
U–22.1 Pu–11.8 Ti	As cast	618	34	Ductile
U–22.1 Pu–11.8 Ti	As cast	717	11	Ductile

extended anneals, grain coarsening and grain-boundary void formation were observed.

(V. W. Storhok)

Plutonium Compounds

Argonne[32] reports a method of preparing single-phase PuC by heating metallic plutonium in a graphite crucible to between 1575 and 1650°C in vacuum. The same laboratory has attempted reaction sintering of UC in preparation for similar processing of mixed (U,Pu)C fuels; however, attempts have not been successful.[33]

The Th–Pu–C ternary is being investigated by the British[34] in the carbon-rich areas of the system. Plutonium dicarbide was shown to be soluble in the monoclinic ThC_2 to the extent of 40 mole % at room temperature. A lattice parameter of 9.68 A was observed for $(Th_{0.6}Pu_{0.4})C_2$. The postulated sesquicarbide $(ThPu)_2C_3$ does not exist at Th : Pu ratios up to 70 : 30. A fuel composition of $(Th_{0.85}Pu_{0.15})C_{2.2}$ has been arc melted, and various properties have been determined.[35] The density is 10.1 g/cm^3, the melting point is 2320 ± 20°C, and the coefficient of thermal expansion (from 10 to 1000°C) is 8.5 ± 0.2 × 10^{-6}/°C. Hardness varies from DPHN 770 at room temperature to DPHN 140 at 900°C. Spherical particles of this material are prepared by granulating mixtures of PuO_2, ThO_2, and graphite and subsequently heating to homogenize and sinter.

Plutonium mononitride (PuN) studies continue at various laboratories. Los Alamos[24] has sintered ball-milled PuN to 89% of theoretical density at 1600°C in a nitrogen atmosphere. Hanford Atomic Products Operation[36] has prepared a single-phase (Pu,Zr)N alloy and claims the preparation of PuN which is stoichiometric, containing 1120 ppm carbon, after reacting PuO_2 and carbon under a nitrogen atmosphere.

Battelle–Northwest is irradiating dispersion fuels of 20 vol.% PuO_2 in type 304 stainless steel with no postirradiation results yet reported. The specimens were prepared by extrusion.[37] In this connection the reported stabilization of PuO_2 against thermal reduction by additives of refractory metals[24] is of interest.

Suboxides of plutonium are anticipated to have desirably high thermal-conductivity characteristics. Beta Pu_2O_3 has been shown in the course of X-ray studies[36] to have no detectable compositional range. Strasser[38] is preparing carbon-stabilized uranium–plutonium monoxide $(U_{0.9}Pu_{0.1})(O_{0.58}C_{0.42})$ by reacting UO_2 and PuO_2 with carbon or uranium metal. Reaction sintering of the mixed dioxides in combination with UH_3 and UC resulted in monocarbo-oxides with densities approaching 94% of theoretical, but they always contained appreciable $(U,Pu)O_2$. Canadian sources[39] have shown by metallographic examination that solid-solution formation apparently occurs in physically mixed $(U,Pu)O_2$ fuels during irradiation in the region of grain growth. However, autoradiographic studies revealed that segregation of the plutonium was still evident. Chalk River research workers[40] have also established that $PuAl_3$ (hexagonal) is stable in the range of 1027 to 1210°C but transforms at 1210°C to a cubic $PuAl_3$ structure. As previously indicated, rhombohedral modifications of the compound are stable below 1027°C. (W. M. Pardue)

Thorium

Eutectics not previously reported were detected between thorium and Th_2Ag at 30 ± 1 at.% silver and 1012 ± 12°C, thorium and Th_2Au at 20 ± 1 at.% gold and 1100 ± 12°C, thorium and Th_7Co_3 at 20 ± 1 at.% cobalt and 1100 ± 12°C by workers in the United Kingdom.[41] The solid solubility of silver, gold, iron, and cobalt in thorium was found to be significantly lower than 2% at the eutectic or peritectic temperatures. The compositions of the eutectics previously reported between thorium and Th_2Cu and between thorium and Th_7Ni_3 were confirmed, but the eutectic temperatures of 1037 ± 12 and 1062 ± 12°C were significantly higher than those given in the literature. It is suggested that this might be due to the impure nature of the material on which the earlier results were obtained.

Investigators at Oak Ridge National Laboratory have determined the hot hardness of numerous thorium-base binary and ternary alloys.[42] The results obtained at 600 and 750°C are given in Table I-6. The binary thorium-base alloys with 4% indium and 5% zirconium were the hardest at 600 and 750°C of any of the alloys investigated. A ternary alloy of thorium with 0.2% each of beryllium and carbon gave exceedingly high hardness at 400°C.

Table I-6 THORIUM-BASE ALLOYS IN ORDER OF DECREASING HARDNESS[42] AT 600 AND 750°C

600°C		750°C	
Alloy (balance thorium), wt.%	DPH	Alloy (balance thorium), wt.%	DPH
4 In	91	4 In	55
2 In	63	5 Zr	37
10 Zr	59	4 In–5 Zr	34
5 Zr	59	5 V–0.2 C	33
2 Zr–0.2 C	54	2 In	31
20 Zr	54	5 Zr–0.2 C	31
5 V–0.2 C	50	5 U–0.2 C	26
4 In–5 Zr	49	20 Zr	25
2 In–0.2 C	49	10 Zr	25
2 Cr–0.2 C	47	8 Nb	25
2 Mo–0.2 C	44	5 Ti–0.2 C	24
5 U–0.2 C	44	5 Ti	23
0.2 Al–0.2 C	43	2 In–0.2 C	23
8 Nb	43	0.2 Be–0.2 C	20
0.2 Be–0.2 C	40	5 V	20
5 Ti–0.2 C	40	2 Cr–0.2 C	20
0.2 C	38	0.2 Al–0.2 C	20
5 Ti	37	0.4 Al	19
20 U	36	0.2 Al	19
0.4 Al	35	20 U	18
8 Cr	35	8 Cr	18
0.2 Al	32	5 U	18
5 V	32	8 Mo	17
5 U	30	2 Mo–0.2 C	17
8 Mo	30	4 Nb	17
0.15 C	29	10 U	15
2 Nb–0.2 C	29	4 Mo	15
10 U	28	2 Nb	14
4 Mo	27	0.2 Be	14
4 Cr	27	0.2 C	13
4 Nb	26	4 Cr	13
2 Nb	26	2 Mo	13
2 Mo	24	0.15 C	11
0.10 C	23	Thorium	11
Thorium	22	2 Cr	11
2 Cr	21	2 Nb–0.2 C	11
0.2 Be	21	0.10 C	9

Some 50 high-purity, binary and ternary, thorium-base alloys were prepared and corrosion tested in distilled water between 120 and 260°C by workers at Argonne.[43] The short-time corrosion tests indicated that the addition of titanium improved the corrosion life of Th–1 wt.% C and Th–0.5 wt.% C binary alloys at 260°C. Additions of from 3 to 7 wt.% aluminum appeared to be beneficial. The Th–10 wt.% Y alloy exhibited a low corrosion rate during a short period of exposure to water at 200°C. The corrosion resistance of all Th–U alloys, in increments of 5 wt.% uranium, to the maximum 40 wt.% uranium was poor. The addition of 4 wt.% zirconium to the Th–15 wt.% U alloy improved its corrosion resistance at 200°C.

(R. L. Martin)

Metal-Ceramic Fuels

Dispersion Fuels

A method has been developed in Germany[44] for producing stable dispersions of fissionable material in an aluminum matrix. A nitride layer was generated on the surface of the aluminum powders with the help of a gaseous or liquid nitrogen-containing substance and mixed with the UO_2 fuel particles. The materials were then pressed and densified.

Workers at North Carolina State College[45] have produced UC–U dispersions approaching ideal densities and uniform distributions of UC particles ($10^{12}/cm^3$) in the uranium matrix. The most successful technique involved blending UH_3 and carbon and hot-pressing the mixtures for a short time at a temperature above the reaction temperature of UC and uranium. Densities obtained by this liquid-phase extrusion technique were above 99% of theoretical. The material contained nearly 1 vol.% UO_2 impurity and 1 vol.% porosity, as observed by metallographic examination.[46]

Workers at Harwell report[47] that dispersions containing 30, 40, and 50 vol.% $(U_{0.75}Pu_{0.25})O_2$–type 316L stainless steel were prepared either by cold pressing and sintering or by hot pressing. Densities were improved from 85 to 95% of theoretical, and pins were prepared for irradiation. Compatibility tests indicated no signs of reactions after 100 hr at 1000°C, or even when the type 316L stainless steel was melted at 1600°C. In addition, workers at Battelle-Northwest report[36] that irradiation capsules containing 20 vol.% PuO_2–stainless steel have been fabricated for testing in the Engineering Test Reactor. The capsules contained two types of pellets—97 and 82% of theoretical density. They were irradiated to 1.6% burnup of the plutonium atoms at calculated centerline temperatures[48] ranging from 1300 to 1415°C. Postirradiation tests indicated that there was no swelling in any specimens.[49] (D. L. Stoltz)

Coated-Particle Fuel Materials

Particle Coating

Measurement of the degree of preferred orientation in pyrolytic carbon (PyC) coating

structures by use of X-ray techniques has been described by General Atomic in a preprint[50] of a paper submitted for publication. In another preprint[51] General Atomic describes the variations in the crystallinity of PyC deposits and suggests that carbon is formed by the following processes:

1. At high methane concentrations carbon is formed from high-molecular-weight planar polymers that form in the gas phase and either condense directly on the bed particles or nucleate homogeneously to form gas-borne droplets. Direct condensation leads to high-density anisotropic carbons, whereas deposition of gas-borne droplets leads to lower density, more isotropic structures.

2. At low methane concentrations (~ 5 vol.%), polymerization is limited and the complexes that form are necessarily smaller. As a result, they are less effectively aligned with one another and the deposition surface. This leads to low-density, less anisotropic carbons that contain a high concentration of misaligned single layers. At very low methane concentration (< 3 vol.%), carbon must be deposited primarily from relatively small hydrocarbon fragments.

Battelle has concluded a study[52] on the preparation of BeO-coated fuel particles. The BeO coatings were deposited on UO_2 particles in a 1-in.-diameter fluidized-bed reactor by each of the following reactions:

$$BeCl_2\ (gas) + H_2O\ (gas) \rightarrow BeO\ (solid) + 2HCl\ (gas) \quad (1)$$

$$BeCl_2\ (gas) + CO_2\ (gas) + H_2\ (gas) \rightarrow BeO\ (solid) + 2HCl\ (gas) + CO\ (gas) \quad (2)$$

$$BeI_2\ (gas) + H_2O\ (gas) \rightarrow BeO\ (solid) + 2HI\ (gas) \quad (3)$$

$$BeI_2\ (gas) + CO_2\ (gas) \rightarrow BeO\ (solid) + CO\ (gas) + I_2\ (gas) \quad (4)$$

$$Be_4O(C_2H_3O_2)_6\ (gas) \rightarrow BeO\ (solid) + \text{unidentified by-products (gas)} \quad (5)$$

Even though the coating quality was equivalent for reactions 1 through 4, reaction 1 was preferred because of convenience and/or economic factors. With reaction 5, carbon contamination (about 8 wt.%) of the coating occurred. It was demonstrated that BeO coatings can be deposited with densities and hardnesses essentially equal to those of single-crystal BeO. However, the grain structure and porosity of the BeO coatings vary with preparation temperature. Dense coatings of large equiaxed grains are obtained at 1400 to 1500°C, but porous coatings with submicron grain sizes are obtained at 600 to 1100°C. At 1250°C the typical structure is that of radially oriented needle-shaped grains of BeO. Heat-treating at 1500°C for 2 hr caused considerable grain growth in the BeO coatings, and, as a result of the coarse grain structure, the coating was weakened. So that the useful temperature range for BeO coatings could be extended, additions of Al_2O_3, MgO, SiO_2, ZrO_2, or carbon during the preparation of coatings were evaluated as grain-growth inhibitors. Only carbon appeared to be effective. (N. D. Veigel)

Irradiation and Evaluation of Coated-Particle Fuels

A large number of specimens of PyC-coated UO_2, UC_2, $(Th,U)O_2$, and $(Th,U)C_2$ particles have recently been evaluated in static capsule irradiations by General Atomic.[53,53a] Conclusions drawn from these experiments include:

1. General Atomic's BISO coatings are equivalent to their Triplex coatings in radiation stability. A 100-μ BISO coating on a 200-μ UC_2 particle survived 20% burnup at 1300°C. The BISO is a two-layered coating, the inner layer porous PyC and the outer layer isotropic PyC; whereas the Triplex has three layers, the inner one porous.

2. Coated oxide particles are equivalent to coated carbide particles in stability.

3. The coating-thickness to fuel-particle-diameter (t/d) ratio is a major factor influencing stability, and the minimum t/d required is a function of irradiation temperature. At 1400°C and below, a ratio of 0.4 is sufficient; whereas at 1700°C a ratio of 0.5 is required.

4. The BISO coatings with a thick buffer layer appeared to be more effective than those with a thin buffer layer. For a 100-μ total coating thickness, a coating with a 33-μ buffer gave less failure than one with a 21-μ buffer.

5. Isotropic coatings deposited at 2000°C (having a density of 1.95 g/cm^3) appeared to be better than those deposited at lower temperatures which had lower density.

Irradiation experiments conducted by General Atomic at greatly accelerated burnup ratios (>10% per month) using large-diameter fuel particles (>400 μ) resulted in higher coating-failure rates than did tests conducted under less stringent conditions. The coating failures are believed to be a result of large thermal gradients produced in the large particles at the high burnup rates.

Irradiation evaluations of PyC-coated particles have also continued at Oak Ridge,[54,55] where they have continued to observe good in-pile performance for the Triplex and Duplex coatings. A General Atomic BISO coating (110 μ thick) on a large (~ 500 μ), porous UO_2 particle performed without failure to 6 at.% burnup at 1370°C. At this point severe failure began to occur, which may have been the result of the very irregular shapes of these particular UO_2 particles.

Large, porous UO_2 particles with monolithic PyC coatings are being evaluated in-pile at Battelle.[56–58] A specimen of 460-μ, 65% dense UO_2 particles coated with 113 μ of laminar PyC has withstood 11 at.% burnup at 815°C without coating failure. The t/d ratio of this material is only 0.25. A similar specimen with 81% dense UO_2 has shown approximately 0.1% failure after 6 at.% burnup. A thinner coating (79 μ) on the 460-μ, 65% dense UO_2 has not failed after 4 at.% burnup at 815°C.

Irradiation studies of coated-particle fuels for the Dragon reactor have been reviewed in a recent article by Hauser.[59] (C. W. Townley)

Coated-Particle Fuel-Materials Compatibility

Lonsdale and Graves[53b] (General Atomic) have completed diffusion studies (tracer level) of thorium in pyrolytic graphite. Recent investigations have been concerned with establishing the dependence of the diffusion coefficient on the structural characteristics of the pyro-

Table I-7 CONDITIONS AND RESULTS OF EXPOSURE OF PyC-COATED CARBIDE FUEL PARTICLES TO WATER VAPOR[55] AT 1000°C

Coated-particle designation*	Initial composition†		Test conditions		Results				
	Pyrolytic carbon, wt.%	Th/U, wt. ratio	Partial pressure of water vapor, torrs	Exposure time, hr	Weight loss, mg	Reaction rate,‡ mg/(g)(hr)	Composition of leach solution		
							Thorium, mg	Uranium, mg	Th/U, wt. ratio
Laminar I	70.9	0	567	1.0	111.2	156	0	13.4	0
			45	4.5	57.7	18	0	0.134	0
Laminar III	65.2	0	567	1.0	224.7	319	0	53.6	0
			567	2.0	208.2	154	0	58.7	0
			47	1.0	18.9	29	0	§	0
			46	5.7	102.7	28	0	0.34	0
			4.6	28.0	121.2	6.5	0	§	0
Granular IV	53.9	5.10	567	1.0	100.9	186	3.97	0.832	4.76
			45	4.5	13.8	5.6	0.028	0.128	0.22
			4.6	28.0	24.1	1.6	§	§	§
Isotropic V	49.0	5.10	567	1.0	68.9	137	22.56	5.66	3.98
			567	2.0	126.5	126	45.30	9.21	4.93
			45	4.5	18.7	8.3	0.137	0.286	0.478
			4.6	27.5	30.3	2.2	0.10	0.016	6.3
Isotropic VI	65.2	19.0	567	1.0	95.2	145	6.25	0.402	15.5
			45	4.7	13.2	4.0	0.69	0.096	0.72
			4.6	28.0	6.7	0.36	0.036	0.016	2.3
Isotropic VII	73.3	4.95	567	1.0	68.0	91	5.93	0.901	6.57
			46	4.5	9.1	2.7	0.012	0.22	0.056
			4.6	27.5	11.3	0.56	0.064	0.023	2.8
NCC-217	57.9	0	567	1.0	84.2	145	0	0.960	0
			567¶	1.0¶	220.7	188	0	13.2	0
			567	2.0	106.1	91	0	4.56	0
			567	4.0	187.2	79	0	33.3	0

*All batches except NCC-217 were prepared by General Atomic. Coating conditions and properties are given in GA-5606 (Part 1), pp. 13-15.
†Based on chemical analysis performed at Oak Ridge.
‡Based on initial weight of pyrolytic carbon.
§Not determined.
¶A 2-g sample exposed at 1100°C. All other samples weighed approximately 1 g.

carbon. Specimens for the diffusion studies consisted of graphite disks coated, along with UC_2 particles, in a fluidized bed. According to the authors the PyC structures deposited on the two substrates are identical. Three basic PyC structures were investigated: laminar, deposited at 1350 to 1400°C; isotropic, deposited at 2000°C; and granular, deposited at 1900°C. All coatings were deposited from methane, with the use of a helium carrier gas. Coating densities ranged from 1.91 to 2.12 g/cm^3. After a mechanical polishing operation to ensure flat faces ($\pm 3\,\mu$), approximately 0.01 to 0.02 μc of ^{228}Th was deposited onto each disk. Following the diffusion anneal, the samples were allowed to come to equilibrium (to allow for the decay of undesirable daughter products) and then sectioned mechanically. The diffusion anneals were performed at temperatures ranging from 1600 to 2000°C. The results of the experiment may be summarized by the following equations:

$$D_{(\text{granular})} = 7.1 \times 10^4 \exp(-152{,}000/RT)$$

$$D_{(\text{isotropic})} = 15.5 \exp(-114{,}000/RT)$$

$$D_{(\text{laminar})} = 1.2 \times 10^4 \exp(-157{,}000/RT)$$

The thorium diffusion coefficient (in a direction perpendicular to the PyC deposition plane) for the laminar coatings was only 3.5 to 4% of the value for the other pyrocarbons. However, since the laminar coatings were deposited at relatively low temperatures (~1350°C), these were preannealed at 2000°C prior to the diffusion anneal. The granular and the isotropic coatings were deposited at temperatures in excess of the temperatures utilized for the diffusion anneals and hence were not subjected to preannealing treatments. The relative importance of the preannealing treatment and its influence on the measured diffusion coefficient for the laminar samples cannot be assessed since no diffusivity data are shown for laminar coatings having the as-deposited structures.

Workers at Oak Ridge[55] have continued the investigations concerned with the compatibility of PyC-coated (U,Th) carbide particles with water vapor. Recent experiments indicate that the incidence of coating failures for a given time and temperature increases with increasing partial pressures of water vapor. Reaction rates (shown in Table I-7) have been obtained for several coating structures, but the effects of coating density and anisotropy have not, as yet, been assessed. (W. H. Pfeifer)

Uranium Oxide Fuel Materials

Preparation of Uranium Oxide Fuel Bodies

Scott and Harrison[60] at Harwell are preparing single-phase single crystals of UO_2 in the oxygen-to-uranium ratio range of 2.00 to 2.25 by a seven-day anneal of crushed fused particles at 800°C in a matrix of UO_2 having an oxygen-to-uranium ratio of 2.44.

Canadian investigators[61] have fabricated sintered UO_2 pellets with a controlled boron content. High-density stoichiometric UO_2 pellets, containing 0, 40, 80, and 120 ppm boron, were prepared using a cold-press-and-sinter technique. In an attempt to minimize the boron loss during sintering, hyperstoichiometric UO_2 was utilized which could be densified under argon at 1325°C. All specimens were cooled under flowing dry hydrogen to ensure a final stoichiometric oxygen content.

Boron additions were made with elemental B, B_4C, B_2O_3, ZrB_2, BN, and $Na_2B_4O_7 \cdot 10H_2O$ (borax). The best boron retention was noted when B_2O_3 and ZrB_2 were used. Pellets containing B_2O_3 exhibited 87 ± 5% retention when sintered under the above conditions.

When correction for the anticipated boron loss was made, stoichiometric UO_2 pellets, having a density of 93% of theoretical, were prepared with a controlled boron content. The standard deviation of the boron content from pellet to pellet was ±0.6%.

Yugoslavian workers[62] have achieved densities of 97% of theoretical with UO_2 powders prepared by direct reduction of ADU after sintering for 2 hr at 1350°C in moist nitrogen. Because of the well-developed surface area, initial neck growth occurred at 900°C and extensive grain growth took place at 1350°C.

(T. R. Wright)

Properties and Behavior of Uranium Oxide Fuels

A British report[63] presents data on fission-product release from UO_2 during in-pile irradiation. The release of ^{85m}Kr, ^{87}Kr, ^{88}Kr,

Table I-8 FISSION-PRODUCT DIFFUSION FROM UO_2 DURING IRRADIATION[63]

Isotope	Specimen	Diffusion coefficient, cm^2/sec, at indicated temperature, °C				
		800	1000	1200	1400	1600
^{87}Kr	1*	1.6×10^{-18}	8.0×10^{-18}	1.7×10^{-16}	4.4×10^{-15}	
	2†	3.2×10^{-18}	3.6×10^{-19}	1.5×10^{-17}	5.5×10^{-16}	1.1×10^{-14}
^{88}Kr	1	9.7×10^{-20}	4.2×10^{-18}	9.1×10^{-17}	1.7×10^{-15}	
	2	1.4×10^{-19}	3.9×10^{-19}	7.7×10^{-18}	1.0×10^{-16}	1.2×10^{-15}
^{85m}Kr	1	1.4×10^{-19}	6.8×10^{-18}	1.3×10^{-16}	3.5×10^{-15}	
	2	2.2×10^{-19}	8.7×10^{-19}	1.4×10^{-17}	3.4×10^{-16}	4.8×10^{-14}
^{136}Xe	1	4.0×10^{-20}	8.0×10^{-19}	5.4×10^{-18}	3.9×10^{-16}	
	2	6.0×10^{-20}	6.0×10^{-19}		4.2×10^{-18}	
^{133}Xe	1	5.7×10^{-20}	1.3×10^{-18}	8.0×10^{-18}	5.7×10^{-17}	
	2	1.8×10^{-19}	2.0×10^{-19}	1.3×10^{-18}	3.8×10^{-17}	
^{135}I	1				$\sim 2.6 \times 10^{-15}$	
	2		3.9×10^{-19}		2.0×10^{-16}	
^{133}I	1				$\sim 1.5 \times 10^{-15}$	
	2		1.2×10^{-19}	5.9×10^{-18}	1.1×10^{-16}	

*Density, 7.90 g/cm^3.
†Density, 10.48 g/cm^3.

^{133}Xe, ^{135}Xe, ^{133}I, and ^{135}I from two UO_2 samples with densities of 7.90 and 10.48 g/cm^3 was determined at 200°C intervals from 800 to 1400°C and 1600°C, respectively. The results of these determinations are presented in Table I-8 in terms of diffusion coefficients. It was found that fission-product release could be separated into temperature-independent and temperature-dependent components, and the diffusion coefficients presented in the table were calculated from the latter. In general, the diffusion coefficients for the denser specimen were found to be about an order of magnitude lower than those of the less dense specimen. This is thought to

Table I-9 COMPATIBILITY OF UO_2 WITH VARIOUS MATERIALS[64]
(Melting Point of UO_2 Is ~ 2760°C)

Material	Symbol	Melting point, °C	Remarks
Alumina	Al_2O_3	2050	Compatible to 1800°C
Aluminum	Al	659.7	Incompatible at 500°C (in vacuum)
Beryllia	BeO	2450	Compatible to 1800°C
Magnesia	MgO	2800	Compatible to 1600°C (sintered bodies)
Molybdenum	Mo	2620	Compatible to 2600°C
Silicon carbide	SiC	Decomposes at 2210	Incompatible at 1925°C
Stainless steel		1420	Compatible for 1000 hr at 800°C and for 24 hr at 1500°C; no interaction > 0.01 in. at 600 to 1000°C for 6 months (stoichiometric UO_2)
Stainless steel, 13% Cr			Compatible to at least 800°C
Stainless steel, 16/12/2½ Mo			Compatible to at least 800°C
Stainless steel, 20/20/1 Nb			Compatible to at least 800°C
Tantalum	Ta	2980	Compatible to 2760°C
Tungsten	W	3380	Compatible to 2760°C
Zirconium	Zr	~ 1855	Very slow reaction at 400 to 650°C; incompatible at 700°C; compatible after 28 days at 600°C (in vacuum)

indicate either that the equivalent sphere model used to calculate the diffusion coefficients requires some refinements or that there are errors in the surface areas used in determining the equivalent-sphere parameters. The in-pile diffusion coefficients for xenon were lower than those observed in postirradiation heating experiments.

Another British report[64] on the compatibility of materials for CO_2-cooled reactors contains a summary of UO_2 compatibility data. These data are presented in Table I-9.

Jones and Murchison[65] have research in progress that looks promising for correlating optical properties of uranium oxides with the oxygen-to-uranium ratio in the composition range $UO_{2.00}$ to $UO_{2.25}$. Reflectivity measurements toward both extremes of the visible spectrum indicate possibilities for differentiating between oxygen contents with sensitivities of ± 0.01 on the oxygen-to-uranium ratios for both sintered compacts and powders.

Recent studies at Chalk River[66] show a correlation between grain growth and fission-gas release in experimental UO_2 irradiations. On the basis of these studies, it has been proposed that grain boundaries may hinder fission-gas release from UO_2. It appears that the fission gases migrate from the matrix of the grain to the grain boundary where bubbles are formed, and release of gas from the fuel occurs mainly by processes such as void migration or cracking of the boundary. In this same study the thermal conductivity of UO_2 was found to vary with the fractional porosity P according to the equation

$$k_p = k\,(1 - 2.6P)$$

where k is the thermal conductivity of 100% dense UO_2 and k_p is the thermal conductivity of the porous material. (R. H. Barnes)

Uranium and Thorium Carbides, Nitrides, and Sulfides

Fabrication

Studies at Harwell[67] indicate that hyperstoichiometric UC powder (up to 5.6 wt.% carbon) can be converted to single-phase UC and sintered to a high density in a single heating cycle at a sintering temperature of 1500°C if sintering is done in a hydrogen atmosphere.

Argonne[68] has converted uranium shot and turnings to UN by nitriding them for several hours at 900 to 1050°C and then raising the temperature to 1300 to 1350°C to complete the conversion. The nitride coating on the uranium contained the molten uranium phase at the higher temperature. The 1300 to 1350°C temperature was held for 20 min, and then the system was evacuated to 5×10^{-5} torr within 15 min. There was no evidence of nitrogen evolution from the reaction product. X-ray analysis indicated that the major phase was UN. Minor phases of U_2N_3 and UO_2 were detected. The UO_2 content was reported as 0.095 wt.%; the N_2 content, as 5.60 wt.%.

Investigators at Harwell[67] have stated that UN will sinter to greater than 95% of theoretical density at temperatures in the range of 1600 to 1700°C under argon without free uranium metal being formed. The particle size after ball milling of the sinterable UN was estimated to be between 0.1 and 0.3 μ by electron-beam microscopy and 0.2 μ by surface-area measurements. The sinterability of these powders was not significantly changed by oxygen and water contaminants picked up from the covering gas after storage in impure argon. Contamination of the powders, initially rapid, appeared to stop after reaching levels of 0.7 wt.% oxygen or 0.3 wt.% H_2O.

Oak Ridge researchers prepared dense ThO_2 spheroids by a sol-gel process and converted these to dense ThC_2 spheres by heating the oxide spheres in the presence of carbon and removing the reaction-product gases. A serious problem encountered by the Oak Ridge researchers was the agglomeration of the ThC_2 microspheres during the conversion reaction. This was prevented in a rotating graphite crucible which stirred the charge 44 times/min. A charge of 300- to 400-μ ThO_2 spheres, with a carbon-to-thoria weight ratio of 1, was completely converted to ThC_2 after 5 hr at 2150°C. Metallography showed that the converted spheres retained their shape and high density. X-ray analysis[54] revealed the presence of only ThC_2. (D. S. Acuncius and E. O. Speidel)

Properties and Behavior

Wallace, Krikorian, and Stone found[69] that UC_2 and GdC_2 form a complete series of cubic solid

solutions at high temperatures. This cubic solid solution decomposes to a complete series of tetragonal solid solutions at temperatures varying from 1785°C for UC_2 to 1155°C for 66 mole % GdC_2 to 1275°C for GdC_2. A eutectic trough exists between these solid solutions and graphite.

Stecher et al.[70] investigated the Ce–U–C and Ce–Th–C systems at 1600°C. At this temperature the solid solutions based on UC and ThC extend to approximately 30 mole % "CeC." These face-centered cubic solid solutions tend to dominate the ternary sections, and ties radiate from them to all other phases in the systems except graphite.

Workers at Harwell noted[67] that the liquidus curve between UC_2 and ThC_2 contains a minimum at 2350°C and 50 mole %. Creep tests performed by Wembley disclosed 1% deformation in 200 hr at 900°C and 6000-psi stress in specimens of uranium plus 49.7 at.% carbon. A deformation of less than 0.04% occurred in 190 hr at 1100°C and 6000-psi stress in specimens of uranium plus 50.8 at.% carbon. A specimen of UC–2 mole % NbC showed 1.2% deformation in 120 hr at 1400°C and 6000-psi stress.

The rate of diffusion of carbon in a chemical concentration gradient in UC has been determined[71] from layer-growth measurements by Chubb, Getz, and Townley. Over the temperature range from 1200 to 2100°C, the rate of growth of UC layers was found to obey the relation x^2/t (cm^2/sec) = 2.8 exp (−66,000/RT). By the use of Wagner's method to estimate the rate of chemical diffusion necessary to support this rate of layer growth, it was found that the chemical diffusion rate obeyed the relation D_{UC} (cm^2/sec) = 0.0002 exp (−22,000/RT).

Atomics International[72] has obtained hot-hardness data on hypostoichiometric UC (4.0 to 4.75 wt.% carbon), which suggest that rapid softening of alloys in this composition range occurs between 500 and 700°C. Such softening has been attributed to the small amount of uranium metal present in these alloys. The average hardness of the alloys tested was 440 DPH at 500°C and 150 DPH at 700°C.

Schmeling[73] has studied gas release from lightly irradiated UC at temperatures ranging from 900 to 2100°C. Diffusion coefficients calculated on the basis of his measurements showed a temperature dependency and gave a mean activation energy of 67 kcal/mole. The highest D value obtained was less than 10^{-10} at 2100°C, which is several orders of magnitude lower than the lowest value reported by Chubb, Getz, and Townley,[71] for any mode of diffusion in UC. Although the diffusion coefficients obtained in the two studies are certainly not directly comparable, the great difference between them suggests that bulk diffusion does not result directly in gas release from UC. Schmeling notes that his diffusion coefficient results are scattered over a range of three orders of magnitude at any given temperature and suggests that this nonreproducibility is related to the nature of UC. It would seem likely that Schmeling meant that the nonreproducibility was inherent in the nature of an as-yet unresolved mechanism of gas release from UC. Mechanisms, such as that suggested by Bauer et al.,[74] involving holdup of gases in bubbles seem to be gaining in popularity.

A tentative phase diagram for the U–US portion of the U–S system has been developed at Argonne[68] and is shown in Fig. I-5. (W. Chubb)

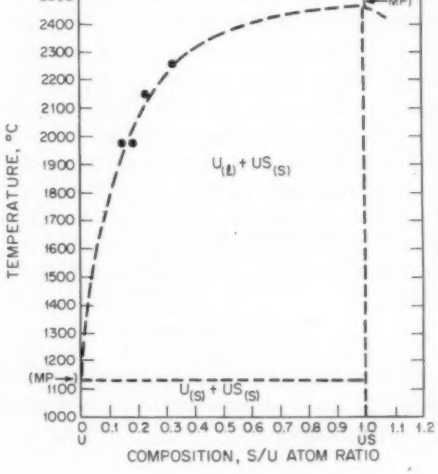

Fig. I-5 Tentative phase diagram for the U–US system.[68]

Basic Studies of Irradiation Effects in Fuel Materials

Metals

At Harwell[75] it has been found that ejection of uranium by fission fragments from a thick

uranium emitter did not stop at the neutron dose at which a single collector holds the maximum deposit. Reejection by fission fragments originating in the collected material occurred at 1/1000 the rate of ejection from the emitter. An early state of dynamic equilibrium between ejection and reejection was found to be caused by bombardment of the collector by fission products escaping from the surface of the uranium emitter. An average fission product originating in the collected material was found to reeject about 10,000 atoms, whereas one originating in the emitter reejected only about 1000 atoms. In other words, fission fragments originating in the collected material were ten times as efficient in causing transfer as those originating in the emitter.

Studies conducted in Russia[76] show that the kinetics of the annealing of the increased electrical resistivity of irradiated uranium cannot be accounted for as a result of the recombination of isolated imperfections only. The results of measurements of the electrical resistance of uranium under irradiation correlate more with the hypothesis that the increase in the electrical resistance is caused by the appearance of loop dislocations which, according to Buckley's theory, are responsible for the irradiation growth of uranium.

A discussion[77] of this Russian research by British authors of earlier work indicates that they are now in agreement that isolated defects cannot give rise to a significant part of the radiation-induced resistivity, as they had assumed earlier.

In Germany[78] liquid-helium-temperature irradiation of pure uranium has been conducted. The initial resistivity increases were measured for various textures of the metal. It was shown that there exists in uranium a very mobile defect that anneals out between 4 and 20°K.

At Harwell[79] the resistivity effect of radioactive self-damage on plutonium was studied in experiments at liquid-helium temperature lasting over 8000 hr and was found to exist in the alpha, beta, and delta phases of the metal. In all cases the resistivity approaches saturation, the rates of increase depending on the crystal structure and isotopic content of the sample. In spite of wide differences in these rates, the functional increase is roughly the same. The temperature dependence of the accumulated resistivities in all three modifications deviates very strongly from a simple additive resistance obeying Matthiesen's rule. The resistivity of fully damaged alpha plutonium is almost temperature independent, becoming smaller than that of the undamaged specimen above about 50°K. Neptunium and ^{233}U also showed resistivity increases with time at helium temperatures, but the effect was too small to decide whether Matthiesen's rule is obeyed in these metals. The observed effects were discussed under the assumption that in plutonium, scattering of electrons at low temperatures is due mainly to a cooperative phenomenon.

Isochronal annealing experiments performed at Oxford University[80] show that the resistivity increases due to radioactive self-damage in alpha plutonium recover in two distinct stages, centered at about 75 and 150°K. In delta-stabilized plutonium the first annealing stage is more pronounced and occurs at lower temperatures, the values of which are dependent on the concentration of aluminum used to stabilize the delta phase. Isochronal annealing experiments were also performed on heavily damaged samples of alpha plutonium and yield further information on the anomalous temperature dependence of the resistivity changes brought about by self-irradiation at low temperatures. The correlation between the observed resistivity changes and changes in the concentration of point defects is discussed.

At Battelle–Northwest[48] the density measurements made on uranium specimens removed from a swelling capsule irradiated at 575°C and 1000-psi external pressure to 0.15 at.% burnup reveal that this pressure reduced the amount of swelling in high-purity uranium by factors of 5 to 15 over that typically observed in uranium irradiated at low pressure. Alloy specimens, U + Fe–Al and U + Fe–Si, exhibited reductions by factors of 2 to 5. The effectiveness of this 1000-psi external, hydrostatic pressure is significantly less at 575°C than was the case for 450°C. At 450°C the reduction for high-purity uranium was by factors of 50 to 100. The 1000-psi pressure is effective in suppressing the crystallographically aligned microtearing typical of low-pressure behavior under irradiation at 575°C, but it does not inhibit the grain-boundary porosity and tearing. This behavior substantiates the concept that defect migration and agglomeration processes are responsible for swelling in the neighborhood of 575°C.

The French[81] studied the behavior of helium in aluminum, with the use of transmission-electron microscopy to determine the swelling mechanisms. The helium was introduced into the aluminum by irradiation of Al–^{6}Li alloys containing small amounts of lithium. The influence of various factors on the nucleation and the swelling of the bubbles was studied, including helium concentration, temperature, and number and distribution of crystal defects in the metal. It was found that the precipitation of rare-gas bubbles could, in certain cases, prevent the recrystallization of the metal as a result of a mechanism depending on the anchoring of the dislocations and grain boundaries by the bubbles.

Ceramics

At Mol, Belgium,[82] studies show that fission fragments in bulk UO_2 single crystals do not create permanent long-range strain fields (not even at low temperatures) that could be detected in the electron microscope, but that they produce only unresolvable point defects. After irradiation with about 10^{17} neutrons/cm^2 (thermal) at 300°C, these defects have coalesced into clusters with diameters of about 25 A and more, which are resolved in the electron microscope. Fission-fragment tracks in UO_2 are not very stable since heating a UO_2 crystal 1 hr at 200°C after irradiation at 20°C is sufficient to anneal out all visible tracks. Only nominally stoichiometric crystals have been examined to any extent after annealing or high-temperature irradiation. The only remaining damage is in the form of loops. Occasionally linear arrangements of small loops are left behind in material irradiated at 20°C and annealed at 200°C. The small loops are more or less polygonal, whereas loops with diameters of 1500 A and more become rounded and seem to be ellipses or nearly circles. Assuming the big rounded loops to be inclined circles, the loop plane was found to be (1 1 0).

At Hahn-Meitner Institut[83] investigations were carried out on the kinetics of the rare-gas release from UO_2 and UC monocrystals during total evaporation in an attempt to determine the influence of evaporation on diffusion measurements. Further research is planned in this area. The results for argon diffusion in KF, KCl, and KBr monocrystals were summarized as follows: KF: $D = 7.7 \times 10^1 \exp(-40{,}4000/RT)$ at 400 to 800°C; KCl: $D = 2.3 \times 10^{-2} \exp(-14{,}100/RT)$ at 400 to 700°C; and $D = 5.5 \times 10^{11} \exp(-55{,}300/RT)$ at 200 to 400°C; KBr: $D = 1.8 \times 10^{-8} \exp(-8200/RT)$ at 500 to 700°C and $D = 1.5 \times 10^6 \exp(-35{,}700/RT)$ at 330 to 550°C.

In Great Britain krypton ions were injected into thin slices cut from synthetic single crystals of UO_2 by use of a heavy-ion accelerator.[84] Krypton bubbles could be formed by pulse-heating the sample in the electron beam of the electron microscope to temperatures where evaporation of UO_2 was rapid. When the samples were annealed, bubble diffusion could be observed. Mechanisms of bubble diffusion are discussed.

At Oak Ridge[85] the possibilities that dislocation movement might play a part in fission-gas release were determined by studying the effects of stress on fission-gas release. Compacts of UO_2 and ThO_2–UO_2 were irradiated at about 100°C to a burnup of about 1.85×10^{15} fissions/cm^3. After a seven-day decay period, these specimens were placed in an apparatus that permitted application of a compressive stress at an elevated temperature. A stream of helium carried fission gas to a liquid-nitrogen trap, where radiation from ^{133}Xe was counted. Specimens were annealed for varying lengths of time; then they were stressed, and the change in fission-gas release was noted. The application of stress caused a fission-gas-release burst and a subsequent increased release rate. The initial release burst was substantially larger than subsequent bursts obtained on reapplication of stress, which were sometimes not detectable.

Oak Ridge studies[86] of continuous in-pile release of fission gas from UO_2 have led to the conclusion that the temperature-dependent release of fission gas is controlled by a trapping process. The defect-trap model assumes that the rate-controlling process for fission-gas release in the temperature-dependent region is the probability of being trapped and the probability of being released from traps. The traps are of three kinds: (1) intrinsic traps that are voids, grain boundaries, or other flaws in the material; (2) point defects that are formed in the wake of a fission fragment; and (3) clustered point defects. The point defects are mobile, are created and destroyed by fission, and are annealed by heat; they reach an equilibrium number at a given temperature and fission rate.

The intrinsic traps are not mobile at the temperatures considered here and act as permanent traps for any gas that diffuses into them.

(F. A. Rough)

References

1. C. L. Angerman and G. R. Caskey, Jr., Swelling of Uranium by Mechanical Cavitation, *J. Nucl. Mater.*, 13: 182-196 (1964).
2. E. C. Sykes and G. W. Greenwood, Tensile Creep Ductility of Neutron-Irradiated Alpha-Uranium, *Nature*, 206(4980): 181-182 (Apr. 10, 1965).
3. J. H. Buddery et al., The Development and Properties of an Oxidation-Resistant Coating for Uranium, *J. Nucl. Mater.*, 13: 169-181 (1964).
4. O. Flint, Protection of Uranium by Flame-Sprayed Metallic Deposits, *Corrosion Sci.*, 5: 19-28 (January 1965).
5. K. R. Riggs and N. F. Neumann, Effect of Alloy Additions on the Quench-Induced Texture of Alpha-Uranium, USAEC Report MCW-1491, Mallinckrodt Chemical Works, April 1965.
6. A. G. Crocker, Stacking Faults in Alpha Uranium, *J. Nucl. Mater.*, 15: 121-124 (1965).
7. G. Clottes, J. C. Jousset, and J. Leteurtre, Polygonization of Very Pure Uranium Between 150 and 300 C (in French), *J. Nucl. Mater.*, 12: 340-344 (1964).
8. J. Morin and F. Jean-Louis, Influence of Temperatures of Intermediate and Final Annealings on the Ductile-Brittle Transition Zone of α Uranium, *Compt. Rend.*, 260: 541-544 (Jan. 11, 1965).
9. J. S. L. Leach and A. Y. Nehru, The Temperature Dependence of the Corrosion of Uranium in Aqueous Solutions, *J. Nucl. Mater.*, 13: 270-274 (1964).
10. N. P. Galkin, B. N. Sudarikov, U. D. Veryatin, Yu. D. Shishkov, and A. A. Mayorov, *Uranium Technology* (in Russian), Atomizdat, 1964.
11. M. M. Haberlin and J. H. Gittus, Continuous-Cooling Transformation Characteristics of Uranium-Iron-Aluminum Alloys, British Report TRG-Report-590, Nov. 10, 1964.
12. T. K. Bierlein, B. Mastel, and C. L. Corey, Electron Microscope Studies of Second-Phase Particles in Dilute Alloys of Uranium, USAEC Report BNWL-43, Battelle–Northwest, Pacific Northwest Laboratory, March 1965.
13. K. N. Woods, Y. E. Smith, and R. D. Leggett, Precipitate Particles in Dilutely Alloyed Uranium Quantitative Metallography, USAEC Report BNWL-30, Battelle–Northwest, Pacific Northwest Laboratory, January 1965.
14. A. R. Kaufman and W. C. Muller, Fundamental and Applied Research and Development in Metallurgy. Development of Uranium-Base Alloys Strengthened by SLIS Techniques. Summary Technical Report to the United States Atomic Energy Commission for the Period July 1, 1963 to June 30, 1964, USAEC Report NMI-1262, Nuclear Metals Division of Textron Inc., December 1964.
15. K. Tangri and D. K. Chaudhuri, Metastable Phases in Uranium Alloys with High Solute Solubility in BCC Gamma Phase, Part I–The System U-Nb, *J. Nucl. Mater.*, 15(4): 278-287 (1965).
16. K. Tangri, D. K. Chaudhuri, and C. N. Rao, Metastable Phases in Uranium Alloys with High Solute Solubility in the BCC Gamma Phase, Part II–The System U-Ru, *J. Nucl. Mater.*, 15(4): 288-297 (1965).
17. P. L. Ryder and J. Nutting, The Precipitation of Intermetallic Compounds in Adjusted Uranium, *J. Inst. Metals*, 93: 178-181 (February 1965).
18. C. Amato, F. S. Saraceno, and T. B. Wilson, Phase Transformations and Equilibrium Structures in Uranium-Rich Niobium Alloys, *J. Nucl. Mater.*, 12: 291-304 (1964).
19. G. Petzow and O. A. Sampaio, The Phase Equilibria in Uranium-Cobalt-Iron Alloys in the Partial System U-UCo_2-UFe_2, *Z. Metallk.*, 56: 14-20 (1965).
20. C. A. W. Peterson and R. R. Vandervoort, Stress-Cracking in the Uranium-10 Wt.% Molybdenum Alloy, USAEC Report UCRL-7767, University of California, Lawrence Radiation Laboratory, Mar. 13, 1964.
21. C. A. W. Peterson, A Stress-Cracking Study of a Gamma-Extruded U-8 Wt.% Mo-0.50 Wt.% Ti Alloy, USAEC Report UCRL-14132, University of California, Lawrence Radiation Laboratory, Apr. 15, 1965.
22. K. G. Hoge, Some Mechanical Properties of Uranium-10 Wt.% Molybdenum Alloy Under Dynamic Tension Loads, USAEC Report UCRL-12357 (Rev. I), University of California, Lawrence Radiation Laboratory, Feb. 25, 1965.
23. G. L. Eggert, Report on the Corrosion of Irradiated U-10Mo Alloy in CO_2 and N_2 at Elevated Temperature, USAEC Report SC-RR-65-28, Sandia Laboratory, February 1965.
24. Los Alamos Scientific Laboratory, Quarterly Status Report on Advanced Reactor Technology (ART) for Period Ending April 30, 1965, USAEC Report LA-3316, May 1965.
25. Los Alamos Scientific Laboratory, Quarterly Status Report on Advanced Reactor Technology (ART) for Period Ending January 31, 1965, USAEC Report LA-3244, February 1965.
26. D. F. Bowersox and J. A. Leary, The Solubilities of Selected Elements in Liquid Plutonium. III. Tungsten, USAEC Report LA-3252, Los Alamos Scientific Laboratory, December 1964.
27. J. E. Fuller, Delta Stabilized Ternary Alloys of Plutonium, USAEC Report RFP-506, Rocky Flats Division of The Dow Chemical Co., Apr. 22, 1965.
28. W. N. Beck, J. H. Kittel, and R. J. Fousek, Irradiations of U-20Pu-10Fs Alloy Fuel Rods, USAEC Report ANL-6750, Argonne National Laboratory, February 1965.
29. Argonne National Laboratory, Reactor Development Program Progress Report, March 1965, USAEC Report ANL-7028, Apr. 20, 1965.
30. H. R. Gardner, The Fatigue Behavior of Pu-1.0 Wt.% Ga Delta Stabilized Plutonium, USAEC Report BNWL-16, Battelle–Northwest, Pacific Northwest Laboratory, Jan. 22, 1965.
31. H. R. Gardner, Physical and Mechanical Metallurgy Studies on Delta-Stabilized Plutonium-Gallium Alloys, USAEC Report BNWL-13, Battelle–Northwest, Pacific Northwest Laboratory, April 1965.
32. R. M. Mayfield and W. G. Tope, Method of Making Plutonium Monocarbide, U. S. Patent No. 3, 170, 759 (to USAEC), Feb. 23, 1965.
33. Argonne National Laboratory, Reactor Develop-

ment Program Progress Report, May 1965, USAEC Report ANL-7046.
34. J. T. Dalton and R. M. Griffin, Initial Investigation of the Thorium-Plutonium-Carbon System, British Report AERE-R-4742, September 1964.
35. B. Riley, Preparation and Some Properties of a Thorium-Plutonium Dicarbide Composition, British Report AERE-M-1478, October 1964.
36. Hanford Atomic Products Operation, Ceramics Research and Development Operation Quarterly Report, October to December 1964, USAEC Report HW-81603.
37. F. W. Albaugh, Reactor and Materials Technology Monthly Report, February 1965, USAEC Report BNWL-C-82 A, Battelle–Northwest, Pacific Northwest Laboratory, Mar. 15, 1965. (Classified; material cited is unclassified.)
38. A. Strasser, D. Stahl, J. Anderson, and K. Taylor, Study of Uranium-Plutonium Monoxides, Progress Report, November 1, 1964 to March 31, 1965, USAEC Report UNC-5117 (EURAEC-1367), United Nuclear Corp., Apr. 15, 1965.
39. H. R. Longfield (Comp.), Atomic Energy of Canada Ltd., October 1964.
40. O. J. C. Runnalls and R. R. Boncher, Polymorphic Transformations in $PuAl_3$, *J. Nucl. Mater.*, 15: 57-64 (1965).
41. J. R. Thomson, Melting and Structural Correlation of Some Thorium Rich Eutectics, *J. Nucl. Mater.*, 15: 88-94 (1965).
42. J. A. Burka and J. P. Hammond, Evaluation of Thorium-Base Alloys for High-Temperature Strength, USAEC Report ORNL-3777, Oak Ridge National Laboratory, April 1965.
43. J. Y. N. Wang, Corrosion of Experimental Thorium-Base Alloys, USAEC Report ANL-7006, Argonne National Laboratory, February 1965.
44. H. R. Roellig, Method of Producing Dispersions of Fissionable Material for Nuclear Fuel Elements, German Patent No. 1,182,363, Nov. 26, 1964.
45. R. F. Stoops and M. W. Haller, A Nuclear Fuel Consisting of Very Small Uniformily Dispersed UC Particles in a Uranium Matrix, Quarterly Report, USAEC Report NCSC-2981-8 (EURAEC-1155), North Carolina State College, June 1964.
46. R. F. Stoops and M. W. Haller, A Nuclear Fuel Consisting of Very Small, Uniformily Dispersed UC Particles in a Uranium Matrix, Final Report, USAEC Report NCSC-2981-9, North Carolina State College, October 1964.
47. J. P. Evans, The Fabrication of $(UPu)O_2$-Stainless Steel Cermets for Irradiation, British Report AERE-M-1314, February 1965.
48. F. W. Albaugh, Reactor & Materials Technology Monthly Report, April 1965, USAEC Report BNWL-C-84 A, Battelle–Northwest, Pacific Northwest Laboratory, May 14, 1965. (Classified; material cited is unclassified.)
49. F. W. Albaugh, Reactor & Materials Technology Monthly Report, March 1965, USAEC Report BNWL-C-83 A, Battelle–Northwest, Pacific Northwest Laboratory, Apr. 15, 1965. (Classified; material cited is unclassified)
50. J. C. Bokros, Absorption Factors for a Modified Bacon Preferred-Orientation Technique, to be published in *Carbon*.
51. J. C. Bokros, Variations in the Crystallinity of Carbons Deposited in Fluidized Beds, to be published in *Carbon*.
52. W. J. Wilson, M. F. Browning, V. M. Secrest, and J. M. Blocher, Jr., Preparation and Irradiation of Beryllia-Coated Fuel Particles, USAEC Report BMI-1718, Battelle Memorial Institute, Mar. 16, 1965.
53. TARGET, a Program for a 1000-Mw(e) High-Temperature Gas-Cooled Reactor, Quarterly Progress Report for the Period Ending February 28, 1965, USAEC Report GA-6113, Mar. 31, 1965.
    a. TARGET, a Program for a 1000-Mw(e) High-Temperature Gas-Cooled Reactor, Quarterly Progress Report for the Period Ending May 31, 1965, USAEC Report GA-6418, June 30, 1965.
    b. Advanced, Graphite-Matrix, Dispersion-Type Fuel Systems and Research on Graphite, Annual Report, April 1, 1964 to March 31, 1965, USAEC Report GA-6233, July 20, 1965.
54. D. B. Trauger and G. D. Whitman, Gas-Cooled Reactor Program Semiannual Progress Report for Period Ending March 31, 1965, USAEC Report ORNL-3807, Oak Ridge National Laboratory, June 1965.
55. W. O. Harms and J. H. Coobs, Coated-Particle Fuels Development at Oak Ridge National Laboratory for Period November 15, 1964 to May 15, 1965, USAEC Report ORNL-TM-1116, Oak Ridge National Laboratory, May 1965.
56. R. W. Dayton and S. J. Paprocki, Progress Relating to Civilian Applications During March 1965, USAEC Report BMI-1721, Battelle Memorial Institute, Apr. 1, 1965. (Classified)
57. R. W. Dayton and S. J. Paprocki, Progress Relating to Civilian Applications During April 1965, USAEC Report BMI-1723, Battelle Memorial Institute, May 1, 1965. (Classified)
58. R. W. Dayton and S. J. Paprocki, Progress Relating to Civilian Applications During May 1965, USAEC Report BMI-1727, Battelle Memorial Institute, June 1, 1965. (Classified)
59. G. Hauser, Irradiation Studies on Fuels for the Dragon Reactor, *Energie Nucl.*, 7(2): 100-112 (March–April 1965).
60. K. T. Scott and K. T. Harrison, The Preparation of Single-Phase Single Crystals of Uranium Dioxide in the O/U Range 2 to 2.25, *J. Nucl. Mater.*, 15: 310-311 (1965).
61. E. Mizzan and R. Stack, Fabrication of Sintered UO_2 Pellets with Controlled Boron Content, Canadian Report FD-127, July 1964.
62. D. Kolar and V. Marinkoric, Sintering of Uranium Dioxide at 900–1350°C, *Rudarsko-Met. Zbornik*, 1: 57-62 (1963).
63. G. Jackson, D. Davies, and P. Biddle, Fission Gas Emission from UO_2 During Irradiation at 800–1600°C, British Report AERE-R-4714, December 1964.
64. B. J. Seddon, Summarized Compatibility Review of Reactor Materials for CO_2-Cooled Graphite-Moderated Reactors, British Report TRG-Report-842, Sept. 23, 1964.
65. J. M. Jones and D. G. Murchison, Optical Properties of Uranium Oxides, *Nature*, 205: 663-665 (February 1965).
66. M. J. F. Notley and J. R. MacEwan, The Effect of UO_2 Density on Fission Product Gas Release and Sheath Expansion, Canadian Report AECL-2230, March 1965.
67. L. E. J. Roberts and J. Williams, Atomic Energy

Research Establishment, Harwell, unpublished, March 1965.
68. Argonne National Laboratory, Chemical Engineering Division Research Highlights, May 1964–April 1965, USAEC Report ANL-7020.
69. T. C. Wallace, N. H. Krikorian, and P. L. Stone, The High Carbon Portion of the Uranium-Gadolinium-Carbon System, *J. Electrochem. Soc.*, 111: 1404-1408 (December 1964).
70. P. Stecher, A. Neckel, F. Benesovsky, and H. Nowotny, Ternary Systems of Cerium and Carbon with Thorium, Uranium, Zirconium, and Molybdenum, *Planseeber. Pulvermet.*, 12: 181-195 (December 1964).
71. W. Chubb, R. W. Getz, and C. W. Townley, Diffusion in Uranium Monocarbide, *J. Nucl. Mater.*, 13: 63-74 (1964).
72. Atomics International, AEC Unclassified Programs, Quarterly Technical Progress Report, October–December 1964, USAEC Report NAA-SR-10850, Feb. 15, 1965.
73. P. Schmeling, Release of Xenon from Polycrystalline Uranium Monocarbide (Rare-Gas Diffusion in Solids 17), Euratom Report EUR-1752.e, Hahn-Meitner-Institut für Kernforschung, 1964.
74. A. A. Bauer, D. L. Morrison, F. R. Winslow, J. Bugl, and T. S. Elleman, Postirradiation Heating Fission-Gas Release from an Iron-20 Wt.% Chromium Alloy, *J. Nucl. Mater.*, 13: 75-86 (1964).
75. M. D. Rogers, Dynamic Equilibrium Between Ejection and Re-ejection of Uranium by Fission Fragments, *J. Nucl. Mater.*, 12: 332-334 (1964).
76. S. T. Konobeevski, Effect of Neutron Irradiation on the Electrical Resistivity of Uranium, *J. Nucl. Mater.*, 13: 107-111 (1964).
77. A. D. Brailsford and K. G. Major, Reply to the Paper by S. T. Konobeevski: Effect of Neutron Irradiation on the Electrical Resistivity of Uranium, *J. Nucl. Mater.*, 13: 112 (1964).
78. G. Burger, K. Isebeck, H. Wenzl, J. C. Jousset, and Y. Quere, Irradiation of Uranium with Neutrons at 4.5 K, *Phil. Mag.*, 11: 621-625 (March 1965).
79. E. King, J. A. Lee, K. Mendelssohn, and D. A. Wigley, Resistivity of Plutonium, Neptunium, and Uranium Due to the Accumulation of Radioactive Self-Damage, *Proc. Roy. Soc. London, Ser. A*, 284: 325-343 (March 1965).
80. D. A. Wigley, Effect of Annealing on the Resistivity of Self Damaged Plutonium, *Proc. Roy. Soc. London, Ser. A*, 284: 344-353 (March 1965).
81. V. Levy, J. Antolin, J. Espinasse, and Y. Adda, Contribution to the Study of Helium Precipitation in an Aluminum-Lithium Alloy, French Report CEA-R-2529, July 1964.
82. H. Blank and S. Amelinckx, Electron Microscope Studies of Precipitates and Fission Damage in Vapor Grown UO_2 Crystals, *Z. Metallk.*, 55: 460-466 (1964).
83. Hahn-Meitner Institut für Kernforschung, Rare-Gas Diffusion in Solids, Quarterly Report No. 17, July–September 1964, USAEC–Euratom Report EURAEC-1245, October 1964.
84. G. K. Williamson and R. M. Cornell, The Behavior of Fission Product Gases in Uranium Dioxide, *J. Nucl. Mater.*, 13: 278-280 (1964).
85. C. S. Morgan, R. B. Fitts, and J. L. Scott, Influence of Stress on Fission-Gas Release, *J. Am. Ceram. Soc.*, 48: 166-167 (March 1965).
86. Oak Ridge National Laboratory, Reactor Chemistry Division Annual Progress Report for Period Ending January 31, 1965, USAEC Report ORNL-3789, April 1965.

Section

II

Reactor Materials

Moderator Materials

Graphite

The effects of annealing on the dimensional and thermal-expansion changes induced in pyrolytic graphite by irradiation at 170°C to 7.7×10^{20} neutrons/cm^2 have been examined by the British.[1] The pyrolytic sample was produced by deposition on a substrate at 2200°C and subsequent heat-treatment at 2700 to 2800°C to increase the perfection and orientation. Figures II-1 and II-2 show the effects of postirradiation annealing on the dimensional changes and thermal-expansion coefficients, respectively. The largest part of the dimensional changes in both directions anneals out between 1200 and 1800°C. These results agree with previous electron-microscope observations, which suggest an annealing process in which vacancies and divacancies diffuse to interstitial clusters and remove interstitial atoms from them. The decrease in the c-axis thermal-expansion coefficient on annealing is associated with changes in the c-axis lattice parameter. The a-axis thermal-expansion coefficient recovered in the lower (<1200°C) temperature range, where the majority of annealing is associated with small interstitial clusters rather than with vacancies. Thus it is suggested that the change in the a-axis thermal-expansion coefficient on irradiation is due mainly to a reduction in the Poisson's ratio contraction of the layer planes as the result of c-axis expansion rather than to modification of the vibrational-frequency spectrum.

A delayed increase in the Poisson's ratio of PGA graphite under fast-neutron irradiation was observed by Brocklehurst and Lynam,[2] as shown in Fig. II-3. For parallel-cut samples irradiated at 150°C, a steady increase occurred, starting at an exposure of about 2×10^{20} neutrons/cm^2. The perpendicular-cut specimens, irradiated under compressive stress at 200 to 250°C, began to increase in Poisson's ratio at about 6×10^{20} neutrons/cm^2. These results are explained as follows. Irradiation causes crystallite c-axis expansion and closure of Mrozowski cracks oriented parallel to the basal planes. This changes the load distribution, tightens up the graphite structure, and causes Poisson's ratio to increase as shown, the maximum limit being 0.5. This would also account for the dependence on irradiation temperature since the effect of micropore closure is observed later under exposure at the higher tem-

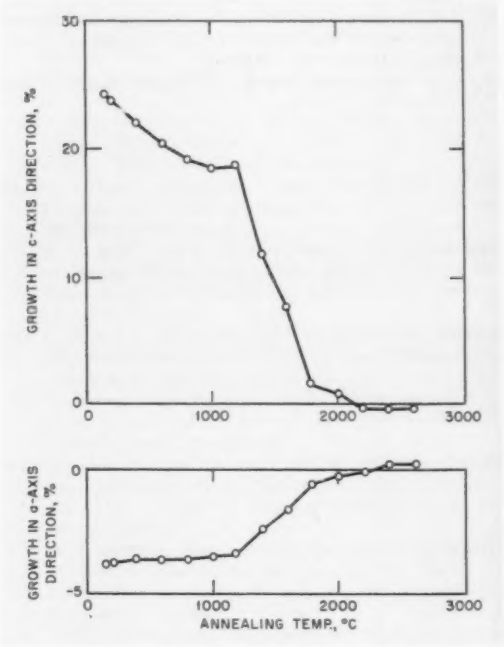

Fig. II-1 Annealing of dimensional changes in pyrolytic graphite[1] irradiated to 7.7×10^{20} neutrons/cm^2 at 170°C.

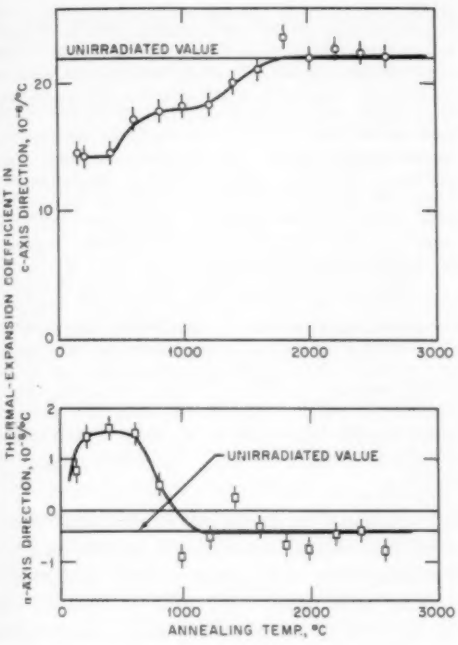

Fig. II-2 Annealing of principal thermal-expansion coefficient in pyrolytic graphite[1] irradiated at 170°C to 7.7 × 10^{20} neutrons/cm^2.

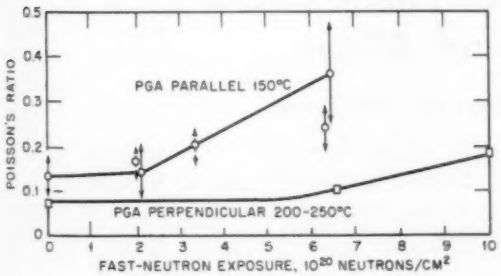

Fig. II-3 Variation of Poisson's ratio of PGA graphite with fast-neutron exposure.[2] Error limits are plus-or-minus standard deviations of a single observation. ↕, measurements of center of specimen. ↕, measurements of one-fourth specimen length.

perature. These results are of practical significance in calculations of the differential stresses in graphite due to differential growth and shrinkage under irradiation.

Fast-neutron-induced dimensional changes in graphites and carbons over the temperature range 150 to 650°C were studied by British investigators.[3] Of special technological interest is the conclusion that the use of different impregnants does not seriously alter the dimensional changes under irradiation of the base graphite (Pile Grade A), even though the irradiation behavior of carbons made completely from these impregnants differs significantly from that of Grade A. In their analysis of the effects of different heat-treatment temperatures on irradiation stability, the authors[3] attribute the increased growth, as well as contraction of poorly graphitized materials (compared with well-graphitized materials), to retention of damage caused by the presence of imperfections that act as sites for interstitial-atom capture.

New data on the effect of irradiation on the tensile-strain limits of graphite were reported by Hanford Atomic Products Operation.[4] A uniquely simple loading device that takes advantage of the high contraction rate of a carbon material was used to conduct tests at either of two strain rates (0.12 or 0.06%/10^{20} neutrons/cm^2). Results to date indicate that the total available strain at 550°C at the higher strain rate is 0.4%.

Graphite reaction rates and hydrogen generation rates have been reported[5] for high-pressure high-temperature steam flowing through a full-scale Experimental Gas-Cooled Reactor (EGCR) fuel-element graphite sleeve (Speer 901-RYL graphite) and a geometrically identical sleeve machined from EGCR moderator graphite (National Carbon Company). The results are summarized in Table II-1. The conclusions drawn from this study are:

1. The significant variables affecting the reaction rate of steam with graphite are (a) temperature; (b) burnoff, which tends to increase the reactive surface area; and (c) the concentration of CO and hydrogen in the fluid boundary layer.
2. Reaction rate is a negligible function of system pressure in the pressure range of 30 to 300 psig.
3. The CO/CO_2 concentration ratio decreases as the steam pressure increases.
4. The reaction rate does not appear to be significantly affected by a fivefold increase in steam Reynolds number.

The reaction rates of a pitch-free petroleum-coke-base graphite with purified hydrogen in the temperature range 1550 to 2260°C were measured by the National Aeronautics and Space Administration, Lewis Research Center.[6] The experimental data agree well with theoretical calculations based on thermodynamic

Table II-1 REACTION OF TWO GRAPHITES WITH STEAM[5]

	Speer 901-RYL* graphite	National Carbon Company* graphite
Activation energy, kcal/mole†	42.8	78.5
Reaction rate, g/(hr)(sq ft)		
1600°F	5.6 (4.0)	16.0 (46.6)
1500°F	2.0 (6.9)	5.0 (36.1)
1400°F	0.7 (7.61)	1.3 (24.1)
Hydrogen production rate, standard cm^3/(min)(sq ft)		
1600°F	270 (4.0)	810 (46.6)
1500°F	98 (6.9)	250 (36.1)
1400°F	34 (7.61)	62 (24.1)

*The percent of burnoff is given in parentheses.

†The test procedure compromised the determination of activation energy in that graphite burnoff (and therefore the steam–graphite reaction rate) was not constant over the temperature range investigated. Actual values would be somewhat higher than those measured.

data for temperatures above 1800°C, which indicate that acetylene is the major reaction product.

Variations in the crystallinity of pyrolytic carbons deposited in fluid beds have been reported[7] by General Atomic Division, General Dynamics Corp. The objective of the research was to study the structure of carbons deposited in the low-temperature region, using X-ray scattering techniques, with specific attention given to variations in the fractions of amorphous carbon and single unassociated layers in the deposits and the average number of layers associated in local regions to form "crystallites." It was found that significant quantities of amorphous carbon can be present in carbons deposited at 1400°C and that the amount present increases with the deposition rate. The concentration of misaligned single layers in these carbons varied from 23% in the low-density carbon deposited from 5% methane to less than 2% in the high-density anisotropic carbon deposited from 40% methane. This decrease in the concentration of single layers with increasing methane concentration occurred regardless of a concomitant increase in deposition rate. The structural variations with deposition conditions for the carbons deposited at 1400°C suggest that carbon is formed by the following processes:

1. At high methane concentrations, carbon is formed from high-molecular-weight planar polymers that form in the gas phase and either condense directly on the bed surface area or nucleate homogeneously to form gas-borne droplets. Direct condensation leads to high-density, anisotropic carbons, because the large planar complexes naturally align themselves with each other and the deposition surface. Deposition of gas-borne droplets, on the other hand, leads to lower density, more isotropic deposits. The formation of droplets is controlled by the contact time and the bed surface area, because at a given methane concentration, these are the variables that control the degree of supersaturation of the gas.

2. At low methane concentrations (~5%), polymerization is limited and the complexes that form are necessarily smaller. As a result they are less effectively aligned with each other and the deposition surface. This leads to low-density, less anisotropic carbons containing a high concentration of misaligned single layers. At very low methane concentration (<3%), carbon must be deposited primarily from relatively small hydrocarbon fragments.

The carbons deposited at 1650°C and above had no detectable amorphous carbon in their structures. The low-density isotropic carbon deposited at a very high rate at 1650°C was found to contain about 10% of single misaligned layers compared with 1 to 2% in the carbons deposited at 1900 and 2000°C.

(M. C. Brockway)

Beryllium Metal and Alloys

Physical Metallurgy

The Brush Beryllium Co. reported[8] on the application of zone leveling as a technique for producing single beryllium crystals of intermediate purity. Zone leveling is, in essence, zone refining in which the direction of the refining pass is alternated. The primary purpose of the process is to provide a more homogeneous distribution of the impurities in the material. Properties of the single crystals were found to improve with decreased rate of zone travel but not with increased number of zone passes. The enhanced basal-plane glide strain was attributed to agglomeration of the elements normally considered insoluble in beryllium, which results in the matrix having a higher capacity for deformation. On the other hand, the elements normally soluble in beryllium, such as copper, nickel, and iron, strengthen the matrix. Considerable reduction of the oxygen, nitrogen, and carbon contents was noted,

but the effect of that factor was not fully evaluated.

Zone leveling was also applied to commercial-grade powder-metallurgy beryllium. In this case the zone leveling was done in the solid state. Although the data reported were very limited, there apparently was some improvement in the overall mechanical properties of the material. In one case a tensile elongation of 6.0% was reported. Again the evidence indicated that the improvement was probably a result of matrix purification. The authors theorized that the $AlFeBe_4$ phase present in hot-pressed material acts as impurity sinks. It was stated that these data demonstrate that proper control of thermal and chemical variables may lead to a notably improved grade of structural beryllium using currently available purity levels.

The influence of oxide distribution and total impurity level on the recrystallization and grain growth of beryllium was studied at the Pechiney Company.[9] Recrystallization temperatures were 700 to 730°C (1290 to 1345°F) for cast SR metal, 760 to 765°C (1400 to 1409°F) for cast QMV, and 800 to 810°C (1472 to 1490°F) for powder-metallurgy materials from both sources. Observations were made by optical and electron microscopy, after various mechanical and thermal treatments, to define the physical processes occurring. At the 700°C fabrication temperature, the cast SR (higher purity) material recrystallized, and the cast QMV had a worked structure. At equal levels of deformation, grain size was finer in the SR material.

In metal of powder origin, the continuous grain-boundary network of oxides was broken up by forging and warm rolling. The rolling process dispersed the oxides in layers parallel to the surface. Brush Beryllium material exhibited grain growth comparable to that in cast material, showing that the oxide network does not provide an insurmountable obstacle to grain growth. However, the powder-metallurgy material did, as a rule, maintain fine grain sizes.

Generally, it was concluded in the study that impurities raised the recrystallization temperature and decreased the tendency for grain growth. Under high deformation the oxide distribution did not seem to vary with different source materials. The oxide layers usually, but not always, restrained grain-boundary motion.

Gross[10] studied the effect of primary recrystallization on the wrought preferred orientation in commercially pure beryllium. Although the texture was produced by wire drawing, the findings are probably applicable to other wrought forms of beryllium. The wrought preferred orientation was partially destroyed by primary recrystallization. No tendency for the formation of an annealing texture was found. There were no critical levels or combinations of time, temperature, or wrought strain found within the limits of the study. Recovery through polygonization preceded primary recrystallization. It was thought that the polygons provided nuclei for primary recrystallization.

In another study reported by the Pechiney Company,[11] the various inclusions and precipitates in beryllium were identified. Binary alloys of aluminum, iron, or silicon with SR-grade beryllium were studied along with cast or powdered CR-grade material. These materials were hot worked into sheet form and then submitted to various thermal treatments. Quenching in oil from as high as 1100°C had no influence on the distribution of aluminum and silicon. However, iron was put into solution at temperatures above 800°C (1470°F) and reprecipitated at 500 to 700°C (930 to 1290°F) as the compound $Be_{11}Fe$. In commercial-purity materials this compound was replaced by Be_5FeAl, primarily in the grain boundaries and subboundaries. On the basis of these data, the authors[11] concluded that aluminum was the predominant impurity responsible for loss in high-temperature ductility. Aluminum apparently decreased the solubility of iron in the matrix at elevated temperatures. If present in excessive amounts, aluminum produced a liquid phase and subsequent weakening of the grain boundaries.

Many other impurities were found in the form of various inclusions. These were (1) intermetallic compounds of the form $Be_{13}M$ (M = Mg, Ca, Zr, Hf, La, Ce, Th, or U) or $Be_{12}X$ (X = Ti, Cr, V, Mn, Nb, Mo, Ta, W, or Ag); (2) carbides and oxides; and (3) free elements such as aluminum and silicon. Quenching and aging did not appear to influence the distribution of these elements.

Nuclear Metals Division of Textron Inc.[12] reported on results of *c*-axis compression tests on ultrahigh-purity single-crystal beryllium. The crystal had a resistance ratio of 3300,

which is the highest purity level reported in the literature to date. The specimen was tested at 225°C, but fracture apparently still occurred on the basal plane. The authors[12] conclude that there were no nonbasal slip modes in high-purity beryllium below this temperature.

Attempts have been made at Nuclear Metals[13] to reduce interstitial carbon and nitrogen in high-purity beryllium by scavenging single crystals with titanium while zone refining. A 1000-ppm titanium addition did not reduce the interstitial content. When 10,000 ppm titanium was added, a two-phase polycrystalline material formed which was presumed to be a dispersion of $TiBe_{12}$ in beryllium. This was thought to be analogous to the effect of BeO in zone refining; that is, the insoluble particles stop the zone-refining action.

Nuclear Applications

In May 1965 this reviewer attended the International Conference on Beryllium Metallurgy in Grenoble, France, and had the opportunity to visit the Center for Nuclear Studies at Saclay. The French are still considering beryllium for fuel-element cladding, which is contrary to U. S., U. K., and Canadian thinking. The cladding material under consideration is a Be–0.4 wt.% Ca alloy cast and extruded tubing. One of the major problems facing investigators in France is how to make the final closure of the tubing.[14] At Saclay they are considering both tungsten-arc–inert-gas (TIG) and electron-beam welding, as well as diffusion bonding. Both welding techniques yield large grains in the weld zones, with a tendency for fracturing. On the other hand, when diffusion bonding was tried, only 70% of the joints were leaktight. Currently, TIG welding is the preferred technique since the tubes can be sealed with helium inside.

Investigators[15a] at Saclay reported on the compatibility of beryllium and its alloys with pressurized CO_2. Many binary alloys were tested, but magnesium- and calcium-bearing alloys provided increased resistance to wet CO_2. Water-vapor contents on the order of 250 ppm by volume did not affect the corrosion resistance of these alloys in the range 600 to 750°C. Corrosion resistance is better in cast Be–Mg than in cast Be–Ca, whereas in the sintered materials Be–Ca alloys are superior. The decrease in the tendency for breakaway corrosion is attributed to the formation of a layer rich in intermetallic compounds at the oxide–metal interface. This layer favors the adherence of the oxide by preventing localized pitting and reducing the relative stresses between the oxide and the metal.

The French are also interested in Be–0.4 wt.% Ca alloys because of their improved mechanical properties. The alloys are cast and extruded into rod, drilled, and then extruded a second time.[15b] Strain to fracture at room temperature is greatly increased[15c] by finish swaging at 400°C and annealing at 800°C. Cast and extruded tubes exhibit 2% elongation circumferentially at room temperature, whereas powder-metallurgy tubes show only 0.2%. On the other hand, Ca–Be alloys show an increase in ductility in the range 200 to 500°C. The swaging operation gives a 25-μ grain size, and the presence of $CaBe_{13}$ intermetallic pins the grain boundaries. The addition of calcium to beryllium also apparently makes it more fabricable.

Fabrication

The Australians[16,17] have reported the results of experiments on the extrusion of beryllium shapes. The primary objective was to fabricate fuel tubes; but, since they were extruding powder-metallurgy products, the general experience with extrusion was reported. Preconsolidated billets gave much better dimensional control in the finished product. Sealed containers were used to minimize oxygen and nitrogen pickup. Mechanical properties were sensitive to extrusion temperatures; residual work hardening increased with lower temperatures in the range 750 to 1050°C. Preferred orientation varied only with reduction, and not with temperature, in this range.

Because of better temperature control, extrusion pressures in the range 750 to 1050°C were found to be lower than those previously reported. Friction between die and billets was reduced by the use of a graphite lubricant. The effect of die configuration, velocity, etc., on deformation of the billets was determined with gridded billets (Inconel wires pressed into the surface of the beryllium billet). With this information the investigators were able to design the trailing edge of the initial billet so that the interface between the final extrusion and its follower came out as a flat plane

and thus reduced the cropping waste to a minimum. (H. D. Hanes)

Beryllium Oxide

The proceedings of The First International Conference on Beryllium Oxide, held in Sydney, Australia, October 21–25, 1963, have been published in the *Journal of Nuclear Materials*.[18] This is the most complete recent compilation of BeO information. It covers the major subject areas of utilization in nuclear reactors, radiation effects, structure and physical properties, sintering and sinterability, fabrication and mechanical properties, corrosion by water vapor, and beryllia-based dispersion fuels.

Additional property data on irradiated BeO have been reported by General Electric Company.[19] Samples exposed to fluxes of 1.5 to 2×10^{14} neutrons/(cm^2)(sec) at 1000°C and dosages of 2 to 3×10^{21} neutrons/cm^2 ($\geq$1 Mev) were characterized as to density, porosity, elasticity, and strength changes. The data are summarized in Table II-2. The open-porosity changes indicate that microcracking occurred in the two large-grain-size materials and possibly in the 5- to 6-μ grain-size low-density samples. In previous work, changes in the elastic constants of 10% or more were associated with microcracking. On the basis of this criterion, the elastic-constant changes in these tests of EBOR and AOX specimens of 18-μ grain size indicate microcracking. The strength changes indicate very little microcracking, at most, in the small-grain-size specimens with densities of 2.75 g/cm^3 or higher, but cracking in all of the remaining types. Two points are noted in regard to strength data. The volume increases were much larger prior to significant decreases in strength than heretofore observed. Also, the increased strength in higher density specimens of 5-μ grain size is one of the clearest indications to date of differences in the behavior of BeO of different densities.

Studies at Denver Research Institute[20] of phase equilibria in the system BeO–ThO_2 indicate that eutectic reaction occurs between 70 and 74 mole % BeO at a temperature of about 2150°C. The solid solubility of BeO in ThO_2 at 2760°C, as indicated by ceramographic inspection, is less than 1.0 mole % BeO. Solid solubility of ThO_2 in BeO at temperatures in excess of 2300°C was indicated to be less than 0.25 mole %. (M. C. Brockway)

Solid Hydrides

Zirconium Hydride

The effect of heating Zircaloy-2 capsules in dry hydrogen has been examined at Hanford.[21] Eight capsules were tested, and it was found that, between 300 and 350°C, hydriding failure is likely to occur in the end-cap region and that, from 350 to 410°C, failures may occur anywhere along the length of the capsule. The times to failure ranged from 5.5 to 40 hr.

Other Ternary Hydrides

The following points along the phase boundaries at high hydrogen contents in the Zr–Nb–H system have been determined at Chalk River:[22]

Temp., °C	$\delta(\delta+\epsilon)$ at.% hydrogen	$(\delta+\epsilon)\epsilon$ at.% hydrogen	Hydrogen pressure, torrs ($\times 10^{-4}$)
360	59.7	61.0	2.50
380	59.9	61.1	6.76
400	60.2	61.2	2.04

These values are in good agreement with those found for the phase boundaries in the pure zirconium hydride system and indicate that the niobium exerts little influence on the system.

A compound, presumably $TiN \cdot TiH_2$, has been prepared at Atomics International[23] by reaction of substoichiometric TiN with hydrogen. It was formed by decomposing TiH_2 mixed with TiN, thereby forming titanium metal, which in turn dissolved in the TiN. When the mixture was cooled, hydrogen was readsorbed to form the ternary hydride. It has a hexagonal cell with a_0 = 3.04 to 3.05 A and c_0 = 5.01 to 5.04 A.

Several binary-system eutectics of LiH have been studied at Argonne National Laboratory.[24] The lithium hydride content and the eutectic melting points are as follows:

System	Mole % LiH	Melting point, °C
LiH–LiCl	34.0	495.6
LiH–LiBr	29.7	453.3
LiH–LiI	23.5	390.8
LiH–NaCl	55.3	565.7

(H. H. Krause)

Table II-2 SUMMARY OF RADIATION EFFECTS IN BeO SPECIMENS[19] IRRADIATED AT 950 TO 1050°C TO 2.5 TO 3.0 × 10^{21} NEUTRONS/CM² (≥ 1 Mev)

Specimen description			Irradiation conditions		Volume expansion, %	Increase in open porosity, %	Elastic constants*							Modulus of rupture at room temperature		
							Young's modulus			Shear modulus						
Composition	Grain size, μ	Nominal density, g/cm³	Flux, 10^{14} neutrons/(cm²)(sec) (≥ 1 Mev)	Exposure, 10^{21} neutrons/cm² (≥ 1 Mev)			10^6 psi	10^{10} dynes/cm²	Percent of unirradiated	10^6 psi	10^{10} dynes/cm²	Percent of unirradiated	Poisson's ratio	10^3 psi	10^3 kg/cm²	Percent of unirradiated
UOX–MgO	6	2.60	1.9	3.0	2.0	0.5	42.0	2.90	94	16.5	1.14	95	0.27	29.8	2.10	95
			1.8	2.8		1.3								29.1	1.90	94
	3	2.75	1.9	3.0	1.8	0.3	46.3	3.19	94	18.7	1.29	94	0.23			
			1.4	2.2	1.4	0.1	45.0	3.10	95	18.3	1.26	95	0.23	38.2	2.69	126
			1.6	2.4	1.5	0.1	45.3	3.12	96	18.4	1.27	95	0.23			
			1.7	2.7	2.0	0.1	46.4	3.20	94	18.8	1.30	95	0.24	34.6	2.43	114
			1.6	2.5	1.7	0.1	45.3	3.12	94	18.4	1.27	95	0.23			
	4	2.90	1.5	2.3	1.1	0.1	50.3	3.47	96	20.8	1.43	97	0.21	44.0	3.09	143
			1.7	2.6	1.7	0.1	51.0	3.52	96	20.9	1.44	96	0.22	41.9	2.95	136
			1.9	3.0	1.8	0.1	51.2	3.53	96	21.0	1.45	96	0.22			
			1.7	2.6	1.5	0.1	50.4	3.47	96	20.8	1.43	97	0.21			
			1.8	2.8	1.8	0.1	51.8	3.57	96	21.2	1.46	96	0.22			
	11	2.90	1.6	2.5	1.9	0.1	52.6	3.63	97	21.0	1.45	96	0.25	35.8	2.52	110
			1.4	2.2	1.6	0.1	52.7	3.63	97	21.0	1.45	96	0.26			
			1.8	2.8	1.8	0.1	52.2	3.60	96	20.9	1.44	96	0.25			
AOX	5	2.60	1.6	2.4	2.5	2.0	38.7	2.67	93	15.3	1.05	95	0.26			
			1.5	2.4	2.2	2.4	39.0	2.69	94	15.6	1.08	97	0.25			
	5	2.60	1.8	2.8	2.3	2.2								23.8	1.67	88
	6	2.75	1.9	3.0		0.2	46.5	3.21	95	19.1	1.32	97	0.22			
			1.8	2.7	1.8	0.3	46.2	3.18	94	19.1	1.32	97	0.21	31.0	2.18	119
			1.4	2.1	1.5	0.5	46.6	3.21	95	19.4	1.34	99	0.20	30.2	2.12	116
			1.6	2.4	1.4	0.1	46.1	3.18	94	18.9	1.30	96	0.22			
			1.7	2.7	1.9	0.7	46.2	3.18	94	18.8	1.30	96	0.23			
	18	2.90	1.5	2.3	1.8	1.7	44.6	3.08	85	18.1	1.25	83	0.23	23.9	1.68	75
			1.7	2.6	2.2	1.3	45.7	3.15	87	18.8	1.30	86	0.22			
			1.6	2.5	2.3	0.9								21.3	1.50	67
			1.7	2.7	2.3	0.7	47.4	3.27	90	19.6	1.35	90	0.21			
EBOR	20 to 28	2.90	1.5	2.3	2.8	4.3†	38.1	2.63	79	16.4	1.13	81	0.18			
			1.7	2.6	2.9	4.3†	41.2	2.84	85	17.2	1.18	86	0.19			
			1.8	2.9	3.2	3.7†	41.6	2.87	85	17.3	1.19	85	0.20			
			1.8	2.9	3.3	3.5†								22.3	1.57	64
			1.6	2.5	2.8	3.2†	38.5	2.65	79	16.0	1.10	80	0.20	16.5	1.16	47

*Elastic constants were derived from resonant vibration frequencies and equations applicable to isotropic material; for the preferentially oriented UOX–MgO materials, this procedure yields apparent rather than true values and leads to particularly high values of Poisson's ratio.

†Open-porosity changes in EBOR specimens are based on comparison with unirradiated specimens from the same production block rather than preirradiation values of the specific samples cited.

References

1. B. T... K. S... sions in F... Brit...
2. J. E... Ratio... diati... 5, 19...
3. B. T... How... Dim... Brit... 1964...
4. J. R... Pro... Dev... Sept... forc...
5. R. F... tion... for... USA...
6. W. ... act... TN-...
7. J. ... ter... and...
8. J. ... era... and...
9. J. ... A. ... Re... the... pur... Gr... (Vo... Na... 19...
10. A. ... Co... 13...
11. M. ... A. ... Re... tic... of...

References

1. B. T. Kelly, W. H. Martin, A. M. Price, and K. Smith, The Effects of Annealing on the Dimensional and Thermal Expansion Changes Induced in Pyrolytic Graphite by Irradiation at 170°C, British Report TRG-Report-909, Dec. 21, 1964.
2. J. E. Brocklehurst and J. T. Lynam, Poisson's Ratio of Reactor Graphite and the Effect of Irradiation, British Report TRG-Report-901(C), Mar. 5, 1965.
3. B. T. Kelly, B. S. Gray, W. H. Martin, V. C. Howard, and M. J. Jenkins, Fast-Neutron-Induced Dimensional Changes in Graphites and Carbons, British Report TRG-Report-885(C), Nov. 23, 1964.
4. J. K. Green (Ed.), Research and Development Programs Executed for the Division of Reactor Development, Quarterly Progress Report, July–September 1964, USAEC Report HW-84384, Hanford Atomic Products Operation, December 1964.
5. R. E. Helms and R. E. MacPherson, The Reaction of Steam with Large Specimens of Graphite for the Experimental Gas-Cooled Reactor, USAEC Report ORNL-TM-984, Oak Ridge National Laboratory, March 1965.
6. W. A. Sanders, Rates of Hydrogen-Graphite Reaction Between 1550 and 2260°C, Report NASA-TN-D-2738 (N65-20481), National Aeronautics and Space Administration, Lewis Research Center, April 1965.
7. J. C. Bokros, Variations in the Crystallinity of Carbons Deposited in Fluidized Beds, USAEC Report GA-6050, General Atomic Division, General Dynamics Corp., Apr. 1, 1965.
8. J. A. Carrabine, A. J. Stonehouse, D. G. Fetsko, and W. W. Beaver, Investigation of the Mechanical Characteristics of Zone-Leveled Beryllium, Report AFML-TR-64-388, The Brush Beryllium Co., November 1964.
9. J. Moriceau, J. M. Logerot, M. Croutzeilles, A. Saulnier, R. Syre, and P. Vachet, Beryllium Research and Development Program, Influence of the Distribution of Oxide and of the Total Impurity Level on Recrystallization and Grain Growth in Beryllium, Report ASD-TDR-62-509 (Vol. VI) (AD-613952), Pechiney Company and Nuclear Metals Division of Textron Inc., January 1964.
10. A. G. Gross, Jr., Primary Recrystallization in Commercially Pure Beryllium, *J. Nucl. Mater.*, 13(1): 1-12 (1964).
11. M. Croutzeilles, J. M. Logerot, J. Moriceau, A. Saulnier, R. Syre, and P. Vachet, Beryllium Research and Development Program, Identification of Inclusions and Precipitates in Beryllium of Different Origins, Report ASD-TDR-62-509 (Vol. VII), Pechiney Company and Nuclear Metals Division of Textron Inc., October 1963.
12. Nuclear Metals Division of Textron Inc., Fundamental and Applied Research and Development in Metallurgy, Monthly Progress Report, December 1964, USAEC Report NMI-2135, Feb. 15, 1965.
13. Nuclear Metals Division of Textron Inc., Fundamental and Applied Research and Development in Metallurgy, Progress Report, October 1964, USAEC Report NMI-2133, Dec. 11, 1964.
14. J. M. Mallen, Centre d'Études Nucléaires, Saclay, France, personal communication, May 12, 1965.
15. Papers presented at an International Conference on Beryllium Metallurgy, Grenoble, France, May 17–20, 1965.
    a. B. Dewanckel, D. Leclerca, and R. Darras, Compatibility of Beryllium and Its Alloys with Pressurized CO_2 at High Temperatures.
    b. J. M. Logerot, J. M. Mallen, R. Molinier, and M. Weisz, Elaboration and Properties of Cast Extruded Beryllium Tubes.
    c. R. Dumas, D. Carpenter, J. Moriceau, and D. Francois, Some Observations on the Recrystallization of Beryllium and Beryllium-Calcium Alloys.
16. W. J. Wright, J. M. Silver, and S. W. Spain, Experiments in Extrusion, Part 2. The Hot Extrusion of Beryllium, Australian Report AAEC/E-131, December 1964.
17. W. J. Wright, J. M. Silver, and J. F. Whatham, Experiments in Extrusion, Part 3. The Mechanics of Extrusion of Beryllium, Australian Report AAEC/E-132, December 1964.
18. R. Smith and J. P. Howe, Beryllium Oxide — Proceedings of the First International Conference on Beryllium Oxide, Sydney, Australia, October 21–25, 1963, *J. Nucl. Mater.*, 14: 1-498 (1964).
19. General Electric Company, Advanced Technology Services, High-Temperature Materials Program Progress Report No. 46, Part A, USAEC Report GEMP-46A, Apr. 15, 1965.
20. H. E. Otto, Determination of Phase Equilibria in the System BeO-ThO_2, USAEC Report DRI-1092-201, Denver Research Institute, Mar. 15, 1965.
21. Hanford Atomic Products Operation, Ceramics Research and Development Operation Quarterly Report, October–December 1964, USAEC HW-81603.
22. W. H. Erickson, paper presented at the meeting of the Electrochemical Society, Buffalo, New York, October 10–14, 1965.
23. Atomics International, AEC Unclassified Programs, Quarterly Technical Progress Report, January–March 1965, USAEC Report NAA-SR-11200, Apr. 15, 1965.
24. Argonne National Laboratory, Chemical Engineering Division Research Highlights, May 1964–April 1965, USAEC Report ANL-7020.

Section

III

Reactor Materials

Nuclear Poisons

Metallic Poison Materials

The grain-growth behavior of arc-melted tungsten and of W–B alloys (0.005 to 0.67 at.% boron) was studied in the 3600 to 4200°F temperature range.[1] The grain-growth kinetics were followed by measuring the decrease in grain-boundary surface area, β, as a function of time at temperature. The relation found at 3600 and 3800°F was $\beta = kt^{-n}$, where k and n are constants. At 4000°F, discontinuous grain growth took place. This discontinuity was attributed to breakup of tungsten boride, which had pinned the grain boundaries, and subsequent solution of the boron into tungsten.

The Russians[2] have measured the vapor pressures of gadolinium and dysprosium. The vapor pressure of gadolinium was found to be represented by $\log P\,(\text{mm Hg}) = 12.03 - 23{,}705/T$ in the 1120 to 1310°C range, whereas that of dysprosium in the 850 to 1075°C range was $\log P\,(\text{mm Hg}) = 0.79 - 15{,}825/T$. Heats of sublimation for gadolinium and dysprosium were 108.5 and 72.4 kcal/mole, respectively.

(M. Kangilaski)

Dispersion and Nonmetallic Poison Materials

Research in neutron-absorbing glass–ceramics has been reported by investigators at the English Electric Company.[3] Glasses based on the systems $CdO-In_2O_3$ and $CdO-In_2O_3-B_2O_3$ were studied for use as reactor control-rod materials. These glasses were found to be impermeable and to have high neutron-absorption coefficients and high mechanical strengths. Also, tests indicated that these glasses are compatible with most potential canning materials and have good resistance to mechanical shock.

In the processing of U–Al alloy fuel elements containing a burnable poison, fabricators have had difficulty in controlling the amount of boron present and its distribution within the alloy. Research at the National Reactor Testing Station (NRTS)[4] has been directed toward alleviating this problem by incorporating the burnable poison as B_4C dispersed in a 1-mil-thick foil of aluminum which is located between the U–Al alloy core and the aluminum-alloy cladding. Sample fuel plates that had a duplex cladding consisting of 1-mil-thick aluminum containing a dispersion of 3.5 wt.% boron as B_4C under a 14-mil-thick outer cladding were fabricated for mechanical and irradiation testing. The presence of the B_4C particles caused a decrease in ductility but did not affect tensile strength. Full-size duplex cladding plates will be fabricated next to determine how uniformly the B_4C can be distributed throughout the plate length.

Progress in research at Combustion Engineering, Inc., concerning the development of UO_2 fuel rods containing additions of burnable poison has been reported.[5] The problem of severe axial boron segregation produced by the migration of B_4C particles during vibratory compaction of fuel rods has been resolved by a combination of incremental loading and intermittent vibration. Rods have been compacted to relative densities of 87 to 88%, and the boron concentration along these rods was maintained within the desired range of ±20% of the mean boron concentration. Compatibility studies of UO_2 and B_4C have been conducted in open (flowing helium gas) containers, and these have shown there is no appreciable thermal migration of boron. For these tests, combined axial and radial thermal gradients of 4500°C/cm and 15°C/cm, respectively, were maintained with a fuel centerline temperature of 2400°C. Closed-container experiments are now being made to yield information on UO_2-B_4C compatibility,

boron migration, and gas release under conditions the fuel rod will encounter during reactor operation.

Results of compatibility studies for B_4C with potential cladding materials for the Advanced Organic Moderated Reactor (AOMR) have been described.[6] The studies included the compatibility of B_4C with copper, types 430 and 304 stainless steels, and AISI 4130 steel at temperatures near and above those considered for the AOMR. Copper and type 430 stainless steel were compatible with B_4C for 10,000 hr at temperatures from 750 to 1300°F. Type 304 stainless steel was also compatible with B_4C for 10,000 hr at temperatures from 750 to 1100°F, but there was extensive reaction at 1300°F. The AISI 4130 steel was compatible for 10,000 hr at 750°F, but reaction became increasingly extensive at higher temperatures. The stoichiometry of the B_4C did not appear to influence the extent of reaction in these tests.

(E. G. Smith, Jr.)

References

1. P. L. Raffo and R. F. Hehemann, Grain Growth in Dilute Tungsten–Boron Alloys, Report NASA-TN-D-2649, National Aeronautics and Space Administration, Lewis Research Center, March 1965.
2. G. P. Kootun, A. A. Kruglykh, and V. S. Pavlov, Vapor Pressure of Gadolinium and Dysprosium, *Ukr. Fiz. Zh.*, 9: 1080-1091 (October 1964).
3. P. W. McMillan and P. B. Hodgson, Neutron-Absorbing Glass–Ceramics, *Glass Technol.*, 2: 142-149 (August 1964).
4. M. J. Graber, W. F. Zelezny, and G. W. Gibson, Annual Progress Report on Reactor Fuels and Materials Development for FY 1964, USAEC Report IDO-17037, Phillips Petroleum Company, November 1964.
5. R. C. Brayer and W. P. Chernock, Burnable Poison Additions to UO_2, Progress Report, July 1–September 30, 1964, USAEC Report CEND-3107-224, Combustion Engineering, Inc., October 1964.
6. R. D. Hahn, Compatibility of Boron Carbide with Potential AOMR Control Rod Cladding Materials, USAEC Report NAA-SR-8702, Atomics International, Mar. 1, 1964.

Section

IV

Reactor Materials

Cladding and Structural Materials

Corrosion

Zirconium-Alloy Corrosion

The kinetics and mechanism of the oxidation of zirconium and Zr–Nb alloys in oxygen at 400, 500, and 600°C and 1 to 760 torrs have been reported by University of Toledo scientists.[1] The rate curves of "degassed" specimens at 400 and 500°C were found to exhibit a horizontal transition region in which the rate of reaction was essentially zero. "Undegassed" zirconium in 760-torr oxygen at 500 and 600°C exhibited parabolic reaction rates. The effect of oxygen pressure on reaction rates was significant, but no simple relation could be established.

The effect of surface contamination on the corrosion of crystal-bar zirconium in steam at 500°C has been investigated at Harwell.[2] Accelerated oxidation was observed from (1) copper contamination deposited on the surface from aqueous solution, (2) an unidentified contaminant due to vacuum annealing in silica capsules, (3) simple immersion in tap or redistilled water due to calcium present, and (4) the normal HNO_3/HF pickle followed by tap-water rinsing. Exposure to HF solution with the rigorous exclusion of calcium had no effect on oxidation rates.

An interpretive literature survey and recent experimental results have been used by Bettis Atomic Power Laboratory[3] to evaluate the effect of environmental factors on the aqueous corrosion and hydrogen-absorption characteristics of Zircaloy. It was found that small quantities of dissolved oxygen or oxidizing agents caused a substantial reduction in hydrogen absorption, with only a slight increase in oxidation kinetics. Large quantities of dissolved hydrogen or reducing agents were required to produce a noticeable increase in hydrogen pickup. It was postulated that hydrogen from the corrosion reaction entered the oxide film at anion vacancy sites as atomic hydrogen and migrated through the film via anion vacancies to the metal surface. The role of dissolved oxygen in reducing hydrogen pickup was believed to be the result of (1) the annihilation of anion vacancies and their reduction in number at the oxide surface (hydrogen entry sites); (2) an accompanying decrease in the number of electrons (which attract protons to the oxide surface and neutralize them to form atomic hydrogen); and/or (3) ionization of the oxygen and its reaction with the protons to form water, thereby preventing the entry of hydrogen into the oxide film.

Hydrogen pickup in Zircaloy-2 and commercially pure zirconium upon exposure to hydrochloric acid has been investigated at Oak Ridge National Laboratory.[4] About 10 to 40% of the hydrogen formed by the corrosion reaction appeared in the metal. Commercially pure zirconium corroded two to four times as fast as Zircaloy-2, although corrosion rates were low for both. Alloying zirconium with 1 wt.% platinum resulted in higher corrosion rates and greater hydrogen pickup than were experienced with unalloyed zirconium.

The oxidation of pure and doped anion-deficient monoclinic zirconia has been reported by Vallecitos Atomic Laboratory[5] for the temperature range 450 to 900°C. A detailed theoretical analysis showed that the parabolic rate constant was a complex function of the diffusion coefficient of oxygen in ZrO_2. Yttrium additions increased the parabolic rate constant for zirconia oxidation by a factor of 300, which was in agreement with the fact that Zr–Y alloys oxidize more rapidly than unalloyed zirconium.

(W. E. Berry)

Aluminum-Alloy Corrosion

The kinetics of the high-temperature corrosion of 99.99% pure aluminum in distilled water have been investigated by Argentine scientists.[6] In the early stages of corrosion at 175 to 225°C, the initial rapid linear-weight-gain rate was followed by a period of essentially no weight change, which in turn was followed by a rapid linear weight gain. The period of no weight change was believed to correspond to crystallization of the oxide and loss of water of hydration.

The Defense Metals Information Center[7] has summarized the information received in reply to a questionnaire on the stress–corrosion cracking of aluminum alloys. The questionnaire was prepared by the Aerospace Research and Testing Committee of the Aerospace Industries Association of America. Approximately 30 alloys were reported as showing varying degrees of susceptibility to stress–corrosion cracking. A variety of specimen types and test environments were also described. (W. E. Berry)

Stainless-Steel Corrosion

The amount of aluminum required to maintain oxidation resistance as the chromium content is varied in Fe–Cr–Al alloys has been determined and plotted by General Electric Company workers.[8] In the temperature range 900 to 1300°C, the critical aluminum content varied from 8 wt.% in an Fe–0 wt.% Cr alloy to 3 wt.% in an Fe–25 wt.% Cr alloy. Experimental Fe–Cr–Al–Y alloys were equal to or superior to commercial alloys in oxidation resistance in steam at 550 to 1100°C.

The effect of metal purity on the corrosion behavior of 18-10 stainless steel is being studied in France.[9] Specimens from commercial-purity heats exhibited lower corrosion rates in 400°C steam than did those from high-purity heats. On the other hand, commercial-purity material corroded intergranularly in boiling nitric acid containing hexavalent chromium, whereas high-purity material did not.

The effect of reactor decontaminating solutions on corrosion behavior at areas of intergranular attack in type 304 stainless steel has been studied at Hanford Atomic Products Operation.[10] The decontaminating processes consisted of repeated cycles of immersion in alkaline permanganate solution, followed by immersion in sulfamic acid or bisulfate solution. It was concluded that the decontaminating solutions would remove grains from areas already subject to intergranular attack but would not cause any additional penetration.

The water chemistry of the pressurized-water loop at the Oak Ridge Research Reactor[4] was studied during operation at 149 to 176°C. Average concentrations (in units of 10^{-9} mole) of corrosion-product iron, nickel, manganese, chromium, and cobalt were, respectively, 200, 150, 14, 3, and 1 as soluble species and 40, 3, 0.1, 5, and less than 0.1 as suspended solids. The solubility of Fe_3O_4 in pure water saturated with 1 atm of hydrogen at room temperature was 0.33×10^{-6} mole (in iron) at 260°C and 1.5×10^{-6} mole at 200°C. (W. E. Berry)

Corrosion of Base Metals and Other Alloys

The outer layer of chemically deposited nickel plate on Pu–Al fuel elements was severely attacked during a one-month in-reactor exposure to water at *p*H 5.5 to 7.3 and temperatures to 260°C in tests conducted at Hanford.[11] The attack proceeded only to the inner Ni–Al diffusion layer. On dummy elements with the same thickness of nickel plate (0.8 mil), the plate was nearly intact.

The corrosion behavior of the construction materials being considered for the core internals of the Advanced Test Reactor has been studied by The Babcock & Wilcox Co.[12] Exposure conditions were up to 4000 hr in static and flowing water at 212 to 250°F, 300 psig, *p*H 5.0 to 6.0, and containing 0, 5, or 11 ppm oxygen. Galvanic, fretting, stress, and crevice corrosion tests were conducted. Included in the materials were beryllium, aluminum alloys, hafnium, Hf–Ta alloys, Haynes 25, Inconel X, and stainless steels. The results of the program indicated that all of the materials tested, except hard-coated aluminum alloys, were suitable for service at the contemplated reactor operating conditions.

An investigation of the factors that affect the hot salt cracking of Ti–8 wt.% Al–4 wt.% Mo–1 wt.% V alloy at 550 and 600°F has been conducted at Langley Research Center.[13] It was found that (1) a reduction in oxygen content and oxygen pressure reduced stress–corrosion cracking; (2) thin oxide films and moisture had no effect in the range investigated; (3) NaCl

caused more cracking damage than ASTM salt (6 parts NaCl to 1 part $MgCl_2$); and (4) moist chlorine produced severe stress–corrosion cracking. (W. E. Berry)

Refractory-Metal Corrosion

OXIDATION

Russian investigators[14,15] determined the effects of alloying additions on the oxidation rates of niobium, tantalum, and tungsten in air at 500 to 900°C. The alloying additions ranged from 5 to 95 wt.%. Additions of titanium, iron, aluminum, nickel, zirconium, and cobalt decreased the oxidation rate of niobium. The effectiveness of nickel and aluminum decreased with increasing temperature. Tungsten and copper additions increased the oxidation rate of niobium. Only iron and cobalt decreased the oxidation rate of tungsten, and only at concentrations greater than 30 wt.%. The effect of iron and cobalt on the tungsten oxidation rate was attributed to the formation of $FeWO_4$, Fe_2WO_6, and $CoWO_4$, which retarded the diffusion of oxygen. In alloys based on tantalum, more than 30 wt.% titanium effectively retarded oxidation. This was ascribed to the formation of TiO_2 and Ti_2O_3.

The influence of up to 50 wt.% molybdenum on the oxidation of Nb–Mo alloys was determined[16] in air at 1000 to 1200°C. At 1000°C, minimum oxidation was observed at 10 wt.% molybdenum. At increased amounts of molybdenum and at higher temperatures, oxidation increased due to the formation of MoO_3. No MoO_3 was found in the scale structure at 1000 to 1200°C.

Kofstad and Espevik[17] studied the oxidation behavior of niobium at 1200 to 1700°C at oxygen pressures ranging from 2×10^{-4} to 0.5 torr. Three stages of oxidation were observed: an initial linear rate was followed by a parabolic stage, which finally transformed to a linear rate. The initial linear stage involved dissolution of oxygen in the metal, and the oxidation was governed by the rate of chemisorption on the metal surface. Parabolic oxidation, the second stage, was due to the formation of protective NbO_2. Further oxidation produced a porous Nb_2O_5 and a second linear rate. At and above 1500°C the presence of liquid Nb_2O_5 affected the oxidation rate. The rate of formation of liquid Nb_2O_5 showed a different dependence on oxygen pressure and temperature than did the growth of solid Nb_2O_5; for example, at low oxygen pressure (e.g., 10^{-3} torr), liquid Nb_2O_5 forms at a lower rate at 1600°C than the solid form at 1400°C.

The formation of several intermediate oxides of niobium produced in the course of the transformation gamma Nb_2O_5 to alpha Nb_2O_5 and the reaction $2Nb_2O_5 + Nb \rightarrow 5NbO_2$ were studied by X-ray diffraction.[18] The structure transformation gamma to alpha was accomplished by passage through two intermediate structures, gamma prime and beta. The gamma prime form was interpreted to have a monoclinic lattice, with parameters $a = 7.34$ A, $b = 5.96$ A, $c = 13.64$ A, and $\beta = 115°30'$. The gamma form was previously considered to be a pentoxide having $12Nb_2O_5$ molecules in its elementary lattice. However, the helium method of density measurement showed two possible compositions for the gamma form—a pentoxide that has $14Nb_2O_5$ molecules in its elementary lattice, or $Nb_{28}O_{69}$.

Bartlett and McCamont[19] studied the influence of crystal orientation on the oxidation of tungsten at temperatures above 1600°C and at an oxygen pressure of 10^{-6} mm Mg. Of the crystal faces examined, the {1 0 0} surfaces oxidized most rapidly, with a reaction probability of 0.4. The {1 1 1} and {1 1 0} faces oxidized at about the same rate as polycrystalline tungsten. The oxidized {1 0 0} faces were smooth, except for occasional stepped octahedral pyramids each bounded by {1 1 1} faces. The {1 1 1} surfaces were also smooth, except for numerous stepped tetrahedral pyramids each bounded by {1 0 0} faces. Extremely irregular surfaces and macroscopic ledges were present on the {1 1 0} surfaces.

The reactions of tantalum with CO_2 and CO were studied in the temperature range[20] 500 to 700°C. It was found that what occurs is substantially oxidation by dissociated oxygen, involving solution of oxygen and the formation of oxides. The oxide phases that were identified include suboxides and Ta_2O_5. The initial stages of the reaction in CO_2 exhibited parabolic behavior where the dissolution of oxygen predominated. Subsequent linear oxidation resulted upon the formation of Ta_2O_5. The rate of reaction in CO below 700°C approximated parabolic behavior during the 8-hr experiments. At 700°C the reaction between CO and tantalum proceeded almost linearly from the start and resulted in the formation of Ta_2O_5.

PROTECTIVE COATINGS

General Telephone & Electronics Laboratories (GT&E) are conducting chemical and metallurgical analyses of protective coatings for refractory metals.[21] Chemical and structural changes that occur in the coatings will be determined and related to exposure conditions and coating performance. Coated specimens, before and after exposure, will be subjected to the following analyses:

1. Metallographic examination
2. Electron-probe analysis
3. X-ray diffraction—room and high temperature
4. Electron diffraction and metallography
5. Hot-stage microscopy
6. Various analytical techniques such as mass spectroscopy

Base metals and coatings selected for the program are given below:

Base alloys, wt.%	Coatings
Nb Nb–5 Mo–5 V–1 Zr (B66) Nb–10 W–1 Zr–0.1 C (D43)	Si (GT&E) Si–Cr (Pfaudler Co.) Ti–Si (GT&E) Ti–Cr–Si (Thompson Ramo Wooldridge Inc.)
Mo Mo–0.5 Ti–0.08 Zr–0.02 C (TZM)	Si (GT&E) Si–Cb (Pfaudler Co.) Si–Cr–B (Chromalloy Corp.)

Boeing Co. is adapting the fluidized-bed coating technique to new coating processes under Air Force sponsorship.[22] This coating technique was previously developed for the now inactive X-20 program. The feasibility of coating selected niobium- and tantalum-base alloys with a vanadium-modified disilicide and Ti–Cr–Si coatings will be determined. Fluidized beds of 4-, 8-, and 18-in. diameters will be used in the program.

Union Carbide Corp. has initiated a program to establish the feasibility of using iridium as a protective coating for niobium and tantalum.[23] This interest in iridium as a coating material resulted from a prior investigation of coatings for graphite.[24] Iridium coatings less than 5 mils thick have protected graphite from oxidation in plasma-torch tests at temperatures approaching 2100°C. Methods for applying iridium to niobium and tantalum will be examined. Chemical and mechanical compatibility of the coating–refractory-metal systems will be determined, and limited oxidation tests will be conducted.

(J. J. English)

Corrosion by Liquid Metals

Difficulties with solubility measurements are illustrated by experiments at the National Aeronautics and Space Administration (NASA) Lewis Laboratory,[25] which indicated the equilibrium solubility of commercially pure iron in 871°F potassium to be approximately 3500 ppm when nickel was used as a crucible material and about 50 ppm when zirconium was the crucible material. Intermediate levels of solubility were obtained when molybdenum, niobium, and tantalum crucibles were used. These observations are related to oxygen levels of the melts, as controlled by the relative gettering ability of the five crucible materials used. The approximately 50-ppm level would appear to be in some agreement with preliminary data from an investigation at Atomics International.[26a] Concentrations of iron dissolved in potassium containing 16 ppm oxygen were found to be approximately 20 ppm at 800°C, from approximately 10 to 80 ppm at 1000°C, and approximately 600 ppm at 1200°C.

The Lewis Laboratory research found also that the equilibrium solubility of cobalt in potassium is less than 5 ppm over the temperature range 668 to 1055°C. Nickel solubility over this range was related by

$$\log \text{ppm nickel} = 3.89 - \frac{3040}{T(^\circ\text{K})}$$

New data[26b] on the solubilities of other materials in potassium show: niobium at 1225 and 1245°C, 7 to 28 ppm; tantalum at 1245 and 1330°C, 6 to 151 ppm.

The minimum-creep-rate data[27] shown in Fig. IV-1 were obtained as a part of the continuing investigation at MSA Research Corp. on the effect of sodium exposures on the mechanical properties of selected steels. Various general results of this research were summarized by Andrews and Tepper.[28a] Some of the highlights for type 316 stainless steel at 1200°F are:

1. It carburizes readily in high-carbon sodium, but the carburization rates for type 304 stainless steel are even higher.

2. Exposures of 4000 hr in various environments produce impact-strength reductions as follows: 47% in helium, 65% in high-oxygen (~300 ppm) sodium, and 82% in high-carbon sodium.

3. The low-strain fatigue life showed the following dependence on environment: longest in low-oxygen (~30 ppm) sodium; shortest in air; and intermediate in high-carbon and high-oxygen sodium.

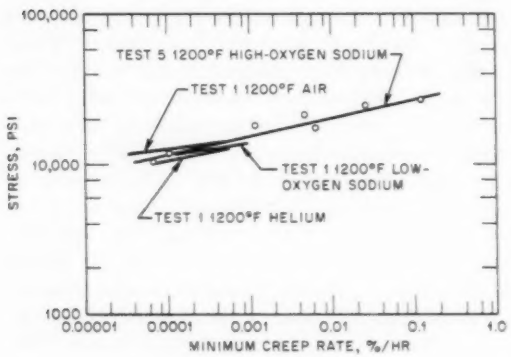

Fig. IV-1 Minimum creep rate[27] of type 316 stainless steel in air, helium, and sodium at 1200°F. Note that all data points shown are from test 5.

Comparisons from exposures of 2.25 wt.% Cr–1 wt.% Mg steel in 1100°F high- and low-oxygen sodium include:

1. Low-strain fatigue life—10 to 20 times longer than in air; approximately equivalent to helium

2. Creep-rupture strength—slight decrease compared to air and helium

3. Stress to produce 1% creep in 10,000 hr—about 14% lower than in air

Workers at Vallecitos have been conducting 1000 to 1200°F sodium tests with pumping loops having hot and cold legs fabricated of type 316 stainless steel, 2.25 wt.% Cr–1 wt.% Mo steel, or 5 wt.% Cr–0.5 wt.% Mo–0.5 wt.% Ti steel. The empirical relation developed from corrosion-tab studies during many thousands of loop-operation hours for steady-state removal of hot-leg metal is[28b]

$$R = V^{0.884}\, O^{1.156} \exp\left(12.845 - \frac{23827}{T + 460} - 0.00676\, L/D_i + \frac{2.26}{t+1}\right)$$

where R = removal rate, mg/(dm^2)(month)
V = flow velocity, ft/sec
O = oxygen level in sodium, ppm
T = hot-leg temperature, °F
L/D_i = diameters downstream from hot leg
t = exposure time, months

Hot- to cold-zone temperature differential, normally thought to affect corrosion behavior, was varied from 250 to 500°F without producing significant changes in measured metal-removal rates. Not represented in the above relation is intergranular corrosion attack, which was observed to occur at a rate of about 1.7 mils/year in the case of the type 316 stainless-steel loop tubing.

Brookhaven National Laboratory is engaged in several kinds of mercury- and sodium-corrosion research. Developments recently reported include:

1. The study of the containment of sodium at temperatures up to 1315°C by various refractory-metal alloys.[29] The Nb–1 wt.% Zr alloy demonstrated excellent corrosion resistance after both thermal-convection and refluxing-capsule experiments of up to about 8000-hr duration. Capsule experiments involving containment by Nb–10 wt.% W–10 wt.% Ta and by Ta–10 wt.% W produced evidence of pronounced attack in both materials.

2. Evaluations to examine the possibility that stress has an effect on the corrosion behavior of niobium-base materials exposed to 760°C mercury liquid and vapor.[29] This constitutes a follow-up of a 7698-hr Nb–1 wt.% Zr loop experiment that failed as a result of a crack which occurred on the neutral axis of a bend in a (760°C) superheater tube.

A series of 90° bend samples were first exposed for 1000 hr with the following results: pure niobium was not affected; two of eight Nb–1 wt.% Zr coupons exhibited cracking at the inside of the bend; all Nb–5 wt.% Zr samples showed intergranular corrosion. Subsequently several 180° bend samples, some of which were stress relieved at 1200°C, were tested. Of these, none exhibited out-of-the-ordinary behavior, except one as-bent Nb–5 wt.% Zr sample exposed to liquid mercury. This sample developed a complete cross-section crack in a zone about ½ in. from the bend.

3. Studies involving additives and pretreatments to mercury-containing low-carbon steel systems are continuing. Thermal-loop experi-

ments were operated for 5000 hr at 593°C (boiler) and approximately 700°C (superheater).[30] Some of the posttest findings are tabulated below.

Additive or pretreatment	Hot-zone attack, μin.	Cold-zone deposits
Titanium addition	<50	~0.5 g of adherent iron
Zirconium addition	<50	~0.2 g of adherent iron (labeled as not discernible)
None	<50	~1 g of adherent iron
Pretest circulation of a liquid Hg–Zr solution for 500 hr at ~600°C; no additive to test charge	300 to 100	~2 g of adherent iron

Brief summaries of findings presented in three reviews of corrosion-loop experiments are given below.

1. Thermal-convection loops[31] of type 316 stainless steel, Haynes 25 alloy, or Inconel were operated with 870°C boiling potassium for 1500 to 3000 hr. Posttest analyses revealed relatively low insert-specimen weight losses (with Inconel the poorest material in this respect); cracking in various zones, especially where fluctuating temperatures occurred (with Haynes 25 alloy poorest in this respect); various quantities of metallic deposits in cold-zone (to about 675°C) regions; and migration of carbon from hot- to cold-zone regions. Overall, the degree of corrosion was not severe, even for a Haynes 25 alloy system that operated with a boiler temperature of 980°C.

2. A thermal-convection loop[32] of Nb–1 wt.% Zr alloy was operated with 1130°C boiling potassium for 2800 hr. Corrosion effects were not pronounced. Metal removal from insert specimens in a 1130°C vapor zone was equivalent to a loss of about 0.1 mg/cm^2; the corresponding losses in an 1130°C liquid zone averaged about 0.01 mg/cm^2.

3. A forced-circulation loop fabricated of type 316 stainless steel with Nb–1 wt.% Zr inserts was operated[33] for 3068 hr with 1200°F (isothermal) NaK. The experiment was designed to fill an information gap between results of similar refractory-metal–stainless-steel experiments in the 1500 to 1600°F range, which indicated significant transport of carbon and other elements, and results of less than 1000°F experiments where no significant interactions occurred. Data early in the experiment indicated that fairly pronounced carbon transport to the niobium alloy was taking place, but this tapered off after about 250 hr of operation. However, nitrogen transport to the alloy occurred throughout the test, with diffusion layers finally appearing to a depth of about 0.01 in. Oxygen migration did not occur to any significant degree.

Cesium corrosion capsule tests[26c] at Hughes Aircraft Co. were operated for 500 hr at 400°C. No significant corrosion was observed for the following materials:

17-4 PH steel	Ti–6 wt.% Al–4 wt.% V	Alumina Al-300
17-7 PH steel	Tungsten	Lucalox
AM 350 steel	Molybdenum	Synthetic sapphire
Nickel	Tungsten carbide	

Among the noticeable effects were: (1) tantalum suffered weight loss and was covered with a nonadherent (presumably oxide) coating, (2) platinum suffered severe weight loss, (3) stainless steels accumulated surface layers, and (4) ceramics lost volume resistivity.

A host of materials was investigated from the viewpoint of response to stress after a 1000-hr exposure to cesium liquid or vapor, followed by a cleanup and a rewetting procedure prior to stressing.[34] The temperature levels employed were 350°C for aluminum and copper-base alloys, 650°C for stainless steels and titanium and nickel alloys, and 1200°C for refractory metals. Generally, the cesium-exposed test metals exhibited noticeable changes in strength and reductions in elongations at fracture, as shown in Table IV-1. However, the reverse effect was noted for Kovar and, surprisingly, for tungsten. It is stated that the elongations for ruptured cesium-exposed specimens of tungsten were definitely measurable, whereas unexposed specimens were completely brittle. A series of Al_2O_3 and Y_2O_3 ceramics was also incorporated in the test program. Whereas the alumina was unaffected by contact with cesium, the yttria was drastically weakened.

It is of interest to note that short-time screening tests were conducted to assess the resistance of ruthenium and iridium to corrosion by a variety of relatively low-melting-point materials at temperature levels in the range of 200°C above their melting points.[35] In the case of iridium, the "no attack" category consists of lithium, sodium, potassium, silver, gold, mer-

Table IV-1 EFFECT OF CESIUM ON TENSILE PROPERTIES[34]

Material	Dry control			Cesium wetted (liquid)†			Cesium vapor‡		
	Ultimate tensile strength, 1000 psi	Yield strength,* 1000 psi	Elongation, %	Ultimate tensile strength, 1000 psi	Yield strength,* 1000 psi	Elongation, %	Ultimate tensile strength, 1000 psi	Yield strength,* 1000 psi	Elongation, %
Titanium	74	63	20.0	70	60	21.8	50	44	13.1
				71	59	20.4	48	37	10.8
Ti–6 Al–4 V	161	152	12.4	151	142	11.2	126	112	7.5
				152	143	11.8	125	110	7.7
302 S.S.	105	73	35.3	81	64	26.7	86	62	18.0
				98	68	35.4	81	60	19.7
Molybdenum	99	96	35.1	97	94	16.0	69	61	17.6
				91	88	34.8	66	60	21.4
Tantalum	88	87	8.3	86	85	7.6	57	56	8.0
	81	78	6.0	81	80	9.3	64	50	13.1
Niobium	62	54	11.4	65	55	14.3	64	50	13.1
				69	59	19.7			

*At 0.2% offset.
†Samples wetted with cesium in the glove box and tested at room temperature at a strain rate of 0.5 in./min.
‡Samples held 1000 hr at temperature (1200°C for Mo, Ta, and Nb; 650°C for others) over a 200°C cesium reservoir and tested at 200°C at a strain rate of 0.5 in./min.

cury, indium, lead, and bismuth. The corresponding grouping for ruthenium is lithium, sodium, potassium, copper, silver, gold, cadmium, mercury, indium, lead, tin, and tellurium.

Attention is called to

1. A compilation[36] of liquid-metal diffusion coefficients which updates an original survey by L. F. Epstein, Static and Dynamic Corrosion and Mass Transfer in Liquid Metals Systems, in *Liquid Metals Technology, Part I*, Chemical Engineering Progress Symposium Series, No. 20, pp. 67-81, American Institute of Chemical Engineers, New York, 1957.

2. A summary[37] of the behavior of niobium in potassium, with emphasis on the role of oxygen in the system chemistry. (J. H. Stang)

Selected Mechanical Properties of Cladding and Structural Materials

Iron- and Nickel-Base Alloys

A thermal-stress-fatigue program was conducted by Advanced Technology Laboratories Division[38] in which stress cycling was induced by thermally cycling a constrained specimen. A major departure from conventional data-presentation methods was made by plotting logarithmic plastic-strain range vs. logarithmic cycles to failure. A summary is presented of results of thermal-stress-fatigue testing on types 304 and 304L austenitic stainless steels; type 403 martensitic stainless steel; types A-302B and A-387D (Croloy $2\frac{1}{4}$) steels; Incoloy 800; and Zircaloy-2. The thermal-stress-fatigue behavior of these alloys was determined under a wide variety of test conditions.

A contribution to the field of fatigue testing was made by the development of a plastic-strain-measuring device and of techniques for graphical manipulation of recorded data. It was thus possible to report fatigue life in a range shorter by an order of magnitude than previously reported data. The use in this study of cyclic plastic strain instead of cyclic stress on graphs of fatigue life resulted in curves largely independent of such test conditions as mean temperature, time, and strain rate. Thus the results can be used, with little or no extrapolation, to estimate thermal-stress-fatigue life. Since the majority of fatigue results from earlier work are plotted on a stress basis, the test results obtained in this program were also plotted on this basis.

The results of comparative creep studies on type 304 stainless steel in Ar–O environments of various oxygen partial pressures at 815°C and 3400 psi were reported by workers at Oak Ridge.[39] At concentrations of oxygen below 70 ppm, the creep rate of 304 stainless steel decreased with increasing oxygen content in the environment. Above 70 ppm the creep rate in-

creased with increasing oxygen content, to a maximum at 256 ppm oxygen. Further increases in oxygen content produced decreases in the creep rate.

Increasing the temperature to 927°C at 2000-psi pressure produced the same trend in creep behavior as at 815°C. Below 70 ppm oxygen an adherent Cr_2O_3 surface scale formed which may act as a barrier to dislocations. A direct correlation was observed between the surface-crack depth and creep rate in the various environments. The maximum crack penetration occurred in the environment giving the highest creep rate (256 ppm oxygen). Even though the surface-crack density increased with higher concentrations of oxygen in the environment, the crack penetration decreased. This indicates that the strengthening effect at high concentrations of oxygen is due to the influence of oxygen in retarding crack growth.

Belgian researchers[40] report that plastic-fatigue tests on two pressure-vessel steels by compression–tension with a fixed maximum load show fairly wide scatter in results, as well as a marked influence of the direction in which the first stress is applied (tension or compression). Plastic-fatigue tests by alternate bending with a fixed maximum strain give more consistent endurance limits, and the data can be represented by a straight line on a plot of log deformation against log number of cycles to failure. Bend tests on specimens previously damaged by alternate bending plastic fatigue have shown them to be embrittled. The embrittlement does not appear to be associated with the presence of fatigue cracks.

Refractory Metals

An investigation was conducted by ManLabs, Inc.,[41] to determine the nature of the tensile-ductility transition in recrystallized molybdenum strip of three different interstitial contents. For a fine grain size the tensile-ductility transition temperature (T_d) and the brittleness transition temperature (T_b) were found to almost coincide, whereas with increase in grain size T_d increases and T_b decreases. The occurrence of a minimum in the fracture stress (σ_F) at T_d appears to be associated with the temperature dependence of the necking stress (σ_N). Prestraining above T_d was found to result in as much as a 20% increase in σ_F as determined at temperatures below T_d. In general, the mode of fracture initiation was found to be intergranular at T_d or below and cleavage above T_d. For test temperatures above and below T_d, crack initiation appears to be the controlling step in fracture. Considering σ_F as a flow stress corresponding to the fracture strain (ϵ_F), the variation of σ_F with temperature above T_d was predicted within about 15%. On the basis of a modification of the Cottrell relation for crack initiation, the increase in σ_F above T_d is associated with a decrease in both the flow-locking parameter (k_f) and the effective grain size.

The strain-rate behavior of the tensile-yielding and flow characteristics of arc-cast polycrystalline molybdenum of 99.97% purity was investigated at Battelle–Columbus[42] within the range of 10^{-6} to 10^{-1}/sec at 243, 293, and 373°K for two grain sizes, 0.027 and 0.098 mm. For 0.098-mm grains the strain-rate dependence of the lower yield stress can be described by a straight line of the form $\sigma_y = \alpha + \beta \log \epsilon$ over the whole range of strain rates examined. However, for 0.027-mm grains, the data fit several consecutive linear relations of the above form. The previous association of these different linear regions with different rate-controlling mechanisms was considered questionable for molybdenum. The semilog strain-rate dependence of the yield stress was consistent with Hahn's model for yielding when the stress dependence of the mobile dislocation density, ρ', was taken into account. Since ρ', from rate-cycling experiments, was found to be relatively insensitive to stress for single crystals, the observed log–log dependence of their yield stresses was also in agreement with the model. A correction for the stress dependence of ρ' changed the activation volume for yielding from a zero to a more realistic inverse function of stress, where the Peierls mechanism was believed to be rate controlling. The grain-size dependence of the lower yield stress was not a monotonic function of strain rate.

The effect of working reduction, stress-relief annealing, and recrystallized grain size on the tensile and notch-tensile properties of molybdenum and Mo–0.5 wt.% Ti was studied at Battelle–Columbus.[43] It was found that increasing the amount of working reduction increased the strength and reduced the tendencies toward brittle behavior. Stress-relief annealing did not alter the strength but lowered the transition temperature. Increasing the recrystallized grain size lowered the strength and raised the tran-

sition temperature. The notch–unnotch strength ratio began to decrease with decreasing temperature at temperatures below those at which the notched ductility fell to zero for all the microstructural conditions investigated.

The nature of fracture in unnotched tensile and notched tensile sheet and round specimens and V-notched and precracked Charpy type sheet specimens of both wrought stress-relieved and recrystallized molybdenum was investigated by Ault[44] over the temperature range −78 to 300°C. A sharp rise in the fracture stress of unnotched tensile samples, as the temperature was increased above the brittleness transition temperature (T_b), was found to be a result of an increase in flow stress due to plastic constraint and an increased strain rate, which resulted from the onset of necking at T_b. Quasibrittle fracture in notched tensile specimens occurred when the tensile stress at the elastic–plastic interface, beneath the root of the notch, reached a maximum critical value, which was independent of test temperature over the range −78 to 25°C, but dependent on microstructure. In the temperature range between 150 and 300°C, unnotched tensile and notched tensile samples alike fractured by a discontinuous ductile fibrous tearing process, as a result of the competition between the processes of tearing, through continued plastic flow, and local work hardening. Results from the V-notched and fatigue-cracked Charpy type impact tests demonstrated that crack initiation is the governing factor in the low-temperature (−78 to 25°C) fracture process for molybdenum.

The tensile properties of high-purity powder-metallurgy tungsten and W–1 wt.% ThO_2 alloy were determined at Westinghouse Electric Corp.[45] at various strain rates and temperatures (800 to 2400°C). The 1 wt.% ThO_2 imparts a slight overall increase in strength properties, although, above one-half the absolute melting temperature, these properties are affected by void formation. The tensile properties of pure tungsten and W–0.35 wt.% Ta single crystals (worked, and worked and recrystallized), investigated from room temperature to 1200°C, were found to be affected by carbon, particularly in the quenched condition. An alloy-screening program was conducted on W–25 wt.% Re, with 1 wt.% ThO_2 and 1 wt.% HfN additions, and on single crystals of W–3.5 wt.% TaC. The yield stress of a quenched W–3.5 wt.% TaC single crystal at 1600°C was found to be 74,000 psi.

Creep data for tungsten, W–25 wt.% Re, TZM molybdenum alloy, and AS-30 niobium alloy are presented by investigators at Thompson Ramo Wooldridge.[46] According to current test results, the creep strength of tungsten is less than that of W–25 wt.% Re sheet alloy at 3200°F. In the case of turbine alloys at 2000°F, preliminary tests show that the TZM alloy in the forged condition has a greater creep strength than cross-rolled AS-30 plate material.

The effects of a carbon addition and subsequent heat-treatments on the tensile properties of W–0.35 wt.% Ta and tungsten single crystals were determined at Westinghouse.[47] The addition of carbon had a pronounced effect on the yield strength of these crystals when they were quenched from 2200 or 2450°C. A maximum strengthening increment of 55,000 psi was observed at 600°C for tungsten crystals and about 45,000 psi for the W–0.35 wt.% Ta crystals. The increased strength was accompanied by a loss in ductility at about 600°C. These phenomena were attributed to precipitation hardening.

Zirconium Alloys

Farrow and Watkins[48] report on the effects of hydrogen on the brittleness of Zircaloy-2 and Zr–2.5 wt.% Nb pressure-tube alloys. Conventional Charpy-impact test specimens cut from plate materials were used to determine the effect of 100 ppm hydrogen. Widely differing results were obtained with different specimen and notch orientations. Therefore a drop-weight test was developed to assess the brittleness of actual pressure-tube sections; this test is described, and preliminary results are presented.

The influence on Zircaloy-2 of various embrittling factors in mechanical testing was examined by Ooestburg[49] utilizing microfractography of impact specimens, tensile tests at different temperatures and strain rates, and delayed-failure tests. It was found that the impact test is not suited for distinguishing brittle-to-ductile transitions in Zircaloy-2. Low-strain-rate embrittlement, detected in Zircaloy-2 and in some other zirconium alloys, was interpreted in terms of hydrogen embrittlement. The occurrence of a yield point was also observed and related to the hydrogen content. The influence of texture, particularly with re-

gard to the appearance of several load maxima and multiple necking, was discussed.

At Battelle–Northwest,[50] Zircaloy-2 pressure tubes were subjected to creep and stress-rupture tests under conditions of biaxial stress at temperatures of 300°C and above. Comparison of the results with the behavior of strip under uniaxial stress shows that tubing requires 60% higher stresses for comparable creep rates. Stress-rupture tests predict a 20-year life for the tubing at stresses more than four times the design stress for the reactor.

The superposition of 1.0% mean strain on constant-deflection cycled bending-fatigue specimens of Zircaloy-4 plate reduces the fatigue strength at both room temperature and 600°F, as reported by Knolls Atomic Power Laboratory.[51] The implications of these test results on recommended fatigue design procedures are examined. Limited studies were conducted on crack propagation in Zircaloy plate. In another study an oxide film formed by exposure to 680°F water for 72 hr was found to be detrimental to fatigue strength at room temperature. (J. A. De Mastry)

Selected Metallurgical Aspects of Cladding and Structural Materials

Zirconium

French investigators[52] have studied the so-called active-eutectoid alpha-zirconium alloys, containing added vanadium or nickel. Hardening of these alloys is caused by (1) rapid decomposition of the beta phase, with the appearance of fine, dispersed particles of ZrV_2 or Zr_2Ni compounds, and by (2) additions of elements soluble in the alpha phase, such as aluminum, titanium, or tin. The Zr_2Ni intermetallic was found to be a less active hardening agent than ZrV_2. The addition of aluminum or titanium had an adverse effect on the corrosion resistance of the alloy in steam. The ternary addition of tin, up to 4 wt.%, results in an alloy having good mechanical properties up to 500°C and good thermal stability after 3000 hr at 500°C. At 350 and 400°C the corrosion rate of Zr–V–Sn alloys remains higher than that of Zircaloy-2, but at 480°C the oxide layer on the vanadium-containing alloy is more adherent. The tensile properties of the most promising alloy, containing 1.5 wt.% vanadium and 1.5 wt.% tin, are as follows:

Temp., °C	Condition	Elastic limit, kg/mm²	Ultimate strength, kg/mm²	Elongation, %
20	Annealed	46	59	17
20	Beta quenched and tempered	69	85	6
500	Annealed	36	43	18
500	Beta quenched and tempered	39	42	15

After 14 days in steam at 400°C and 106 kg/mm² pressure, the hydrogen absorption of this alloy was less than 10% of the hydrogen theoretically produced.

The combined effects of oxygen and hydrogen on the mechanical properties of zirconium were examined by Westlake.[53] Polycrystalline tensile specimens of various Zr–O–H alloys were tested at 298, 178, and 77°K. Hydride precipitation and dissolved oxygen in quenched systems made individual contributions to the 0.2% offset yield strength which combined to produce a resultant strength increment, $\sigma_{0.2} = (\sigma_O^2 + \sigma_H^2)^{1/2}$. Ductility changes that were observed can be interpreted in terms of the various oxygen and hydrogen concentrations, testing temperatures, and dispositions of the hydride.

An X-ray study[54] of tempering in a ternary zirconium martensite has been conducted by Douglass. The stability of martensite in Zr–2 wt.% Nb–2 wt.% Sn, which was formed by quenching from the beta phase, was studied for times up to 2000 hr at temperatures in the range from 400 to 700°C. Both the a_0 and c_0 lattice parameters increased with tempering. Activation energy for the process was 58 kcal/mole. According to the phase diagram, the compound Zr_4Sn should be rejected from the supersaturated martensite, the a_0 parameter should increase, and c_0 should decrease. The observed increase in both parameters indicated that niobium precipitated with the tin and that the compound was not the suggested Zr_4Sn. Changes in hardness with time were similar to those found in age-hardening alloys. Hardness maxima were noted at 950 hr at 400°C and at 200 hr at 500°C. Overaging occurred in less than 20 min at both 600 and 700°C and resulted in coarser precipitates than those noted in the aged alloy. Fourier analysis of the broadened

peaks indicated that several nonuniform microstrains existed in the lattice initially. The microstrains were increased by tempering, but some strain remained after overaging of the martensite occurred. Retention of hardness after extensive tempering was probably due to both microstrains and the dispersed phase.

Investigators at the University of Cincinnati[55] have determined the isotherms of the Zr–Cr–O ternary system at 1200, 1500, and 1700°C, using metallographic and X-ray diffraction analyses of selected alloys.

Refractory Metals

The effects of temperature and strain rate on the yield strength of single-crystal niobium investigated[56] with the ⟨1 1 0⟩ direction parallel to the compression axis seem to be characterized by a modified form of the rate-process equation. Within the range of variables studied, the frequency factor has been found to be independent of stress, temperature, and microstructure and has a value of about 10^7/sec for the material investigated. The activation volume has been found to be dependent upon stress, but independent of microstructure. The internal (frictional) stress has been shown to vary as the square root of the dislocation density, as determined by etch pitting and optical microscopy.

The internal friction of niobium wires containing both oxygen and nitrogen was measured by van Ooijen and van der Goot[57] by means of the torsion-pendulum method. It was found that, after suitable heat-treatment (about 1000°C), of cold-worked wires containing oxygen, part of the oxygen atoms do not contribute to the internal friction nor to the normal Snoek peak (which is lowered), nor to the cold-work peak (which is completely absent). This is explained in terms of the formation of domains having ordered structures of oxygen atoms. In cold-worked wires containing both oxygen and nitrogen, the oxygen atoms were first found to precipitate or segregate spontaneously at dislocations, but, after a slight increase in the temperature (up to about 400°C), they were replaced irreversibly by nitrogen atoms. The Snoek peak caused by oxygen was found to be broadened owing to an interaction between the oxygen and nitrogen. In some cases an additional peak appeared.

The effects of strain aging on the room-temperature mechanical properties and internal-friction-relaxation peaks due to interstitial impurities in commercial niobium have been determined at the Battersea College of Technology.[58] The results showed that the strain-aging behavior of niobium is, in general, similar to the behavior of mild steels. The mechanism of aging is, however, different in that oxygen plays an important part in the aging of niobium by diffusing to free dislocations and then being replaced by carbon. In addition, it is suggested that carbon contributes to strain aging by cluster formation.

Studies at Boeing[59] on modifications of Nb–W–Hf alloys with yttrium additions have led to the successful development of C-129Y alloy, with the composition Nb–10 wt.% W–10 wt.% Hf–0.1 wt.% Y. This alloy has shown good strength at temperatures to 3500°F, excellent formability and weldability, and a subzero ductile-to-brittle transition temperature. Tungsten-arc welds of the alloy display 0.5T minimum bend radius in the as-welded condition, compared with 8T for the C-129 alloy. Weld strength was equal to that of the parent C-129Y alloy. The "Disil" oxidation-protective coating does not adversely affect the strength or ductility of C-129Y sheet material, but the coating does reduce the room-temperature ductility of fusion welds.

Investigators at the Massachusetts Institute of Technology have determined the constitution diagrams of the Nb–Ir and Nb–Rh systems by metallographic and X-ray techniques.[60,61] The solubility limits of terminal and intermediate phases, and solidus and transformation temperatures, were determined. In the Nb–Ir system, five intermediate phases were found, two of which melt congruently; three eutectic and three peritectic reactions occur. In the Nb–Rh system, there are nine intermediate phases; two eutectic, five peritectic, two eutectoid, and three peritectoid reactions were encountered.

Dunn and Webster[62] have described the necessary rolling and annealing procedures for developing the (1 1 0) preferred orientation in tantalum for use as a thermionic-emission material where electrodes of a uniform, high work function are needed. The development of a (1 1 0) [0 0 1] annealing texture is also reported. A preferential growth process due to low (0 0 1) gas–metal surface energy is considered an explanation of the observed growth of (1 1 0) grains.

At the University of California, Lawrence Radiation Laboratory,[63] single crystals of a series of Mo–Ta alloys were used to determine the mechanisms for the occurrence of cleavage and to increase the knowledge of electrical transport in transition-metal alloys. The investigation revealed that the alloys in the composition range of Mo–19 wt.% Ta to Mo–58 wt.% Ta cleave on the (100) planes. No intermediate phases or long- or short-range order of a dimension greater than 300 A were detected by lattice-parameter measurements or transmission-electron microscopy. The increase in critical resolved shear stress for plastic flow with increasing tantalum content results from a corresponding increase in the Peierls-Nabarro friction of dislocations produced by alloying, compositional deviations on {100} or {110}, and concomitant changes in the elastic coefficients. Cleavage occurs owing to a violation of the strain-energy restrictions on the elastic coefficients in a local region of the crystal. Alloying and the existence of composition deviations change the elastic coefficients, in the range of alloys which cleave, to values that marginally fulfill the strain-energy restrictions. The presence of a critical density of dislocations in a local region produces changes in the values of the elastic coefficients such that the crystal is locally energetically unstable. The crystal then cleaves on the {100} plane, which relieves the maximum strain energy.

Marked changes in the slope of the curve of electrical resistivity ($\rho_{273°K} - \rho_{4.2°K}$) vs. alloy composition at Mo–20 wt.% Ta, Mo–50 wt.% Ta, and Mo–88 wt.% Ta reveal that there is a relatively large change occurring in the density of states in the *d* and *s* bands, and/or marked changes in the elastic coefficients at these alloy compositions.

The effect of plastic deformation on the fine structure of molybdenum single crystals was studied[64] by Russian investigators. Molybdenum single crystals, 99.77% pure, obtained by electron-beam zone refining from twice-vacuum-arc-melted molybdenum, were cold rolled with a 2% maximum reduction per pass. The single crystals were highly ductile and sustained a total reduction of more than 90% at room temperature without failure. A study of deformation-induced changes in the single-crystal substructure revealed fragmentation and disorientation of the blocks whose boundaries were in the active slip planes. With increasing degree of deformation, the blocks turn in the direction of the force, and the disorientation increases. A fibrous structure begins to form when the deformation becomes greater than 80%. No hardness anisotropy was observed in as-cast single crystals. The microhardness along the (100), (110), and (111) planes was 156 to 157 kg/mm^2. The density of the etch pits was of the order of 10^3/cm^2 in both the (100) and (111) planes.

Passmore[65] has shown that transitions from ductile-to-brittle behavior of high-purity molybdenum occur with both decreasing temperature and increasing grain size. On the basis of the assumed temperature independence of the critical-stress criterion for cleavage fracture, both of these transitions were interpreted largely in terms of the plastic-strain dependence of this critical fracture stress.

An investigation of the yield-point phenomenon in molybdenum has been conducted by King and Spretnak[66] by determining changes in dislocation densities during discontinuous yielding. Tensile specimens were deformed various amounts up to and beyond the Lüder's strain, and the dislocation densities were measured over the entire deformed portion of the gauge sections. It was found that the dislocation density tends to increase linearly with plastic strain up to and beyond the Lüder's strain. The rate of multiplication at the end of the Lüder's strain increased with temperature up to 185°C, and, above 225°C, it decreased with increasing temperature.

Wronski and Fourdeux[67] have investigated the ductile-to-brittle transition temperature of polycrystalline tungsten and found it to be approximately 100°C higher in sintered material than in melted material of coarser grain size and probably higher purity. Whereas the brittle fracture stress of recrystallized swaged single crystals increased with decreasing temperature, no reproducible behavior was detected on testing sintered material. Reasons for this were sought using conventional metallurgical techniques, as well as replica and transmission-electron microscopy. It is only the last of these techniques that showed reproducibly that in sintered tungsten there are small gas bubbles or voids, which are not found in melted tungsten. The behavior of the bubbles in the as-received (warm-worked) sintered rod was studied as the material was annealed at 1080, 1550, and 1730°C to yield the fully recrystallized state.

Stanford University Press has recently published a book[68] for information on the general behavior of refractory metals, with property data for unalloyed metals included. Mechanical, oxidation, and thermal properties of chromium, niobium, molybdenum, rhenium, tantalum, tungsten, and vanadium are discussed and tabulated. Properties, cost, and size-availability data for commercial refractory-metal sheet alloys are appended.

A compilation of specific-heat, thermal-expansion, and thermal-conductivity data for materials of possible structural usefulness above 2500°F has been prepared at Battelle.[69] Data are presented graphically, with notations as to measurement methods and test conditions. Prominent laboratories currently making thermal-property measurements are identified.

Investigators at General Electric[70] have published the results of their enthalpy and thermal-expansion measurements on several of the refractory metals and alloys up to 2500°C.

Nickel-Base Alloys

The recrystallization behavior of Ni–Ta alloys, with and without the presence of fine precipitates in the structure, was studied in Germany.[71] The progress of primary recrystallization was followed in alloys of nickel with 0.01, 0.1, and 1.0 at.% tantalum. It can be shown that, in one particular alloy containing 0.1 wt.% tantalum and 0.02 wt.% oxygen, a large grain structure (0.5 mm in diameter) could be developed by primary recrystallization in thin sheets which had been cold worked to 97.5% reduction in thickness. Electron-transmission microscopy demonstrated that this phenomenon was linked to the occurrence of fine precipitates at subboundaries. A discussion is included on how fine precipitates under certain circumstances can exert a rather distinct retarding effect on nucleation rate. (N. M. Griesenauer)

Diffusion Studies

Numerical solutions of the equations for gas release from various shapes of crystals were carried out in Germany[72] with the aid of a digital computer. Results are given for spheres, 20 different forms of cylinders, and 30 different specific forms of parallelepipeds. Solutions are not exact, but sufficient accuracy is obtainable for any specific form, with proper interpolation from the graphs, to be useful in correlating actual fission-gas-release experiments. Graphs were prepared in the form of F vs. α or α^2, where F is the fractional gas release and α is a function of time, the diffusion coefficient, and characteristic length of the body. The authors indicate that a previously used approximation of Fick's equation for diffusion release of rare-gas atoms was adequate for $F \leq 0.25$, but not for $F > 0.25$. The release pattern may cover the whole range up to $F = 1$, and the graphs and tables have been prepared to include F values from 0 to 1. It should be noted that experimental results on fission-gas release indicate that the release process does not follow simple diffusion behavior.

Murray, Kuzuu, and Klints[73] have presented evidence of escape of helium by diffusion when irradiated zirconium is heated above the alpha-to-beta transformation temperature. Helium was introduced into commercial-grade zirconium by transmutation of 0.1 at.% boron added to zirconium. Diffusion anneals were conducted in the temperature range of 600 to 1400°C, and the fractional gas release at each temperature was determined by mass spectrometry. The diffusion coefficient of helium in beta zirconium was calculated to be $D = 2.3 \times 10^{-4} \exp(-35{,}600/RT)$ cm²/sec. Gas released from zirconium above the alpha-to-beta transformation temperature varied between 5 and 12% of the total gas content, and diffusivities at these temperatures were time independent. Below the alpha-to-beta transformation temperature, less than 1% of the total gas was released, and the diffusivities were time dependent. The authors point out that the small gas release and "apparent" diffusion in alpha zirconium is typical of other inert-gas–irradiated-metal systems which have been investigated, but the high fractional gas release and "true" diffusivities observed in beta zirconium show that helium can escape by solid-state diffusion.

Basic diffusion studies in refractory metals include a study of the self-diffusion and solute diffusion in molybdenum[74] using radioactive isotopes ^{99}Mo, ^{60}Co, and ^{95}Nb. Diffusion anneals were made in an argon atmosphere in the temperature range of 1850 to 2350°C. Serial sectioning methods were used to make the analysis. A reduction in the lattice diffusion coefficient of ^{60}Co in molybdenum apparently was caused by the use of argon, reducing the coefficient by

a factor of 6.3 at 1850°C and by 2.8 at 2350°C. Diffusivity results on polycrystalline materials are expressed by the following relations: $D = 0.5 \exp(-96{,}900/RT)$ cm²/sec for self-diffusion in molybdenum, $D = 18 \exp(-106{,}700/RT)$ cm²/sec for solute diffusion of ^{60}Co in molybdenum, and $D = 14 \exp(-108{,}100/RT)$ cm²/sec for solute diffusion of ^{95}Nb in molybdenum. Self-diffusion in molybdenum for single crystals was given as $D = 0.1 \exp(-92{,}200/RT)$ cm²/sec.

Measurements have also been made of the self-diffusion in single-crystal tungsten and the solute diffusion of rhenium by radioactive-tracer methods.[75] The isotopes ^{185}W, ^{183}Re, and ^{184}Re were produced by deuteron bombardment, and diffusion heating was accomplished in high vacuum by induction heating. The diffusivities of the two systems were expressed as $D = 42.8 \exp(-153{,}100/RT)$ cm²/sec for self-diffusion of tungsten, and $D = 275 \exp(-162{,}800/RT)$ cm²/sec for the solute diffusion of rhenium tracers.

The interdiffusion in Nb/Nb–8.5 at.% Ti and Nb/Nb–35 at.% Ti couples has been measured[76] at temperatures between 1300 and 2000°C. Concentration–penetration data were obtained from electron-microprobe scans of the diffusion couples. Plots of log D vs. $1/T$ appeared to be linear up to 1500°F, but at higher temperatures the plots showed some curvature, which increased with increasing titanium alloy. Values for the activation energy and frequency factor for self-diffusion of ^{95}Nb in niobium were reported as 110,000 cal/gram atom and 500 cm²/sec, respectively, and can be compared with data from Steedly et al. (Q = 95,000 cal/gram atom, D_0 = 1.3 cm²/sec) and from Graham et al. (Q = 105,000 cal/gram atom, D_0 = 12.4 cm²/sec).

(A. N. Ashurst)

Ceramic Technology

The mechanical behavior of both single-crystal and polycrystalline MgO has been compared at different temperatures by Day and Stokes.[77] With increasing temperature, single crystals showed increasing interpenetrability and multiplicity of slip systems. Above 1700°C, slip was very flexible. Slip systems with different Burgers vectors completely interpenetrated each other, and slip occurred over a variety of slip planes. Rearrangement of dislocations by polygonization was observed, and in certain cases recrystallization could be obtained. Polycrystalline ceramics showed a brittle-to-ductile transition with increasing temperature. At low temperatures any structural discontinuity capable of blocking slip dislocations, including subgrains and grain boundaries, induced cleavage crack nucleation and brittle fracture. At intermediate temperatures (1400 to 1700°C), more slip occurred, but grains could not conform adequately to each other's changes in shape to allow the ceramic to behave as if it were flexible. The constraints caused intergranular crack nucleation and brittle fracture. At temperatures above 1700°C, as with single crystals, the polycrystalline MgO had flexible slip. The polycrystalline matrix deformed plastically and necked down to a ductile fracture. Polygonization and recrystallization of the deforming grains also contributed to relaxation of internal stresses. Slight porosity caused an increase in the brittle-to-ductile transition temperature.

The structure of explosively shocked MgO single crystals was investigated[78] by Battelle–Columbus. Although ionic crystals with the rock-salt structure, such as MgO, have been used as models to study the basic processes involved in plastic flow at low deformation rates, little is known about their response to high-velocity deformation. In this investigation the structural changes induced in MgO crystals by plane shock waves were studied by etch-pit metallography and by electron-spin resonance. Dislocations and cracks were generated at a pressure estimated to be about 47 kbars. In general, the density of slip bands in the shocked crystals, about 10^4 to 10^5 dislocations/cm², was greater than for crystals deformed in slow compression to the same or greater strain, suggesting that more dislocation sources are activated during shock loading. The microstructure suggests that slip preceded cracking and that some of the cracks were nucleated at the intersections of diagonal edge-dislocation slip bands, where stress concentrations were high. Vacancies detectable by electron-spin-resonance measurements were created in MgO crystals by explosive shocking. None could be detected in crystals deformed in slow compression.

A review of rare-earth cermets has been prepared by Samsonov.[79] It includes the preparation, methods, and uses of rare-earth bo-

rides, carbides, nitrides, silicides, and sulfides.

The fission-fragment-induced expansion of several ceramic materials has been studied[80] by Battelle–Columbus. The technique used was to recoil fission fragments into one face of thin, flat, ceramic specimens and then measure the spherical curvature caused by the irradiation. Fission-fragment-induced expansion increased in the order: MgO < SiO_2 < BeO < graphite < Al_2O_3 < ZrO_2 < pyrolytic carbon < SiC. No difference in expansion was observed for single-crystal and polycrystalline specimens. The expansion of single-crystal alpha Al_2O_3 was found to be independent of crystallographic orientation, and the expansion normal to the surface was at least three times the expansion in the surface plane. It appeared that fission-fragment-induced stresses were preferentially relieved by expansion normal to a free surface. Damage annealing during postirradiation heating was measured, and approximate values for radiation expansion coefficients and stresses in irradiated specimens were calculated.

The crystal structure of $TiNb_{24}O_{62}$ ($TiO_2 \cdot 12Nb_2O_5$) has been defined by Roth and Wadsley.[81] The $TiNb_{24}O_{62}$ is monoclinic, with a = 29.78, b = 3.821, c = 21.12 A, and β = 94.9°, and its space group is C2. The structure, refined by two-dimensional Fourier methods, contains ReO_3 type blocks of metal–oxygen octahedra, 3 by 4 and infinite in extension along b. These join up in pairs, and the double blocks pack together by additional edge sharing, with metals in tetrahedral coordination at each of the junctions. (D. J. Bowers)

Radiation Effects in Nonfuel Materials

Studies were carried out at Harwell[82] on a 0.24 wt.% carbon ferritic steel to investigate strengthening and embrittlement as functions of neutron dose, irradiation temperature, and metallurgical structure. The kinetics of recovery of radiation-induced hardening were studied by postirradiation annealing for various periods of time at several temperatures. The maximum changes in properties were found for irradiation temperatures below 190°C, where $\Delta\sigma_y$, the increase in lower yield strength, and ΔT, the increase in ductile-to-brittle transition temperature, can be represented by the following:

$$\Delta\sigma_y\,(\text{psi}) = 14.6\ (\phi t)_f^{1/4}$$

$$\Delta T(°\text{C}) = 38.0\ (\phi t)_f^{1/4}$$

Here $(\phi t)_f$ is fission-neutron exposure in units of 10^{18} neutrons/cm^2. (The British practice of reporting fission-neutron dose is not easy to compare with the U. S. practice of giving exposure to neutrons of over 1-Mev energy.)

It was noted that recovery of radiation-induced property changes occurred during irradiation for irradiation temperatures greater than 250°C and became more pronounced as the temperature was increased. A quenched-and-tempered structure showed only small changes in ΔT for exposures of 9.0×10^{18} neutrons/cm^2 (thermal) and 7.6×10^{17} neutrons/cm^2 (fast). Specimens in all other conditions of heat-treatment showed an increase of about 30°C in ΔT for the same exposure. Postirradiation annealing at 450°C produced nearly a 90% recovery of $\Delta\sigma_y$ and ΔT. A calculated activation energy for this recovery process was approximately 3.18 ev.

In similar studies, mild and low-carbon steels were irradiated at about 20°C to an exposure of 1.70×10^{18} neutrons/cm^2 (fast) and subsequently annealed for 1 hr at temperatures up to 400°C. The effects of this irradiation and annealing on the mechanical properties were noted.[83]

A method developed by workers at Argonne National Laboratory[84] for measuring and reporting neutron exposure for radiation-damage studies uses a calculated neutron-spectrum shape whose magnitude is determined by the reaction $^{54}Fe(n,p)^{54}Mn$. A unit, called RDU, is used for reporting exposure. Steel specimens were irradiated in three very different reactor spectra, and the resulting embrittlements were compared.

A procedure used to obtain estimates of the changes in the ductile-to-brittle transition temperature of ferritic steel due to neutron irradiation was developed by Bettis[85] researchers. A postulated damage model, which accounts for neutron spectral differences between irradiation locations, was used to obtain a physically more meaningful measure of exposure than the usually cited neutron exposure above 1 Mev. Changes in transition temperature for A-302B pressure-vessel steel were successfully correlated with this newer exposure parameter.

Studies were made at Vallecitos[86] to determine if the radiation stability of reactor-

pressure-vessel steels is altered by the simultaneous application of stress. The specimens were cut from a plate of the same heat of ASTM A-302 grade B steel as was used in construction of the Dresden Nuclear Power Station reactor pressure vessel. The specimens were stressed and unloaded at least 30 times owing to reactor shutdown and scrams. Neutron exposure, as indicated by a nickel flux monitor, was 4.35×10^{19}/cm^2 (>1 Mev) for the stressed specimen and 2.64×10^{19}/cm^2 (>1 Mev) for the unstressed control specimen. The impact strength of the stressed material was found to be greater than the impact strength of the unstressed material, in spite of the somewhat lower exposure on the unstressed bar.

Internal friction studies were made by Brookhaven[87] workers in an investigation of the effect of irradiation on the precipitation of carbon from solid solution in alpha iron. An enhancement of precipitation, which was found to saturate after a fast exposure of 3×10^{15} neutrons/cm^2, was attributed to the formation of nucleation sites during irradiation. Bombardment with 2-Mev electrons to an exposure of 1.8×10^{15} electrons/cm^2 did not produce enhanced precipitation.

The Russians[88] found that the wear resistance of carbon steel, which had been annealed and quenched at 850°C, was lowered by exposure to 1×10^{18} neutrons/cm^2 (presumably at reactor ambient temperature, approximately 100°C). Low irradiation exposures reduced the hardness of annealed specimens; further irradiation improved the wear resistance. These effects were attributed to the neutron bombardment rather than to any thermal treatment.

A review article[89] that discusses potential uses of stainless steels in reactors also reports a summary of the effects of neutron irradiation on the mechanical properties, structure, and phase changes. These radiation-induced property changes, particularly the adverse effect on the tensile ductility, were discussed by Harwell[90] researchers. It is believed that the reduction in ductility at elevated temperature is a function of thermal-neutron exposure rather than fast exposure. The ductility cannot be restored by postirradiation annealing. It was found, however, that some control could be exercised over these radiation-induced changes in properties by initial cold working and annealing to produce a fine grain size. Coarse precipitates within the grains were also beneficial.

A second austenitic stainless steel being studied at Oak Ridge[91] is a niobium-stabilized Fe–20 wt.% Cr–25 wt.% Ni alloy. The effect of heat-treatment on the stress-to-rupture properties under constant stress during irradiation at 650°C was studied. The stress-to-rupture data are shown in Fig. IV-2, and the effects of heat-treatment on the fracture ductility of the material after irradiation are given in Table IV-2. Although the times to rupture were not markedly affected by the irradiation, the exposure reduced the ductility at fracture significantly.

Research done at Battelle–Northwest[92] on the effect of neutron irradiation on the deformation behavior of molybdenum showed that slip lines formed by equivalent strains were coarse and distinct in the irradiated material and unresolvable in the unirradiated. Researchers at the Franklin Institute[93] have shown that irradia-

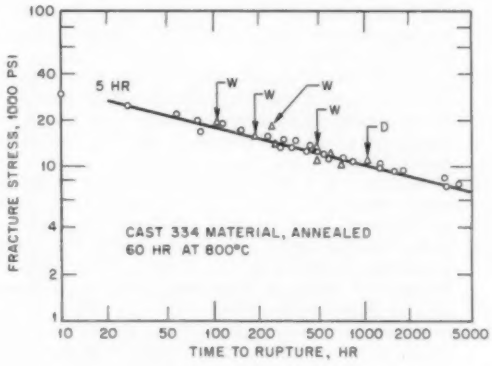

Fig. IV-2 Effects of heat-treatment and irradiation on stress-rupture properties of niobium-stabilized 20 wt.% Cr–25 wt.% Ni stainless steel[92] at 650°C. D, test discontinued; W, fracture at weld; Δ, in-reactor results; ○, out-of-reactor results.

Table IV-2 EFFECT OF HEAT-TREATMENT AND IRRADIATION ON THE FRACTURE DUCTILITY OF NIOBIUM-STABILIZED 20 WT.% Cr–25 WT.% Ni STAINLESS STEEL[91] AT 650°C

Material designation	Annealing treatment		Strain at fracture,* %	
	Temp., °C	Time, hr	Unirradiated	Irradiated
Cast R121	1050	½	3.8	1.9
Cast 334	800	60	20.4	4.4

*Average values for all specimens tested.

tion of zone-refined molybdenum to a total neutron exposure of 8×10^{17} neutrons/cm^2 at 600°C produces a low density of large prismatic dislocation loops. There were about 2×10^{13} of these loops per cubic centimeter, and they had an average diameter of 1100 A. Diffraction-contrast experiments established that the loops were formed by the aggregation of interstitial atoms. (F. R. Shober)

References

1. O. Zmeskal and K.-H. Lin, A Study of the Oxidation of Zirconium-Niobium Alloys in the Temperature Range 300°–500°C, USAEC Report COO-1000-1, University of Toledo, Mar. 3, 1965.
2. J. T. Demant and J. N. Wanklyn, The Effects of Contamination on the Oxidation of Zirconium in Steam, British Report AERE-R-4788, March 1965.
3. E. Hillner, Hydrogen Absorption in Zircaloy During Aqueous Corrosion, Effect of Environment, USAEC Report WAPD-TM-411, Westinghouse Electric Corp., Bettis Atomic Power Laboratory, November 1964.
4. Oak Ridge National Laboratory, Reactor Chemistry Division Annual Progress Report for Period Ending January 31, 1965, USAEC Report ORNL-3789, April 1965.
5. D. L. Douglass and C. Wagner, The Oxidation of Anion-Deficient Zirconia and Its Relationship to the Oxidation of Zirconium, USAEC Report GEAP-4544, General Electric Company, Vallecitos Atomic Laboratory, July 31, 1964.
6. J. Mazza and J. R. Galvele, Corrosion of Superpure Aluminum in Distilled Water at High Temperature, *J. Nucl. Mater.*, 13(1): 92-99 (1964).
7. J. D. Jackson and W. K. Boyd, Stress-Corrosion Cracking of Aluminum Alloys, Report DMIC-Memo-202, Battelle Memorial Institute, Defense Metals Information Center, Feb. 15, 1965.
8. General Electric Company, Nuclear Materials and Propulsion Operation, High-Temperature Materials and Reactor Component Development Programs, Volume I. Materials, USAEC Report GEMP-334A, Feb. 26, 1965.
9. G. Chaudron, Quarterly Summary [Report] No. 9 [On Corrosion of Stainless Steels Under Stress], July 1–September 30, 1964, USAEC Report EURAEC-1213, Centre National de la Recherche Scientifique, 1964.
10. A. P. Larrick, The Effects of Reactor Decontaminating Solutions on Intergranularly Corroded Type 304 Stainless Steel, USAEC Report HW-SA-3628, Hanford Atomic Products Operation, Oct. 9, 1964.
11. Hanford Atomic Products Operation, Metallurgy Research Operation. Quarterly Progress Report, October–December 1964, USAEC Report HW-84573, Jan. 15, 1965.
12. D. W. Koch, K. F. Riskevics, and E. E. Ritchie, Advanced Test Reactor. Investigation of the Corrosion Behavior of Materials of Construction, USAEC Report IDO-24460, The Babcock & Wilcox Co., Aug. 1, 1963.
13. D. N. Braski, Preliminary Investigation of Effect of Environmental Factors on Salt Stress Corrosion Cracking of Ti–8 Al–4 Mo–1 V at Elevated Temperatures, Report NASA-TM-X-1048, National Aeronautics and Space Administration, Langley Research Center, December 1964.
14. R. F. Voitovich, Kinetics of Oxidation of Niobium Alloys, *Mekhanizm Vzaimodeistviya Metal. i Gae. Akad. Nauk SSSR, Inst. Fiz. Khim.*, 154-159 (1964).
15. I. N. Frantsevich and R. F. Voitovich, Oxidation of Binary Alloys, *Mekhanizm Vzaimodeistviya Metal. i Gae. Akad. Nauk SSSR, Inst. Fiz. Khim.*, 135-142 (1964).
16. D. A. Prokoshkin, E. V. Vasil'eva, and A. M. Ryabyshev, Oxidation Kinetics and Mechanisms of Niobium-Molybdenum Alloys, *Issled. po Zharoproch. Splavam, Akad. Nauk SSSR, Inst. Met.*, 10: 233-239 (1963).
17. P. Kofstad and S. Espevik, Low-Pressure Oxidation of Niobium at 1200-1700°C, *J. Electrochem. Soc.*, 112(2): 153-160 (February 1965).
18. N. Terao, Structure of Oxides of Niobium: Transformation of the γ-Nb_2O_5 to α-Nb_2O_5 and the Formation of NbO_2 (in French), *Japan. J. Appl. Physics*, 4: 8-15 (January 1965).
19. R. W. Bartlett and J. W. McCamont, The Influence of Crystal Orientation on the Oxidation of Tungsten, *J. Electrochem. Soc.*, 112: 148-152 (February 1965).
20. F. Saegusa, Oxidation of Tantalum in Carbon Dioxide and Carbon Monoxide, Report WVT-6416 (AD-610494), Watervliet Arsenal, September 1964.
21. D. J. Bracco, L. Sama, and P. Lublin, Identification of Microstructural Constituents and Chemical Concentration Profiles in Coated Refractory Metal Systems, Quarterly Progress Report No. 1, TR-64-717.3, General Telephone & Electronics Laboratories, Oct. 15, 1964.
22. Boeing Co., Fluidized-Bed Techniques for Coating Refractory Metals, First Interim Engineering Progress Report, 8 December 1964–8 March 1965, Report IR-8-184 (I), Mar. 8, 1965.
23. E. B. Bitzer, J. Rexer, and R. G. Fenish, High Temperature Protective Coatings for Refractory Metals, Progress Report No. 1, Union Carbide Corp., Jan. 23, 1965.
24. J. M. Criscione, R. A. Mercuri, E. P. Schram, A. W. Smith, and H. F. Volk, High Temperature Protective Coatings for Graphite, Report ML-TDR-64-173(Pt. II), Union Carbide Corp., August 1964.
25. J. H. Swisher, Solubility of Iron, Nickel, and Cobalt in Liquid Potassium and Effect of Oxygen Gettering Agents on Iron Solubility, Report NASA-TN-D-2734, National Aeronautics and Space Administration, Lewis Research Center, March 1965.
26. Papers presented at AEC-NASA Liquid Metals Information Meeting, Gatlinburg, Tenn., Apr. 21–22, 1965.
    a. R. L. McKisson and R. L. Eichelberger, Status Summary: Solubility and Diffusion Studies of Ultra Pure Transition Elements in Ultra Pure Alkali Metals.
    b. W. S. Ginell and R. J. Teitel, Solubility of Transition Elements in Molten Potassium.
    c. P. M. Winslow, Synopsis of Cesium Compatibility Studies.

27. MSA Research Corp., Effect of High-Temperature Sodium on Austenitic and Ferritic Steels. Physical Properties of Materials, Progress Report No. 53, January 1965, USAEC Report MSAR-65-28, Feb. 24, 1965.
28. Papers given at Sodium Component Program Development Committee Information Meeting, Chicago, Ill., June 16–17, 1965.
    a. R. C. Andrews and F. Tepper, The Effect of Sodium on the Mechanical Properties of Austenitic and Ferritic Steels.
    b. R. W. Lockhart and R. S. Young, General Electric Sodium Mass-Transfer Program.
29. Brookhaven National Laboratory, Nuclear Engineering Department Annual Report, December 31, 1964, USAEC Report BNL-900, April 1965.
30. A. H. Fleitman, A. J. Romano, and C. J. Klamut, Corrosion of Carbon Steel by Boiling and Superheated Mercury, *Nucl. Sci. Eng.*, 22(1): 24-32 (May 1965).
31. D. H. Jansen and E. E. Hoffman, Type 316 Stainless Steel, Inconel, and Haynes Alloy No. 25 Natural-Circulation Boiling-Potassium Corrosion Test Loops, USAEC Report ORNL-3790, Oak Ridge National Laboratory, June 1965.
32. D. H. Jansen and E. E. Hoffman, Niobium-1% Zirconium, Natural-Circulation, Boiling-Potassium Corrosion Loop Test, USAEC Report ORNL-3603, Oak Ridge National Laboratory, May 1964.
33. C. J. Lymperes, J. D. Chapman, and G. F. Schenck, Interactions in a Type 316 Stainless Steel–NaK Cb–1 Zr Alloy System, USAEC Report TIM-896, Pratt & Whitney Aircraft Division, United Aircraft Corp., June 23, 1965.
34. D. W. Levinson, Stress-Dependent Interactions Between Cesium and Other Materials, Report IITRI-B215-22, Illinois Institute of Technology Research Institute, Nov. 18, 1964.
35. D. W. Rhys and E. G. Price, Resistance of Indium and Ruthenium to Liquid-Metal Attack, *Metal Ind. (London)*, 105(7): 243-245 (August 1964).
36. L. F. Epstein, J. D. Mottley, and J. Q. Pon, Diffusion Coefficients in Liquid Metals—A Compilation of Published Literature, Report N65-16551, General Electric Company, Vallecitos Atomic Laboratory, October 1964.
37. A. P. Litman, The Effect of Oxygen on the Corrosion of Niobium by Liquid Potassium (thesis), USAEC Report ORNL-3751, Oak Ridge National Laboratory, July 1965.
38. K. E. Horton and J. M. Hallander, Investigation of Thermal-Stress-Fatigue Behavior of Stainless Steels. Final Report, USAEC Report ATL-A-144 (EURAEC-1299), American Radiator & Standard Sanitary Corp., Advanced Technology Laboratories Division, Oct. 31, 1964.
39. P. Rodriguez, High-Temperature Creep Behavior of Type 304 Stainless Steel in Argon–Oxygen Environment of Different Oxygen Partial Pressures, USAEC Report ORNL-TM-1124, Oak Ridge National Laboratory, May 5, 1965.
40. National Metallurgical Research Center, Belgium, Study of the Embrittlement by Plastic Fatigue of Steel Used for Reactor Vessels, Quarterly Report No. 3, July 1–September 30, 1964, USAEC–Euratom Report EURAEC-1207.
41. B. S. Lement and K. Kreder, The Tensile Ductility-Transition in Molybdenum, Report WADD-TR-61-181(Pt. IV), ManLabs, Inc., July 1964.
42. R. N. Orava, The Strain-Rate Dependence of Yielding and Flow in Molybdenum, *Trans. AIME*, 230: 1614-1622 (December 1964).
43. A. G. Imgram, J. W. Spretnak, and H. R. Ogden, Effect of Metallurgical Structure on the Tensile and Notch-Tensile Properties of Molybdenum and Mo–0.5 Ti, *Trans. AIME*, 230: 1345-1352 (October 1964).
44. R. T. Ault, Fracture of Molybdenum, *Trans. AIME*, 230: 1443-1453 (October 1964).
45. H. G. Sell, G. W. King, R. H. Schnitzel, and N. F. Cerulli, Physical Metallurgy of Tungsten and Tungsten-Base Alloys, Report WADD-TR-60-37 (Pt. V), Westinghouse Electric Corp., May 1964.
46. J. C. Sawyer and C. H. Philleo, Generation of Long-Time-Creep Data of Refractory Alloys at Elevated Temperatures, Report NASA-CR-54287, Thompson Ramo Wooldridge Inc., Jan. 15, 1965.
47. R. H. Schnitzel, The Effects of a Carbon Addition on the Tensile Properties of W–0.35 Per Cent Ta and Tungsten Single Crystals, *Trans. Am. Soc. Metals*, 58: 74-84 (1965).
48. M. Farrow and B. Watkins, The Effect of Hydrogen on the Embrittlement of Zirconium-Base Pressure Tubes, *J. Nucl. Mater.*, 15: 208-219 (1965).
49. G. Ooestberg, Some Observations on the Ductility of Zirconium Alloys with Special Reference to the Effect of Hydrogen, *J. Inst. Metals*, 93: 223-228 (March 1965).
50. R. C. Aungst, Stress Rupture Tests of Zircaloy-2 Pressure Tubes, USAEC Report BNWL-8, Battelle–Northwest, Pacific Northwest Laboratory, January 1965.
51. D. F. Mowbray, Effects of 1.0% Superimposed Mean Strain on the Bending Fatigue Strength of Zircaloy-4, *Nucl. Appl.*, 1: 39-48 (February 1965).
52. R. Syre, A. Guilhaudis, J. Orsag, M. Croutzeilles, R. Bourbon, and J. Bonmarin, Zirconium Alloys. Final Report No. 1, April 1, 1962–March 31, 1964, USAEC–Euratom Report EURAEC-1270, Campagnie Pechiney, Paris, July 1964.
53. D. G. Westlake, The Combined Effects of Oxygen and Hydrogen on the Mechanical Properties of Zirconium, *Trans. AIME*, 233: 368-372 (February 1965).
54. D. L. Douglass, An X-Ray Study of Tempering in a Ternary Zirconium Martensite, *J. Nucl. Mater.*, 15: 49-56 (1965).
55. S. K. Rhee and M. Hoch, The System Chromium-Zirconium-Oxygen at 1200, 1500, and 1700°C, *Trans. AIME*, 130: 1687-1690 (December 1964).
56. D. C. Huffaker, Yield Behavior of Niobium Single Crystals, USAEC Report TID-21599, University of Illinois, September 1964.
57. D. J. van Ooijen and A. S. van der Goot, Internal Friction Caused by Oxygen and Nitrogen in Niobium, *Philips Res. Rept.*, 19: 505-519 (December 1964).
58. Z. C. Szkopiak and L. W. Derry, Some Strain Aging Effects in Commercial Niobium, *J. Nucl. Mater.*, 13: 130-136 (1964).
59. R. T. Torgerson, Development and Evaluation of C-129Y (Cb–10 W–10 Hf–0.1 Y) Columbium Alloy, Report D2-20282-1, Boeing Co., Mar. 20, 1964.
60. B. C. Giessen, R. Koch, and N. J. Grant, The Niobium (Columbium)-Iridium Constitution Diagram, *Trans. AIME*, 230: 1268-1273 (October 1964).
61. D. L. Ritter, B. C. Giessen, and N. J. Grant, The

Niobium (Columbium)-Rhodium Binary System. Part I—The Constitution Diagram, *Trans. AIME*, 230: 1250-1259 (October 1964).
62. C. G. Dunn and H. F. Webster, Development of a (1 1 0) Preferred Orientation in Rolled and Annealed High-Purity Tantalum, *Trans. AIME*, 230: 1567-1570 (December 1964).
63. L. I. Van Torne, The Electrical Transport and Mechanical Properties of Tantalum–Molybdenum Alloy Single Crystals, USAEC Report UCRL-11752, University of California, Lawrence Radiation Laboratory, January 1965.
64. E. M. Savitskii and N. M. Bokareva, Effect of Plastic Deformation on the Fine Structure of Molybdenum Single Crystals, *Dokl. Akad. Nauk SSSR*, 159: 1137-1139 (Dec. 11, 1964).
65. E. M. Passmore, Correlation of Temperature and Grain Size Effects in Ductile-Brittle Transition of Molybdenum, *Phil. Mag.*, 8(11): 441-450 (March 1965).
66. G. W. King and J. W. Spretnak, An Investigation of the Yield-Point Phenomenon in Molybdenum, *Trans. AIME*, 230: 1481-1484 (October 1964).
67. A. Wronski and A. Fourdeux, The Ductile-Brittle Transition in Polycrystalline Tungsten, *J. Less-Common Metals*, 8: 149-158 (March 1965).
68. T. E. Tietz and J. W. Wilson, *Behavior and Properties of Refractory Metals*, Stanford University Press, Stanford, Calif., 1965.
69. W. D. Wood and H. W. Deem, Thermal Properties of High-Temperature Materials, Report RSIC-202, Battelle Memorial Institute, June 1, 1964.
70. J. B. Conway, R. A. Hein, R. M. Fincel, Jr., and A. C. Losekamp, Enthalpy and Thermal Expansion of Several Refractory Metals to 2500°C, USAEC Report GE-TM-64-2-8, General Electric Company, Advanced Technology Services, February 1964.
71. K. Detert and J. Ziebs, The Recrystallization Behavior of Ni–Ta Alloys and the Role of Fine Precipitates, *Trans. AIME*, 233: 51-56 (January 1965).
72. T. Lagerwall and K. E. Zimen, The Kinetics of Rare-Gas Diffusion in Solids, USAEC–Euratom Report EURAEC-772, Hahn-Meitner-Institute für Kernforschung, Berlin, 1964.
73. G. T. Murray, H. Kuzuu, and V. Klints, The Diffusion and Precipitation of Helium in Zirconium, *J. Nucl. Mater.*, 15: 140-142 (1965).
74. J. Askill, Tracer Diffusion Studies in Molybdenum, Report CONF-691-9, presented at the Conference on Diffusion in Body-Centered Cubic Materials, Gatlinburg, Tenn., September 1964.
75. R. L. Andelin, J. D. Knight, and M. Kahn, Diffusion of Tungsten and Rhenium Tracers in Tungsten, *Trans. AIME*, 233: 19-24 (January 1965).
76. T. C. Reuther, Jr., Diffusion in Columbium-Rich Columbium–Titanium Alloys with Consideration of the Possibility that the Diffusion Coefficient Is Time Dependent, Report NRL-6221, Naval Research Laboratory, Dec. 14, 1964.
77. R. B. Day and R. J. Stokes, Grain Boundaries and the Mechanical Behavior of Magnesium Oxide, Report CONF-641116-4, presented at the Conference on the Role of Grain Boundaries and Surfaces in Ceramics, Raleigh, N. C., 1964.
78. M. J. Klein, The Structure and Annealing Behavior of Explosively Shocked MgO Crystals, Report AROD-4434:2, Battelle Memorial Institute, Jan. 5, 1965.
79. G. V. Samsonov, Rare Earth Cermets, Report JPRS-28165, translated from *Tugoplavkie Soedineniya Redkozemel'nykh Metallov s Nemetallami* (Russian), pp. 53, 59-62, 88-92, 112-114, 170, 185, 214-215, 224, 239-240, 1964.
80. T. S. Elleman, R. B. Price, and D. N. Sunderman, Fission-Fragment-Induced Expansion in Ceramic Materials, *J. Nucl. Mater.*, 15: 164-178 (1965).
81. R. S. Roth and A. D. Wadsley, Mixed Oxides of Titanium and Niobium. The Crystal Structure of $TiNb_{24}O_{62}$ ($TiO_2 \cdot 12Nb_2O_5$), *Acta Cryst.*, 18: 724-730 (Apr. 10, 1965).
82. D. R. Harries, C. Judge, and B. Edmondson, Radiation Damage and Recovery in a 0.24 Wt.% Carbon Steel, British Report AERE-R-4846, January 1965.
83. D. R. Harries, A. G. Ardy, and A. F. Bartlett, Radiation Hardening in Mild and Low Alloy Steels, *J. Iron Steel Inst. (London)*, 202: 518-522 (June 1964).
84. A. D. Rossin, Comparison of Neutron Embrittlement of Steel in Different Reactor Spectra, *Nucl. Struct. Eng.*, 1: 76-82 (January 1965).
85. K. Shure, Radiation Damage Exposure and Embrittlement of Reactor Pressure Vessels, USAEC Report WAPD-TM-471, Westinghouse Electric Corp., Bettis Atomic Power Laboratory, November 1964.
86. M. B. Reynolds, The Effect of Stress on the Radiation Stability of ASTM A302 Grade B Pressure Vessel Steel, *Mater. Res. Std.*, 3: 644-645 (August 1963).
87. A. C. Damask, Effect of Neutron Irradiation on Precipitation of Carbon in Alpha–Iron, USAEC Report BNL-8418, Brookhaven National Laboratory, 1964.
88. E. A. Markovskii and M. M. Krasnoshchekov, Antifriction Characteristics of Neutron-Irradiated Steel, *At. Energy USSR*, 18: 72-73 (January 1965).
89. G. Rossi and A. Cignolini, Problems Arising from the Use of Some Types of Stainless Steels in Nuclear Reactors, *Met. Ital.*, 56: 482-492 (October 1964).
90. P. C. Pfeil and D. R. Harries, Effects of Irradiation in Austenitic Steels and Other High Temperature Alloys, Report CONF-446-49, presented at the American Nuclear Society Tenth Annual Meeting, Philadelphia, Pa., June 1964.
91. Oak Ridge National Laboratory, Gas-Cooled Reactor Program Semiannual Progress Report For Period Ending March 31, 1965, USAEC Report ORNL-3807, June 1965.
92. J. L. Brimhall, The Effect of Neutron Irradiation on Sliplines in Molybdenum, USAEC Report BNWL-44, Battelle–Northwest, Pacific Northwest Laboratory, March 1965.
93. J. D. Meakin and I. G. Greenfield, Interstitial Loops in Neutron Irradiated Molybdenum, *Phil. Mag.*, 8(11): 277-290 (February 1965).

Section V

Reactor Materials

Special Fabrication Techniques

Melting, Casting, and Working

Nuclear Metals Division of Textron Inc.[1,2] is concentrating on extruding and drawing the W–25 wt.% Re alloy into ¼-in.-OD tubing with a 20-mil wall and 0.080-in.-OD tubing with an 8-mil wall. The effects of temperature and reduction are being investigated using Mo–CaC_2 cores and extrusion temperatures of 1200 and 1500°C. Inconsistent results and poor extrusions were obtained. Satisfactory techniques for smoothing the internal surfaces prior to drawing and a method of loosening the drawn tube from the mandrel are still being sought. Ball swaging was explored and appears to offer promise for the latter, but the technique requires modification to remove the spiral pattern that results.

The Bureau of Mines[3] research in this area seems to have been concentrated on producing W–25 wt.% Re alloy sleeves suitable for extrusion. The sleeves were sintered by heating for 15 hr at 2400°C in flowing hydrogen. Sintered densities were found to range from 18.82 to 19.34 g/cm³; rhenium contents were from 24.1 to 25.1 wt.%; and out-of-straightness measured 10 to 18 mils over the 8-in. length of the sleeves.

High-deformation-rate extrusion of thin-walled tungsten hemispheres has been investigated at Los Alamos Scientific Laboratory.[4] A model 1210 Dynapak was used in these studies in an effort to produce 4-in.-diameter hemispheres with ¼-in.-thick walls. During preliminary runs, aluminum, copper, and type 321 stainless steel were employed as stand-ins for the tungsten. A tungsten carbide coating was applied to the die to eliminate the welding of the stainless-steel die to the American Iron and Steel Institute (AISI) 4340 steel die during extrusion. A 2-in.-diameter by 2⅛-in.-long tungsten rod was extruded at 1870°C, with the extrusion filling 85% of the die cavity. Therefore it is stated that the feasibility of the process has been demonstrated, but a larger capacity extrusion unit would be required.

Fabrication studies on tantalum-base alloys are also being conducted at various sites. The results of a study of four alloys (Ta–5 wt.% W–2.5 wt.% Mo, Ta–10 wt.% W–2.5 wt.% Mo, Ta–17 wt.% W, and Ta–10 wt.% W–1 wt.% Zr) have been reported by Battelle Memorial Institute.[5] The first three compositions were successfully processed to 6-in.-wide strip by extruding, forging, and rolling. The ingots were prepared by consolidating powders and chips of the elements into consumable electrodes, using nonconsumable-electrode arc-melting techniques. The electrodes were then double consumable arc melted into 4¼-in.-diameter ingots. The zirconium-containing ingot proved difficult to melt and exhibited some segregation. The first three compositions were then extruded at 2600 to 3000°F with a reduction ratio of 4 to 1. Forging of these alloys was accomplished at 2200°F with reductions of 45 to 60%. The Ta–W–Mo alloys were reduced approximately 60% at 1000°F by rolling and then finish rolled at room temperature with reductions of 65 to 70%. The Ta–17 wt.% W alloy was breakdown rolled at 1800°F, then rolled at 1000°F, and finished at 700°F. This alloy was stiffer than those containing molybdenum and exhibited the highest hot strength (17,600-psi ultimate tensile strength at 3500°F). Since marked deoxidation occurred in the alloys during melting, the total interstitials averaged less than 200 ppm.

Argonne is continuing work on the V–20 wt.% Ti alloy and melt-refining studies. The consolidation and fabrication techniques employed in producing the 20 wt.% titanium alloy are de-

scribed in detail in an Argonne topical report,[6] and later studies are included in Argonne progress reports.[7,8] Four melt-refining runs and skull-oxidation runs were carried out with yields of 93 to 95%.

The preparation of W–Tc alloys is being investigated at Hanford Atomic Products Operation.[9] The technetium is being obtained from reactor operations. It is reported that, after a W–Tc alloy was arc melted, the furnace exhibited a reading of 50,000 counts/min owing to the ^{99}Tc beta activity. It is also reported that there is reason to believe that the technetium forms a carbide, whereas rhenium does not.

(N. E. Daniel)

Cladding

Rolling, Swaging, and Coextrusion

A program in support of the Argonne Advanced Research Reactor (AARR) was conducted at Battelle[10] to investigate fabrication procedures for 37 wt.% UO_2–stainless steel by roll bonding. The authors observed that the commonly used high-fired UO_2 will crush and stringer severely when cold rolled in excess of 3% reduction, whereas sol-gel UO_2 was not significantly crushed or stringered in a duplicate dispersion after a 16% cold reduction. However, because of availability and lower cost, high-fired spherical UO_2 was used for the fabrication development work. A reduction of 6 to 1 in thickness, with heavy initial roll reductions of 40% followed by 25% reductions at 1200°C, was observed to produce the best combination of results with regard to dimensional control and dispersion structure. Small plates for property tests containing depleted high-fired UO_2 and irradiation test plates containing plasma-sprayed enriched UO_2 were prepared and forwarded to Argonne for testing and evaluation.

(R. J. Diersing)

Pressure Bonding

Solid-state joining of beryllium components, without diffusion-bonding aids, was described[11] at the International Conference on Beryllium, held in October 1964 at Philadelphia. Surface-preparation methods included chemical milling, mechanical abrasion, machining, cold rolling, and grit blasting of beryllium surfaces, which were subsequently bonded for 4 hr and 10,000 psi at temperatures ranging from 1550 to 1850°F (843 to 1010°C). Joint strengths comparable to the parent-metal strength were obtained with grit-blasted and HNO_3-washed surfaces bonded at temperatures of 1650°F (898°C) and above. These techniques have been used successfully in the fabrication of fuel elements and structural members, such as box beams and I beams. Generally, iron tooling has been utilized. For bonding at the higher temperatures, molybdenum, graphite, and BeO have been found to be promising barriers to diffusion between the iron and beryllium.

A Canadian patent[12] describes the use of diffusion barriers in aluminum-clad uranium fuel elements bonded at 600°C (1112°F) and 1150 psi. Nickel coatings 5 to 7 μ thick are deposited on the inside surfaces of the fuel sheath, and the uranium surfaces are coated with 4 to 6 μ of nickel. Both surfaces are then coated with 3 to 5 μ of chromium. Bonded assemblies of this type show very little reaction between cladding and core.

The application of hot isostatic pressing to powder-metallurgy parts is reviewed in Ref. 13. Bonding conditions and results for the refractory metals tungsten, tantalum, niobium, and rhenium are described. Consolidation of spherical tungsten powders has permitted the fabrication of final tungsten forms without recrystallization. Full-density rocket nozzles, nose cones, forging billets, bars, rods, and tubes have been produced at 2900°F and 15,000 psi. The resulting material shows a greatly reduced tendency to recrystallize on heating. Only 50% recrystallization has been observed after heating to 3630°F. Metallographic examination after nozzle test firing at 6500°F has shown a retained fine-grain size. With many of the refractory-metal powders, it is often necessary to preform the shapes by cold hydrostatic pressing or explosive treatment. The required bonding temperature can be significantly reduced by utilizing explosive techniques. Beryllium has been consolidated into various forms with random-oriented structures and theoretical densities at temperatures of 1400 to 1600°F (760 to 871°C) and pressures of 10,000 to 15,000 psi. Superalloy materials, including A-286 and high-nickel alloys, have been consolidated to 99% density by a combination of cold hydrostatic pressing and hot isostatic pressing at 1800 to 2200°F (982 to 1204°C).

The fabrication of nonmetallic materials by hot isostatic pressing is also described in the above-mentioned paper.[13] Graphite and carbides bonded at temperatures from 2900 to 4200°F (1593 to 2315°C) have been consolidated to densities of 93 to 98%. Oxides of aluminum, beryllium, magnesium, and uranium have been successfully consolidated in the temperature range of 2100 to 2500°F (1148 to 1371°C) at pressures of 10,000 psi. Nonstable materials such as ferroelectrics and piezoelectrics have been fabricated by hot isostatic pressing with a high degree of purity and good structural properties.

Studies of zirconium and aluminum self-bonds at Battelle have continued.[14] These couples were assembled in an expansion jig to provide the bonding pressure during treatment in vacuum of 10^{-8} to 10^{-9} mm Hg. The zirconium surfaces were prepared by mechanical abrasion on 600- and 80-grit paper. Holding at 1500°F (815°C) for 2 hr produced bonds having 30% of the parent-metal yield strength. This was consistent with the amount of observed grain growth across the original interface. Shaper-machined aluminum components bonded at 900 to 1000°F (480 to 540°C) for 1 hr exhibited 20% of the parent-metal yield strength. Metallographic examination showed bonding only between asperities of the original surfaces.

(S. W. Porembka)

Canning

Work on the compaction of irregular-shaped particles has been completed at Argonne.[7] The relation between the packing efficiency of a single component and the size of the particle has been found by computer to be

$$Pe_1 = 0.635 - (0.032/d_1) - 0.072 \exp(-0.207D/d_1)$$

where Pe_1 is the packing efficiency, D is the diameter of the container, and d_1 is the diameter of the single component. The fit of the equation to the data points yields a standard deviation of packing efficiency of 0.009 for particle dimensions greater than 300 μ.

The packing efficiency of a second angular component in the matrix formed by the first component is expressible as

$$Pe_2 = 0.484 - 0.192 \exp(-0.098\, d_1/d_2)$$

The standard deviation is 0.026.

With the aid of the two preceding equations, the total packing-density fraction of a binary system of angular materials reduces to

$$0.812 - (0.017/d_1) - 0.037 \exp(-0.207D/d_1) - 0.070 \exp(-0.098\, d_1/d_2)$$

The value of 0.812 is the limiting density of a binary system of angular (approximately tetragonal) grit.

Fabrication of UO_2–PuO_2 vibrationally compacted (VIPAC) fuel rods for the Saxton Reactor has been started in the Plutonium Fuels Laboratory at Hanford.[15] The Zircaloy cladding for the fuel rods will be 1 m long, with a 0.9-cm inside diameter and a 0.06-cm-thick wall. The core material will be produced by pneumatically impacting (NUPAC) fused normal UO_2–6.6 wt.% PuO_2 (8% ^{240}Pu). The NUPAC powder will be compacted in the fuel tubes to 86 to 88% of the theoretical density by vibrational compaction.

Stress studies were conducted at Battelle–Northwest,[16] to determine the stresses encountered in Experimental Boiling Water Reactor (EBWR) Zircaloy-2 tubing during vibratory compaction on the M-B electrodynamic shaker unit. Strain-gauge measurements were made in the tubing immediately above the end-cap clamp assembly with comparisons obtained between a normal clamp arrangement, a normal clamp mounted on a reinforced resonance plate, and a modified tapered end-cap holder on a reinforced resonance plate.

Under an applied load of 20 g, maximum cladding stresses from excited bending modes ranged from 11,000 to 15,000 psi, the higher values being associated with the modified clamp. An applied load of 40 g increased the cladding stresses up to 25,000 psi with a normal clamp arrangement.

(V. D. Linse)

Electroplating

Among recent developments in electrolytic processes, progress has been made in utilizing chemically reduced and electrodeposited coatings for protection against oxidation at high temperatures. Electroless nickel appears promising for inhibiting oxide scaling of refractory metals such as Nb–1 wt.% Zr during thermal-cycling tests at Argonne.[7,17] The outer layer of the coating on one specimen showed slight flaking after 14 cycles to 1500°F. Five other specimens were unchanged after 14 cycles to

1500°F, one cycle to 1700°F, one to 1820°F, and one to 1920°F. Cycle 18 to 1940°F caused slight peeling of the outer layer of nickel on three specimens, and cycle 19 to 2000°F caused slight peeling on the remaining specimens.

Dense, high-purity refractory-metal coatings with good mechanical properties were electrodeposited by Union Carbide Corporation in high-temperature salt mixtures of the refractory-metal fluoride and alkali fluorides.[18] When niobium was electrodeposited, for example, a 10 wt.% mixture of niobium fluoride (NbF_5) and alkali fluorides was maintained at 775°C. Deposition at a cathode current density of 50 ma/cm^2 (5 amp/dm^2) yielded niobium with a density of 99.8% of the theoretical. Dense and smooth structures with a hardness of 85 to 100 DPH were obtained with deposits up to 1/4 in. thick. Similar procedures were satisfactory for electroplating chromium, hafnium, molybdenum, tantalum, tungsten, vanadium, and zirconium. These metals were deposited on steel, graphite, copper, and other materials.

Dense rhenium electrodeposits were applied adherently by the Russians[19] on molybdenum and tungsten when the substrate surfaces were etched with an a-c density of 30 amp/dm^2 in a 15 wt.% sodium hydroxide solution. After 2 μ (0.00008 in.) was electroplated and heat-treated in an inert atmosphere at 800 to 1000°C for 10 to 20 min, another dense 2-μ-thick layer could be deposited. Adherence was unsatisfactory when more than 2 μ was deposited without intermediate heat-treatment. The electrolyte contained 12 or 60 g of $HReO_4$ per liter, 40 or 60 g of H_2SO_4 per liter, and 30 or 100 g of $(NH_4)_2SO_4$ per liter. Its pH was 1, and its temperature was 18 to 20°C. Cathode current density was 20 amp/dm^2.

A boronizing procedure for diffusing up to 20 wt.% boron in steel by electrolysis in fused borax at 900°C was developed in Japan.[20] Boron deposited on the steel cathode diffuses into carbon steel, stainless steel, and high-chrome steels. The anode is a graphite rod.

(W. H. Safranek)

Nonelectrolytic Chemical-Plating Techniques

Singleton and coworkers[21] studied the effects of plating parameters on the orientation, microhardness, and microstructure of tungsten deposited from WF_6 by CVD. They also discuss the formation of freestanding CVD tungsten structures and the joining of tungsten tubing by CVD.

In the area of CVD coatings for corrosion protection, Venker[22] studied the deposition of niobium on uranium and aluminum. Evaporation or sputtering of the coating metal from an anode produced good deposits of silver and copper but not of niobium. Niobium was deposited by hydrogen reduction of $NbCl_5$ in an electric discharge at a temperature below that at which deposition occurs in the absence of a discharge. Uniform, adherent niobium coatings were obtained by reduction of $NbCl_5$ vapor with zinc vapor at 400 to 600°C. The deposits contained about 2.5 wt.% zinc, which could be partially removed by heat-treating the deposit at 500°C at 1-torr pressure.

Plunkett[23] has reviewed major NASA research on inorganic coatings for thermal protection and lubrication, including oxidation-resistant coatings for refractory metals and methods of application. (C. F. Powell)

Metals Joining

Welding and Brazing

Recent reports indicate that laser (optical maser) welding is finding its niche in industry. Electronic circuitry welded by the laser process is reported on by Pfluger and Maas.[24] Excellent fusion welds were made in fine nickel wire and ribbon, Kovar, and copper wire, using a pulsed ruby laser having a total energy output of 1.5 joules. Cross-wire and parallel-wire joints

were studied. In general, it was concluded that the parallel-wire joint design was superior, mainly because the light beam finds the joint area directly. This would indicate the need for redesign of existing circuitry for laser welding if it were used in place of the proven resistance-welding techniques. The advantages, disadvantages, and areas requiring further study are discussed.

Welding engineers at AiResearch have demonstrated the usefulness of laser welding for welding very close to ceramic seals, etc.[25] The laser used was capable of 10 pulses/sec at 10 joules/pulse and was set up for manual or automatic firing. Laser welding was used successfully to weld retainer rings to the heat-treated races of ball bearings. Other welding processes, including electron-beam welding, failed because it was impossible to prevent damage to the bearing races or the lubricant. A small electronic-sensing device that proved very difficult to fabricate by other joining methods was made practical through laser welding. The materials joined and reported by AiResearch were type 440C to type 321 stainless steels, 6061 T-6 aluminum, gold, and AISI type 1151 steel to type 321 stainless steel.

In an Air Force-sponsored laser-welding program,[26] seam welds having base-metal properties were made in several materials, including René 41, titanium, and molybdenum. It was concluded that the major deterrent to wide usage of laser welding for thin materials is the need for a continuous laser beam.

The development of brazing filler metals for use with the refractory metals and their alloys continues. Investigators at General Electric Company[27] have reported on the stress-rupture properties of lap joints in W–Re and Ta–W alloys. The data are shown in Table V-1. All tests were made in hydrogen with the joint under a shear stress of 1.422×10^{-4} psi. Remelt-temperature tests were run on the Ta–10 wt.% W joints brazed with Nb–40 wt.% V. The results indicate considerable increase in remelt temperature. The joint did not fail at 4350°F after annealing for 2 hr at 2910°F. The melting temperature of the Nb–40 wt.% V alloy is about 3360°F.

General Electric[27] is also evaluating other brazing filler metals. This work is summarized in Table V-2. Significant results are: (1) the high porosity recorded when Nb–Pd filler metals are used at brazing temperatures above 3630°F, (2) the intolerable cracking of W–Re–Ru and W–Ru filler metals when the ruthenium plus rhenium totals over 50 wt.%, (3) the ductility of joints in tungsten brazed with W–Rh and W–Ir filler metals, and (4) excessive grain-boundary attack and vaporization when tungsten is brazed with the Mo–Re–Pd alloys.

Table V-1 STRESS-RUPTURE TEST RESULTS[27] FOR LAP-SHEAR BRAZE JOINTS* AT 1600°C (2910°F)

Braze alloy wt.%	Time to rupture, hr	Type of failure
Ta–10 Wt.% W Base Metal†		
None	8.6	Intragranular
V‡	29.9	Intragranular, adjacent to fillet
V§	7.8	Intragranular, adjacent to fillet
Nb–40 V‡	16.2	Intragranular, adjacent to fillet
Nb–40 V‡	14.6	Intragranular, adjacent to fillet
W–25 At.% Re Base Metal		
None	15.1	Intergranular
Cr–20 Ru	1.09	Shear through braze joint
Cr–20 Ru	0.13	Shear through braze joint
Cr–20 Ru	3.95	Shear through braze joint
Nb–40 V	11.7	Intergranular, adjacent to fillet
Nb–40 V	12.1	Intergranular, adjacent to fillet
V–25 Nb	18.4	Intergranular, adjacent to fillet

*All specimens were annealed for 2 hr at test temperature in hydrogen before testing.
†Tested with tantalum-foil covering to reduce contamination.
‡No tantalum-foil covering during brazing.
§Tantalum foil was covered during brazing.

Northrop Corp.,[28] in their brazing-alloy development programs for tantalum and molybdenum, have published limitations on the titanium and vanadium in alloys used to braze refractory-metal honeycomb structures. The limits minimize embrittlement of the core caused by fillet evaporation. They are: (1) a limit of three 1-hr exposures at 3000°F for titanium-base systems; and (2) a limit of 6%, or complete elimination of these metals from systems which must be reusable at 3500°F. The presence of beryllium in titanium-base alloys retards the embrittlement of tantalum. A Ti–30 wt.% V–4 wt.% Be alloy appears suitable for service at 3000°F. Alloys of Hf–Mo show promise for continued use at 3000°F, and Hf–Ta, for use at 3500°F. A thin vapor deposit of tantalum over a brazed fillet was shown to be an effective

Table V-2 SUMMARY OF REFRACTORY-METAL BRAZING SYSTEMS STUDIED[27]

Composition, wt.%	Cold workability	Brazing temp.,* °C	Fillet characteristics	Base-metal erosion, cm	Fillet microstructure
Brazing Alloys for Tantalum-Base Metal					
Nb–30 Pd	Slight	1950	Medium	None	Slight second phase
Nb–20 Pd	Slight	2150	Large	None	Slight porosity
Nb–10 Pd	Slight	2300	Medium	None	Severe porosity
Brazing Alloys for Tungsten-Base Metal					
W–10 Re–20 Ru	None	2550	Medium	0.010	Two or three phases
W–15 Re–25 Ru	None	2525	Medium	0.007	Two phase
W–20 Re–10 Ru	None	2825	Large	None	Two phase, slight porosity
W–40 Re–15 Ru	None	2500	Medium	None	Slight cracking
W–31 Ru	None	2300	Small	None	Two phase
W–28 Rh	Slight	2275	Small	None	Two-phase eutectic
W–35 Rh	Slight	2200	Small	None	Two-phase eutectic
W–42 Ir	Slight	2500	Medium	None	Two phase
100 Mo	Slight	2600	Large	None	Large grained
Mo–50 Re–15 Pd	None		None		Excessive vaporization
Mo–30 Re–30 Pd	None		None		Excessive vaporization
Mo–1 B	Moderate	2600	None		No melting
Mo–20 V	None	2450	Medium	None	Severe porosity

*Dry hydrogen atmosphere.

inhibitor of the coating–brazing alloy interaction.

The alloy Hastelloy W has been used for some time as a filler metal for welding superalloys. Battelle–Northwest investigators[29] have been concerned with a possible loss of weld-metal ductility during aging and consequently have set up a program to study this effect. Bend and tensile tests of joints made with Hastelloy W and Hastelloy X in type 316 stainless steel and Haynes 25 are being used. To date, tests of specimens aged for 500 and 1000 hr at 1400 and 1600°F have been completed. As expected, the ductility was lowered and the yield strength was raised. More important, however, was the fact that aging of the Hastelloy W weld metal was the most sluggish; and, at 1000 and 1200°F, Hastelloy W welds have more remaining useful ductility.

The weldability of Fe–Cr–Al–Y alloy has been limited in the past by the formation of YFe_9, which melts at 2460°F compared with the 2640°F melting point for the matrix.[27] Thus interdendritic films are formed in the weld which embrittle the joint. Postweld heat-treatments at 2200 to 2375°F spheroidize the YFe_9 and improve ductility. General Electric investigators have reported that reducing the yttrium content of the alloy from 0.7 to 0.8% to 0.1 to 0.3% also improves ductility and does not lower the oxidation resistance.

The program at General Electric[30] to develop techniques for joining TD nickel has entered Phase II. The results of Phase I indicated that flash welding, resistance welding, and brazing were the processes which have the least effect on the base-metal thoria dispersion and which give the greatest joint efficiency. Two brazing alloys, 60 Pd–40 (Ni + Li) and 71 Ni–19 Cr–10 Si (wt.%), were evaluated for oxidation resistance and diffusion characteristics at high temperatures. The oxidation tests indicated the need for a protective coating on sheet-metal components. Figure V-1 shows the results of these tests. Diffusion was evaluated metallographically. Significant internal oxidation and delamination were encountered. Delamination was attributed to the diffusion of carbon from the brazing alloy and its reaction with

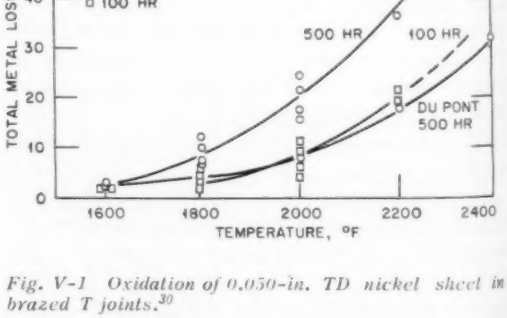

Fig. V-1 Oxidation of 0.050-in. TD nickel sheet in brazed T joints.[30]

oxygen to form CO_2. Tentatively, a maximum of 200 ppm carbon is considered tolerable.

An extended study of the mechanical properties of fusion-welded René 41 alloy sheet, plate, and tubing was conducted by Boeing Co.[31] during the development of the X-20 reentry vehicle. Experiments included static tests of longitudinal fillet-welded joints. Most tests were conducted on both original and repaired welds. Specimens were subjected to a variety of thermal-exposure conditions. The results were analyzed using the standards of Military Handbook No. 5 as far as possible to determine the various allowable stresses. The allowable stresses and other results obtained are considered applicable to designs with requirements similar to those encounted on the X-20.

(R. M. Evans)

Explosive Welding and Cutting

In a paper[32] presented at the Western Metals Congress in February 1965, it was predicted that explosive welding would find important applications for joining dissimilar metals and alloys, for joining heat-treated and welded components, and for welding in geographic areas remote from conventional energy sources and supporting services. Research indicates that any metal or alloy that can withstand the explosive shock without damage can be explosively welded.

Aluminum alloys, magnesium alloys, mild steel, and copper have been self-joined by explosive welding at the Frankford Arsenal.[33] Lap, seam, and spot-welded joints were made and evaluated. The quality of the explosive-welded joints was determined nondestructively by visual examination, ultrasonic inspection, and radiography. Destructive evaluation included peel, bend, and tensile-shear tests. Metallography and hardness surveys were used to evaluate the condition in the vicinity of the weld interface. In general, the welded plates were just as strong as the unwelded base metals, a significant accomplishment when one considers that several of the alloys were in their heat-treated conditions for optimum strength prior to welding.

In recent studies conducted by Battelle,[34] the feasibility of using shaped charges to drill holes explosively in mild steel has been demonstrated. Holes with depth-to-diameter ratios of 5 to 1 have been drilled in mild steel. In addition, cable-cutting, tube-cutting, and spot-welding operations have been performed. The object of performing these conventional operations in an unconventional manner was to demonstrate the usefulness of controlled explosions as a primary source of energy for operations in remote areas or other areas where conventional forms of energy are unavailable. (R. H. Wittman)

Nondestructive Testing

Ultrasonic Techniques

Aeroprojects Inc.[35] has developed and installed an ultrasonic level indicator in the Molten Salt Reactor Experiment (MSRE) fuel-processing tank at Oak Ridge. The components are believed to be resistant to the highly corrosive, high-radiation environment. The probe consists of a sensing bar brazed to the end of a steel acoustic transmission line. The transducer is located at the opposite end of the bar in a safe environment. The transducer operates nominally at 2915 kc. Sensing is based on a change in acoustic reaction when the sensing bar contacts the liquid.

Savannah River investigators[36] are combining Hall elements and ultrasonic sensors to advantage for detecting the presence of nickel in clad elements after the bonding process and for measuring nickel-plate thickness, end-cladding thickness, grain size of the uranium cores, and nonbond between aluminum cladding and the core in U–Ni and Al–Ni fuel elements. The Hall elements for detecting nickel in clad elements and the ultrasonic transducers for detecting nonbond between core and cladding are mounted in the same head, which is contoured and spring loaded to maintain contact with the element. The ultrasonic frequency is 1 mc, which is low enough that the propagation of the ultrasound is essentially unaffected by variations in grain size.

The ultrasonic grain-size tester is used before cladding is applied. Average grain size is determined by measuring the attenuation of 5.0-mc pulses at a pulse repetition rate of 2000 per second in a water-immersion system.

Savannah River makes good use of specialized analog computing circuits in the systems. For instance, automatic compensation is made for the effects of temperature on attenuation in determining bond integrity, and computing circuits determine whether average grain size is ac-

ceptable. The time constant of the integrating circuit is adjusted so that the core is rejected if, during any one-third revolution of the core, the average grain size is found to be outside preset limits.

Hanford investigators[37,38] believe that they can detect fatigue in aluminum, stainless steel, and copper at about 20% of the fatigue life using "critical-angle" ultrasonic techniques. A receiver transducer, scanned across the reflected wave front of a beam incident near the critical angle, detects a signal null and a maximum. The null signal stems from the interference between energy that enters the surface and that which is reflected from it. The energy entering the surface and reflected at a translated position is called the boundary signal.

Also, Hanford has been studying the water-surface-distortion technique of ultrasonic imaging.[37,38] An object is ultrasonically illuminated from behind, and the transmitted beam impinges upon a water surface. A shadow image of the object is formed by distortion of the water surface. Where the ultrasound is most intense, the water surface bulges upward, and shadowed areas are depressed by comparison. Although the distortion is normally only a few thousandths of an inch, the shadow image is made clearly visible with collimated light. Photographs of a few images thus produced show fair contrast.

(D. Ensminger)

NDT Techniques Other Than Ultrasonic

Investigators at the Reactor Materials Laboratory, Culcheth, Great Britain,[39] have found that a thermoelectric test is useful for detecting undesirable heat-affected zones of fusion welds. The test identifies conditions that will result in low corrosion resistance of heat-affected zones in a Zr–2.5 wt.% Nb alloy. The test is performed by measuring the thermoelectric potential between a heated metallic point probe in contact with particular regions of the weld and adjacent metal. The simple equipment required can be obtained by modifying commercially available devices. In the Zr–2.5 wt.% Nb alloy, it was found that, if the thermoelectric potential of any part in the zone is near that of the alloy in the state induced by rapid quenching from 1000°C, the weld is likely to have unsatisfactory corrosion resistance in a steam environment.

Investigation of the multiparameter eddy-current system is being continued at Battelle-Northwest.[38] An oscilloscope image provides a cross-section display of the tubing being tested and serves to show both the location and relative size of detected flaws. Artificial flaws were prepared in the inner and outer walls of the type 304L stainless-steel tube, which had a wall thickness of $\frac{1}{8}$ in. and a diameter of $2\frac{3}{4}$ in. In a setup having a sensitivity of about 3% of wall thickness for OD defects and 20% for ID defects, a 0.040-in.-ID flaw and a 0.012-in.-OD flaw at the same location were simultaneously detected and displayed. Although the flaws were in the same location, their signals were independently recorded at the proper magnitude.

(A. F. Leatherman)

References

1. Nuclear Metals Division of Textron Inc., Fundamental and Applied Research and Development in Metallurgy, Progress Report for the Month of November 1964, USAEC Report NMI-2134, Jan. 25, 1965.
2. Nuclear Metals Division of Textron Inc., Fundamental and Applied Research and Development in Metallurgy, Progress Report for the Month of February 1965, USAEC Report NMI-2137 (NYO-2784-8), Apr. 8, 1965.
3. Bureau of Mines, Albany Metallurgy Research Center, Quarterly Metallurgical Progress Report No. 26, January 1–March 31, 1965, USAEC Report USBM-RC-1158.
4. J. M. Dickinson, High-Deformation-Rate Extrusion of Thin-Walled Tungsten Hemispheres, USAEC Report LA-3181, Los Alamos Scientific Laboratory, Aug. 1, 1964.
5. J. B. Hallowell, D. J. Maykuth, and H. R. Ogden, Final Report on Tantalum Alloy Processing Development, Report ML-TDR-64-63, Battelle Memorial Institute, March 1964.
6. W. R. Burt, Jr., W. C. Kramer, R. D. McGowan, F. J. Karasek, and R. M. Mayfield, Consolidation and Fabrication Techniques for Vanadium-20 Wt.% Titanium (TV-20), USAEC Report ANL-6928, Argonne National Laboratory, February 1965.
7. Argonne National Laboratory, Reactor Development Program Progress Report, March 1965, USAEC Report ANL-7028, Apr. 20, 1965.
8. Argonne National Laboratory, Reactor Development Program Progress Report, May 1965, USAEC Report ANL-7046.
9. Hanford Atomic Products Operation, A Study of Tungsten-Technetium Alloys, Quarterly Progress Report, October 1, 1964–January 1, 1965, USAEC Report HW-84550, Jan. 1, 1965.
10. D. S. Acuncius, D. E. Lozier, D. E. Kizer, and D. L. Keller, Development of Fabrication Procedures for the AARR Fuel Plates, USAEC Report BMI-X-327, Battelle Memorial Institute, Feb. 1, 1965.

11. E. S. Hodge, P. J. Gripshover, and H. D. Hanes, Solid-State Bonding of Beryllium, USAEC Report CONF-729-2, presented at the International Conference on Beryllium, Philadelphia, 1964.
12. W. Blomeyer and G. Schneider, Fuel Element for Nuclear Reactors and Process for Its Manufacture, Canadian Patent 700,831, Dec. 29, 1964.
13. E. S. Hodge, Hot Isostatic Pressing Improves Powder Metallurgy Parts, *Mater. Design Eng.*, 61(5): 92-97 (May 1965).
14. R. W. Dayton and S. J. Paprocki, Progress Relating to Civilian Applications During April 1965, USAEC Report BMI-1723, Battelle Memorial Institute, May 1, 1965. (Classified)
15. Hanford Atomic Products Operation, Ceramics Research and Development Operation Quarterly Report, October–November 1964, USAEC Report HW-81603.
16. F. W. Albaugh, Reactor and Materials Technology Monthly Report, March 1965, USAEC Report BNWL-C-83A, Battelle–Northwest, Pacific Northwest Laboratory. (Classified; material cited is unclassified)
17. Argonne National Laboratory, Reactor Development Program Progress Report, February 1965, USAEC Report ANL-7017, Mar. 18, 1965.
18. G. W. Mellars and S. Senderoff, Electrodeposition of Coherent Deposits of Refractory Metals, *J. Electrochem. Soc.*, 112: 226-272 (March 1965).
19. I. M. Kvokova and V. I. Layner, Electrodeposition of Rhenium on Molybdenum and Tungsten, *Izv. Vysshikh Uchebn. Zavedenii, Tsvetn. Met.*, 4: 142–146 (July–August 1964).
20. M. Kawakami, The Cementation of Boron to Steels by the Methods of Electrolytic Deposition, in *Physics and Material Problems of Reactor Control Rods*, Conference Proceedings, Vienna, 1963, pp. 357-364, International Atomic Energy Agency, Vienna, 1964 (STI/PUB/81).
21. R. H. Singleton, N. D. McMurray, and K. E. Muszar, Fabrication of Tungsten Thermionic Emitter Surfaces by Chemical Vapor Deposition, Report CONF-640103-1, presented at the Seventh Refractory Composites Group Meeting, Fort Worth, Tex., 1964.
22. H. Venker, Attempts at Plating Uranium and Aluminum with Niobium, Euratom Report EUR-2111.d, October 1964.
23. J. D. Plunkett, NASA Contributions to the Technology of Inorganic Coatings, Report NASA-SP-5014, University of Denver Research Institute, 1964.
24. A. R. Pfluger and P. M. Maas, Laser Beam Welding Electronic-Component Leads, *Welding J.* (N. Y.), 44(6): 264s-269s (June 1965).
25. K. J. Miller and J. D. Nunnikhoven, Production Laser Welding for Specialized Applications, *Welding J.* (N. Y.), 44(6): 480-485 (June 1965).
26. S. Reich, Laser (Optical Maser) Beam Fusion Welding, Report AFML-TR-65-33, TRG Inc., Subsidiary of Control Data Corp., February 1965.
27. General Electric Company, Advanced Technology Services, High-Temperature Materials and Reactor Component Development Programs, Fourth Annual Report, Vol. I. Materials, USAEC Report GEMP-334A, Feb. 26, 1965.
28. A. H. Freedman, L. H. Stone, and E. B. Mikus, Tantalum and Molybdenum Brazing Techniques, Sixth Quarterly Progress Report, Report NOR-65-68, Northrop Corp., April 1965.
29. F. W. Albaugh, Reactor and Materials Technology Monthly Report, April 1965, USAEC Report BNWL-C-84A, Battelle–Northwest, Pacific Northwest Laboratory, May 14, 1965. (Classified; material cited is unclassified)
30. T. K. Redden, R. E. Kutchera, and R. G. Carlson, Development of Joining Techniques for TD-Nickel, Interim Progress Report No. 3-8-211, Report DM-65-61, General Electric Company, Feb. 1, 1965.
31. B. P. Rich, Strength Evaluation of Fusion Welded René 41 Nickel Alloy, Report D2-81283, Boeing Co., Sept. 24, 1964.
32. R. J. Carlson, Explosive Welding, paper presented at Western Metals Congress, Los Angeles, Calif., 1965, American Society for Metals Technical Report W-6-3-65.
33. H. J. Addison, Jr., Explosive Welding, Report A-64-13, Frankford Arsenal, May 1964; also, ASME Paper 64-MD-47.
34. C. C. Simons, Battelle Memorial Institute, personal communication, July 1965.
35. Aeroprojects Inc., Applications of Ultrasonic Energy: Ultrasonic Instrumentation for Nuclear Applications, USAEC Report NYO-2910-9, April 1965.
36. R. H. McKane and D. L. Honkonen, Nondestructive Testing of Reactor Fuel, Target, and Control Elements, USAEC Report DPSPU-65-30-11 (CONF-650509-1; SM-63/43), Savannah River Laboratory, March 1965.
37. J. K. Green (Ed.), Research and Development Programs Executed for the Division of Reactor Development, Quarterly Progress Report, July–September 1964, USAEC Report HW-84384, Hanford Atomic Products Operation, December 1964.
38. J. K. Green (Ed.), Research and Development Programs Executed for the Division of Reactor Development, Quarterly Progress Report, October–December 1964, USAEC Report HW-84609, Hanford Atomic Products Operation, December 1964.
39. R. F. Hanstock and D. C. B. Walker, Nondestructive Examination of the Heat-Affected Zone of Welded Zirconium–Niobium Alloy, British Report TRG-Report-950, Mar. 1, 1965.

Index

Reactor Materials

Volume 8

Note: The page range for each of the four issues of Vol. 8 is as follows: No. 1, pages 1 to 56; No. 2, pages 57 to 118; No. 3, pages 119 to 174; and No. 4, pages 175 to 233.

3Z1
  compatibility with UC, 11

A

A-286
  hot isostatic pressing, 226
A-286 (irradiated)
  ductility and stress-rupture properties, 155-56
A-356
  welding, 115
Acetylene
  pyrolysis, 108
Alloys (bcc group A)
  local order, 150-51
Alloys (high-temperature)
  Nb use in, 151
Alloys (irradiated)
  mechanical properties, 100
Alloys (rare earth)
  properties, 97
Alloys (refractory)
  coatings of, 48
  enthalpy, 218
  mechanical properties, 91-93
  solid-solution alloying effects, 150
  thermal expansion, 218
  welding, 168
Alloys (refractory metal)
  contamination in vacuum, 38-39
Alloys (super-)
  hot isostatic pressing, 226
  Nb use in, 151
  weight loss in vacuum systems, 150
  welding, 230
Almag 35
  welding, 115
Alumina Al-300
  corrosion, 211
Aluminum
  annealing, 150
  bonding, pressure, 107, 227
  compatibility with UO_2, 189
  corrosion, 27-28, 207
  electroplating on, 165
  electroplating with oxides, 108
  fatigue detection using ultrasonics, 232
  reaction with UO_2, 9-10
  reaction with water, 31-32
  weld testing, 116
Aluminum (irradiated)
  damage, 101
Aluminum (M-257)
  creep-rupture properties, 148
Aluminum (M-583)
  creep-rupture properties, 148
Aluminum (molten)
  corrosive effects, 89
Aluminum (Nb-coated)
  preparation, 228
Aluminum (SAP-895)
  creep-rupture properties, 148
Aluminum (SAP-915)
  creep-rupture properties, 148
Aluminum alloy (X 8001)-uranium dioxide, zirconium dioxide (Nb-coated) dispersions (Alclad 6061-clad)
  interactions, 64-65
  microstructure, 64
Aluminum alloy (X 8001)-uranium octoxide dispersions (Alclad 6061-clad)
  microstructure, 64
Aluminum alloys
  corrosion, 86, 207
  stress-corrosion cracking, 207
  tensile properties, Cs effects on, 211
  welding, 114-15, 231
Aluminum alloys (1100)
  corrosion, 27
  welding, 168
Aluminum alloys (1100)(Cu-clad)
  eddy-current testing, 116
Aluminum alloys (1100)(irradiated)
  corrosion and mechanical properties, 30
Aluminum alloys (6061)
  Ni plating on, 48
  welding, 115, 168
Aluminum alloys (6061)(irradiated)
  mechanical properties, 34
Aluminum alloys (6061 T-6)
  welding, laser, 229
Aluminum alloys (7075)
  corrosion, 27
Aluminum-boron carbide-uranium octoxide plates (Al(6061)-clad)
  fabrication, 10
Aluminum-boron system
  fabrication, 24
Aluminum-carbon-thorium system
  corrosion, 184
  hot hardness, 183
Aluminum-chromium-iron alloys
  oxidation, 207
Aluminum-chromium-iron-yttrium alloys
  corrosion, 87
  ductility, 149
  impact properties, 91
  oxidation, 143, 207
  welding, 113, 230
Aluminum-chromium-titanium-vanadium alloys
  use in brazing, 113
Aluminum-copper alloys (irradiated)
  diffusion in, 98
Aluminum-copper-nickel alloys
  embrittlement, 35-36
Aluminum-gallium-plutonium alloys
  properties and stability, 180
Aluminum-iron alloys
  U diffusion in, 153
Aluminum-iron-silicon-uranium system
  fabrication, 120
  hardness, 58
  hot hardness, 58-59
  microstructure, 58-59
Aluminum-iron-uranium alloys
  development, 119-20
  hot hardness, 120
  phase studies, 1-2
  transformation, 176
Aluminum-iron-uranium alloys (irradiated)
  swelling, pressure effects on, 191
Aluminum-lithium alloys (irradiated)
  He precipitation, 130-31
  swelling, 192
Aluminum-molybdenum alloys
  phase studies, 35
Aluminum-molybdenum-titanium-vanadium alloys
  phase studies, 153
  stress-corrosion cracking, 207-8
Aluminum-nickel alloys (Ni-clad)
  ultrasonic testing, 231
Aluminum-nickel-zirconium alloys
  corrosion and hardening, 215
Aluminum oxide
  bonding to Cr, pressure, 47
  compatibility with UO_2, 189
  corrosion, 211
  crushing, electrohydraulic, 41
  heat transfer, effects of high-rate, 99
  hot isostatic pressing, 227
  tensile properties, Cs effects on, 211
  tensile-strength testing, 41
Aluminum oxide (irradiated)
  expansion, 220
Aluminum oxide-calcium oxide-uranium dioxide-zirconium dioxide system
  reaction with water, 13
Aluminum oxide coatings

development, 67
Aluminum oxide-gadolinium oxide system
fabrication, 25
Aluminum oxide-plutonium dioxide system
phase studies, 63
Aluminum oxide powder
bonding, pressure, 106
densification, 154
pressure bonding, 106
Aluminum oxide whiskers
preparation, 108
Aluminum oxide-yttrium oxide system
W adherence to, 99
Aluminum plates
ultrasonic testing of thin, 49
Aluminum-plutonium alloys (Ni-plated)
corrosion, 207
Aluminum-plutonium intermetallic compounds
polymorphic transformations, 183
Aluminum-silicon-uranium system
hot hardness, 58-59
microstructure, 58-59
particle precipitation in, 176
preparation, 176
Aluminum-thorium alloys
hot hardness, 183
Aluminum-thorium dioxide dispersions (Al-clad)
coextrusion, 46
Aluminum-titanium-vanadium alloys
corrosion and Cs effects on tensile properties, 211
Aluminum-uranium alloys
B_4C incorporation in fuel, 204
phase studies, 119
Aluminum-uranium alloys (molten)
corrosive effects, 89
Aluminum-uranium dioxide dispersions
production, 184
Aluminum-uranium dioxide dispersions (Al-clad)
coextrusion, 46
Aluminum-uranium octoxide dispersions
reaction kinetics, 124-25
Aluminum-uranium plates (Al-clad)
roll bonding, 46-47
Aluminum-uranium silicide dispersions (Al alloy-clad)
fabrication and properties, 6
Aluminum-vanadium-zirconium alloys
corrosion and hardening, 215
Aluminum-Zircaloy systems
interdiffusion, 154
Aluminum-zirconium systems
interdiffusion, 154
Americium-plutonium alloys
phase studies, 123, 178
Antimony (molten)
corrosive effects, 89
AS-30
creep, 214

B

B-66
bonding, diffusion, 168
coatings for, 209
corrosion, 146
stress-rupture properties, 93
transition temperature, 48
welding, 48, 112, 150, 167-68
B-66 (Cr-Si-Ti-coated)
evaluation, 144
B120VCA
stress-corrosion cracking, 27
use in brazing, 113
Ball bearings
laser welding of retainer rings to races, 229
Beryllides
degradation, 80
Beryllium
analysis, activation, 20
analysis for impurities, 136
bonding, pressure, 164
casting, 19-20
compatibility with CO_2, 200
corrosion, 19, 30, 207
deformation, 77
extrusion, 200-1
forging, 76-77
forming, 77
grain growth, 199
hot isostatic pressing, 226
inclusions in, identification of, 199
joining, solid-state, 226
machining effects, 136
mechanical properties, 136, 199
metallurgy, 20
metallurgy, powder, 76
oxidation, 19
precipitates in, identification of, 199
preferred orientation, wrought, 199
properties of forged, 77
purification, 20, 76
reactions with air, CO, N, and O, 19
recrystallization, 199
strength of extruded, 20
tensile properties of extruded, 19
vapor pressure, 80
vaporization from $LaBe_{13}$ and YBe_{13}, 80
working, hot, 19-20
Beryllium (irradiated)
damage, 20, 136
enthalpy, 77
Beryllium (Ni-coated)
preparation, 136, 166
Beryllium alloys
compatibility with CO_2, 200
Beryllium-calcium alloys, 200
Beryllium-carbon-thorium system
hot hardness, 183
Beryllium-carbon-uranium system
fabrication, 45
particle precipitation in, 176
preparation, 176
Beryllium-carbon-uranium-Zircaloy-2 system
fabrication, 45
Beryllium-copper alloys
electroplating of, 108
welding, 168
Beryllium-magnesium alloys
compatibility with CO_2, 200
Beryllium-molybdenum intermetallic compounds
interdiffusion, 39
Beryllium-niobium alloys
preparation and properties, 80
Beryllium oxide
compatibility with UO_2, 189
conference, 201
enthalpy, 77
expansion at transformation, 77
hot isostatic pressing, 227
rupture, 77
self-diffusion, 21
stabilization, 137
Beryllium oxide (irradiated)
expansion, 20-21, 77, 80, 220
properties, 201
rupture, 77
Beryllium oxide coatings
development, 67
Beryllium oxide-plutonium dioxide system
phase studies, 4, 63
Beryllium oxide-plutonium dioxide-thorium dioxide system
phase studies, 63
Beryllium oxide powder
bonding, pressure, 106
Beryllium oxide-thorium dioxide system
phase studies, 201
Beryllium powder
bonding pressure, 106
metallurgy, 76
pressing, vacuum hot, 136
Beryllium sheet
crystallography and mechanical properties, 76
Beryllium single crystals
compression tests, 199-200
deformation, 18-19
dislocations in deformed, 75-76
flow stress, heat treatment effects on, 75
mechanical properties, 136
production by zone leveling, 198-99
scavenging using Ti, 200
slip, 75
Beryllium-thorium alloys
hot hardness, 183
Beryllium-titanium alloys
use in brazing, 229
Beryllium-titanium-vanadium alloys
use in brazing, 229
Beryllium tubing
fabrication, 20
Beryllium-uranium alloys
fabrication, 45
hardness, 45
preparation, 176
strength, 176
Beryllium-uranium alloys (irradiated)
stability, 176
Beryllium-Zircaloy-2 alloys
use in brazing Th-U alloys (Zy-2-clad), 5-6
Beryllium-zirconium braze
corrosion, 28
Bismuth (molten)
corrosive effects, 89, 146, 211-12
Bismuth-lead alloys (molten)
corrosive effects on Ta, 146
Borides
preparation of ultrahigh-purity, 154
use in control rods, 25
Borides (refractory)
entropies and heats of formation, 40
Boron
diffusion in steel, 228
effects on stainless steel, 24
plating, chemical, 108
vapor deposition, 166
Boron carbide
addition to UO_2 fuel, 204-5
compatibility with cladding materials, 205
incorporation in Al-U alloy fuel, 204
Boron carbide-graphite dispersions (irradiated)
properties, 25
Boron carbide powder
thermal conductivity, 140
Boron carbide tubing
fabrication, 108
Boron-carbon system
chemical deposition, 108
phase studies, 154-55
Boron-chromium-silicon system coatings
for refractories, 209
Boron coatings
preparation on transition metals, 48
Boron filaments
chemical deposition, 108
Boron-hydrogen-zirconium system, 81
Boron-molybdenum system

phase studies, 139
use in brazing, 229
Boron monocarbide-copper composites
fabrication and testing, 140
Boron nitride-molybdenum disilicide-zirconium diboride composites
tensile properties, 25
Boron oxide-cadmium oxide-indium oxide system glasses
properties, 204
Boron-plutonium system
crystal structure and lattice parameters, 178
Boron-tungsten system
grain growth, 204
Brass plates
ultrasonic testing of thin, 49
Brazing, 112-15, 171

C

C-129 Y
development, 216
evaluation, 216
welding, 112, 150, 168
C-129 Y (disilicide-coated)
preparation, 144-45
Cadmium (molten)
corrosive effects, 212
C-129 Y (V-modified disilicide-coated)
preparation, 144-45
Cadmium-indium-silver alloys
properties, 139
Cadmium-indium-silver alloys (irradiated)
damage, 139
density, 84
Cadmium-indium-silver braze
corrosion, 28
Cadmium oxide-indium oxide system glasses
properties, 204
Cadmium-plutonium alloys
phase studies, 61
Calcium fluoride (irradiated)
Ar diffusion in, 15
Calcium oxide-zirconium dioxide system
high-temperature properties, 155
Calcium-oxygen-tungsten system
phase studies, 143
Calcium-tungsten alloys
oxidation, 143
Carbides
hot isostatic pressing, 227
preparation of ultrahigh-purity, 154
technology, 10
Carbides (Group 4a, 5a, and 6a)
properties and purification, 41
Carbides (refractory)
constitution, 68
entropies, 40
heats of formation, 40
properties, 68
Carbon
(see also Graphite)
chemical deposition, 108
diffusion in UC, 190
PyC deposition on, 48
Carbon (irradiated)
dimensional changes, 197
Carbon (pyrolytic)
actinide diffusion in, 8-9
crystallinity, 185, 198
deposition, 48, 166
structure, 18
Carbon (pyrolytic)(irradiated)
expansion, 220
Carbon (pyrolytic) coatings
crystallite size, 126
development, 67
fission product diffusion through, 7
microvoids, 65
preferred orientation, 184-85
preparation, 7
preparation on C filaments, 166
properties, 126
structure, 125
Carbon (pyrolytic) coatings (irradiated)
behavior on ThO_2-UO_2, UC_2, and UO_2 particles, 67
Carbon (vitreous)
preparation and properties, 74-75
Carbon-cerium-thorium system
phase studies, 190
Carbon-cerium-uranium system
phase studies, 190
Carbon-chromium-thorium system
hot hardness, 183
Carbon dioxide
reaction with H, kinetics of, 74
Carbon filaments
coating with PyC, 166
Carbon-gadolinium-uranium system
phase studies, 189-90
Carbon-hafnium carbide system
thermal expansion of fused, 140
Carbon-hafnium-hydrogen system
properties, 81
Carbon-hafnium system
phase studies, 154
strength, 140
Carbon-hydrogen-titanium system
properties, 81
Carbon-hydrogen-zirconium system
properties, 81
Carbon-indium-thorium system
hot hardness, 183
Carbon-molybdenum-thorium system
hot hardness, 183
Carbon-molybdenum-titanium system
microstructure and tensile properties, 36
Carbon-molybdenum-titanium-zirconium system
microstructure and tensile properties, 36
Carbon-molybdenum-uranium system
phase studies, 10
Carbon-nickel-thorium system
phase studies, 129
Carbon-niobium-thorium system
hot hardness, 183
Carbon-oxygen-plutonium system
properties, 5
Carbon-plutonium system
metallography, 123-24
Carbon-plutonium-thorium system
phase studies, preparation, and properties, 183
Carbon-plutonium-uranium system
properties, 4
Carbon-plutonium-uranium system (irradiated)
compatibility with Nb, 4
Carbon-silicon system
chemical deposition, 108
Carbon-tantalum system
phase studies, 154-55
Carbon-tantalum-uranium system
phase studies, 10-11
Carbon-thorium system
hot hardness, 183
phase studies, 129
Carbon-thorium-titanium system
corrosion, 184
hot hardness, 183
Carbon-thorium-uranium system
hot hardness, 183
Carbon-thorium-vanadium system
hot hardness, 183
Carbon-thorium-zirconium system
hot hardness, 183
Carbon-uranium system, 176
Cb-752
aging, 150
bonding, pressure, 164
Cb-752 (Cr-Si-Ti-coated)
preparation, 144-45
Ceramic coatings
development of reinforced, 41
Ceramic-fuel (ceramic-coated) dispersions
use in gas-cooled reactors, 67
Ceramic-fuel (PyC-coated) dispersions
use in gas-cooled reactors, 67
Ceramic fuels
Geneva Conference papers, 53-54
thermochemical deposition, 68
Ceramic powders
bonding, pressure, 106
Ceramics
coating with metals, 166-67
heat transfer, effects of high-rate, 99
joining to metals, 47, 106
preparation of ultrahigh-purity, 154
tensile-strength testing, 41
Ceramics (Al_2O_3-base) (metal-coated)
preparation, 100
Ceramics (ferroelectric) (Al-Cu-coated)
preparation, 100
Ceramics (ferroelectric)(Al-Au-coated)
preparation, 100
Ceramics (glass)
properties, 204
Ceramics (irradiated)
expansion, 220
fission gas release, 15
Ceramics (metal-coated)
preparation, 99-100, 166-67
Cerium
electrodeposition, 165
Cerium-cobalt-plutonium alloy - sodium couples (irradiated)
fission product distribution, 123
Cerium-cobalt-plutonium alloys
segregation, 122-23
Cerium-cobalt-plutonium alloys (molten)
corrosive effects, 179-80
viscosity, 122
Cerium-gallium-plutonium alloys
properties and stability, 180
Cerium-magnesium alloys
recrystallization and stress-rupture properties, 35
Cerium-manganese alloys
phase studies, 153
Cerium-nickel alloys
mechanical properties and phase studies, 94
Cerium-plutonium alloys (molten)
viscosity, 62
Cermet cores (metal-clad, metal-capped)
preparation, 165
Cermet dispersions, 106
Cermets (rare-earth)
review, 219-20
Cesium (molten)
corrosive effects, 31, 211
effects on tensile properties of materials, 211
Cesium (vaporized)
corrosive effects, 146, 211
effects on tensile properties of materials, 211
Cesium-cobalt-plutonium alloys (molten)
corrosive effects, 30
Chromium
bonding to Al_2O_3, pressure, 47
compatibility with Eu oxides, 84
corrosion, 30
electrodeposition, 228
mechanical properties, 218

oxidation, 218
plating using, chemical, 109
reaction with UN, 130
thermal properties, 218
Chromium alloys
corrosion, 28
Chromium films
formation on ceramics, 166-67
Chromium-gadolinium alloys
phase studies, 84
Chromium-gadolinium-iron alloys
properties, 24
Chromium-iron alloys
U diffusion in, 153
Chromium-nickel alloy coatings
deposition on UO_2 pellets, 65, 67
Chromium-nickel alloys
corrosion and self-diffusion, 97
Chromium-nickel-silicon system
use in brazing, 230-31
Chromium-nickel-titanium alloys
brazing using, 48
Chromium-niobium alloys
interdiffusion, 39
$NbCr_2$, precipitation, 38
Chromium-niobium-titanium-vanadium alloys
corrosion, 29
Chromium-oxygen-zirconium system
phase studies, 216
Chromium-plutonium dioxide-uranium dioxide dispersions
properties, 7
Chromium-rhenium alloys
internal friction, N effects on, 153
Chromium-silicon system coatings
for refractories, 209
Chromium-silicon-titanium system coatings
for refractories, 209
Chromium-tantalum compounds
thermochemical properties, 153
Chromium-thorium alloys
hot hardness, 183
Chromium-titanium alloys
use in brazing, 112-13
Chromium-titanium-vanadium alloys
corrosion, 145
Chromium-uranium alloys
phase transformation, 1
tempering, 120
Cladding materials, 86-100, 142-60, 206-22
compatibility with B_4C, 205
Coatings
(see also specific coatings)
crack propagation in duplex, 126
ductility of oxidation-resistant, 144
for refractories, 209
review, 67
technology of inorganic, 228
Coatings (refractory alloy), 48
Cobalt
solubility in molten K, 209
Cobalt alloys (MAR-M-302)
properties, 34
Cobalt alloys (MAR-M-322)
properties, 34
Cobalt-iron-uranium alloys
phase studies, 177
Cobalt-oxygen-tungsten system
phase studies, 143
Cobalt-plutonium alloys
transformation, 61
Cobalt-thorium alloys
eutectics, 183
Cobalt-tungsten alloys
oxidation, 143
temper hardening, 94
Cobalt-zirconium diboride system
oxidation, 25
Conferences (Third Geneva)
materials information presented, 52-56
Control materials
Geneva Conference papers, 55-56
Control rod materials
high temperature uses, 25
Copper
compatibility with B_4C, 205
creep-rupture properties, 36
electrodeposition on Zy-2, 165
electroplating on, 165
electroplating on Zy, 108
fatigue detection using ultrasonics, 232
fluoridation, 88
welding, 168, 228-29, 231
Copper (Au-coated)
preparation, 46
Copper (molten)
corrosive effects, 89-90, 212
Copper (refractory-metal-coated)
preparation, 228
Copper alloys
tensile properties, Cs effects on, 211
Copper coatings
failure of, on U, 175
Copper-nickel alloys
self-diffusion, 97
Copper-Nimonic-75 couples
interdiffusion, 140
Copper-niobium-zirconium alloys
oxidation, 142
Copper-plutonium alloys
crystallography, 3
Copper single crystals (irradiated)
yield stress, microstrain, 101
Copper-stainless steel (V2A) couples
interdiffusion, 140
Copper-thorium alloys
eutectics, 183
Corrosion
Geneva Conference papers, 54-55
Croloy 2 1/4
corrosion, 145
Croloy 9M
corrosion, 146-47
Crystals
gas release from, 218
Cutting (explosive)
uses, 231

D

D6ac
welding, 170-71
D-36
bonding, diffusion, 168
brazing, 112-13
D-43
aging, 150
bonding, diffusion, 168
coatings for, 209
electrical resistivity, 150
emittance, total hemispherical, 150
stress-rupture properties, 93
transition temperature, 48
welding, 48, 112, 150, 168
D-43 (coated)
transition temperature, 48
Diborides (refractory)
entropies, 40
Disilicide coatings (V-modified)
feasibility for Nb and Ta alloys, 209
Dysprosium
heat of sublimation and vapor pressure, 204
Dysprosium ceramics
preparation of ultrahigh-purity, 154
Dysprosium intermetallic compounds
crystal structure, 24
Dysprosium oxide-graphite assembly (Hastelloy X-clad)
heat generation in, 140-41

E

Eddy-current testing, 116
Electroplating, 107-8
Europium dioxide particles (PyC-coated)
compatibility, 8
Europium-molybdenum oxide
compatibility with metals and stainless steel, 84
Europium oxide
consolidation and melting, 84
Explosive cutting
uses, 231
Explosive forming, 167
Explosive joining, 109-12
Explosive welding
uses, 231

F

Fabrication
techniques, special, 45-49, 105-17, 163-72, 225-32
Fast Reactor Test Facility
structural materials, 147
Ferroelectrics
hot isostatic pressing, 227
Fertile materials, 1-15, 57-71, 119-32, 175-93
Forming
techniques of explosive, 167
FS-85
welding, 150
FS-85 (Cr-Si-Ti-coated)
preparation, 144-45
Fuel (ceramic-coated)-graphite dispersions
use in gas-cooled reactors, 67
Fuel materials, 1-15, 57-71, 119-32, 175-93
Fuel materials (irradiated)
annealing effects on bubbles, 71
properties, 130-32
Fuel particles
production of spherical, 128
Fuel particles (coated)
symposium, 7-8
Fuel particles (coated)(irradiated)
properties for Dragon reactor, 186
Fuel particles (PyC-coated)
development, 65
Fueled-graphite spheres
bond testing using infrared radiometer, 49
Fuels
corrosion of blanket, in PWR, 27
Geneva Conference papers, 52-54
Fuels (canned)
vibratory compaction, 107
Fuels (irradiated)
testing, 125
Fuels (SS-clad)
corrosion in OMRE, 28

G

Gadolinium
heat of sublimation and vapor pressure, 204
Gadolinium dicarbide-uranium dicarbide system
phase studies, 189-90
Gadolinium intermetallic compounds
crystal structure, 24

Gadolinium-manganese intermetallic compounds
crystal structure and density, 25
Gadolinium-scandium alloys
phase studies, 24
Gallium-iron-plutonium alloys
properties, 180, 183
Gallium-plutonium alloys
fatigue behavior, 180
properties, 180
stability, 180
transformation, 61
Gallium-plutonium alloys (molten)
density, 62
Gallium-plutonium-zinc alloys
properties and stability, 180
Gas Cooled Reactor Experiment
fuel development, 125
Geneva Conference
materials information presented, 52-56
Glasses
crushing, electrohydraulic, 41
heat transfer, effects of high-rate, 99
properties of ceramic, 204
Gold
welding, laser, 229
Gold (irradiated)
damage, 101
Gold (molten)
corrosive effects, 211-12
Gold-thorium alloys
euctectics, 183
Graphite
(see also Carbon)
bonding, pressure, 164
coatings for, 166
hot isostatic pressing, 227
metal diffusion in, 39
oxidation inhibition, 18
reaction with H, 197-98
reaction with steam, 197
reaction with vitreous C, 75
Graphite (boronated)
thermal conductivity, 140
Graphite (Ir-coated)
oxidation, 135, 209
Graphite (irradiated)
annealing effects, 196
dimensional changes, 197, 220
Poisson's ratio increase, 196-97
preparation, 74
stability, 135
tensile-strain limits, 197
Graphite (pyrolytic)
Th diffusion in, 186-87
vapor deposition, 47
Graphite (refractory-metal-coated)
preparation, 228
Graphite (TiN-ZrO_2-coated)
preparation, 109
Graphite (TiN)(ZrO_2-coated)
preparation, 109
Graphite (Y_2O_3-ZrO_2-coated)
preparation, 109
Graphite joints (irradiated)
performance of cemented, 18
Graphite powder
bonding, pressure, 106-7
Graphite single crystals (irradiated)
defects, 18
Graphite spheres (fueled)
bond testing using infrared radiometer, 49

H

Hafnium
annealing, 93
corrosion, 24, 207
electrodeposition, 228
heat capacity, 40
N diffusion in, 84
oxidation, 139
O diffusion in, 83-84
phase transformation, 139
stress relaxation, 93
vapor deposition, 166
welding to Zircaloy, 24-25
Hafnium (irradiated)
tensile properties, 139-40
Hafnium boride
preparation, 40
Hafnium carbide
casting, 105
emissivity, 140
fluorination, 40
oxidation, 40
preparation, 40
Hafnium ceramics
preparation of ultrahigh-purity, 154
Hafnium diboride, 40, 84
Hafnium dioxide powder
preparation of ultrahigh-purity, 154
Hafnium halides, 40
Hafnium-iridium alloys
phase studies, 83
Hafnium-molybdenum alloys
use for brazing, 168, 170, 229
Hafnium-molybdenum-vanadium alloys
use for brazing, 168, 170
Hafnium-molybdenum-zirconium alloys
use for brazing, 168, 170
Hafnium monocarbide
development of fused, 163
heat capacity, 40
heat of formation, 99
Hafnium mononitride-rhenium-tungsten system
tensile properties, 214
Hafnium-nickel alloys
mechanical properties and recrystallization, 24
Hafnium-niobium alloys
phase studies, 37, 83
Hafnium-niobium-zirconium alloys
use for brazing, 168, 170
Hafnium-rhenium-tungsten alloys
phase studies, 37
Hafnium-tantalum alloys
corrosion, 207
oxidation, 29
phase studies, 83
use for brazing, 168, 170, 229
Hafnium-tantalum-tungsten alloys
(see T-111)
Hafnium-tin alloys
phase studies, 24-25
Hafnium-tungsten alloys
mechanical properties, 148
Handbooks
high-temperature materials, 39
Hastelloy 280
corrosion, 28
Hastelloy B
corrosion, 28
Hastelloy C
corrosion, 28, 146-47
Hastelloy N
corrosion, 28, 146-47
ductility, 35
oxidation, 87
Hastelloy W
use for welding, 230
Hastelloy X
carburization, 87
corrosion, 28
nitridation, 87
use for welding, 230
Hastelloy X (irradiated)
ductility, 155-56
mechanical properties, 33
stress-rupture properties, 155-56
Hastelloy X-280
carburization, 143
corrosion, 87
oxidation, 143
Haynes 25
carburization, 87, 143
corrosion, 30, 207, 211
nitridation, 87
oxidation, 143
welding, 230
High-Temperature Lattice Test Reactor
corrosion of alloys, 28
High-temperature materials
handbook, 39
HP 9-4-20
welding, 170-71
HP 9-4-25
welding, 170-71
HP 9-4-45
welding, 170-71
Hydrogen-iridium-lithium system
properties, 137-38
Hydrogen-lithium-rhodium system
properties, 137-38
Hydrogen-niobium-zirconium system
phase studies, 201
Hydrogen-niobium-zirconium system (irradiated)
strength, 81
Hydrogen-nitrogen-zirconium system
structure, 81
Hydrogen-platinum-plutonium dioxide system
interaction, 63
Hydrogen-uranium-zirconium system
combustion, 81
Hydrogen-zirconium system
equilibrium dissociation pressures, 22
phase studies, 22, 81

I

Incoloy (irradiated)
corrosion, 143
Incoloy 800
corrosion, 28-29, 87
thermal-stress fatigue, 212
Incoloy 800 (irradiated)
properties, 156
Inconel
corrosion, 28, 89, 211
creep-rupture properties, 36
stability, metallurgical, 36
Inconel (irradiated)
corrosion, 143
Inconel 600
corrosion, 28, 87
welding to Zy, explosive, 109-12
Inconel 600 (irradiated)
properties, 156
Inconel 625 (irradiated)
properties, 156
Inconel 718
corrosion, 87
Inconel 718 (irradiated)
properties, 156
Inconel X
corrosion, 28, 207
Indium (molten)
corrosive effects, 146, 211-12
Indium-plutonium alloys
phase studies, 178
Indium-thorium alloys
mechanical properties, 63, 183
Indium-thorium-zirconium alloys
hot hardness, 183
INOR-8

stress-rupture properties, 34
Inorganic coatings
technology, 228
Iridium
corrosion, 211-12
Iridium coatings
behavior on graphite, 135, 209
feasibility for Nb and Ta, 209
Iridium-molybdenum alloys
phase studies, 37
Iridium-niobium alloys
phase studies, 37-38, 216
Iridium-tantalum alloys
phase studies, 37-38
Iridium-tungsten alloys
interdiffusion, 39
use for brazing, 229
Iron
compatibility with Eu oxides, 84
corrosion, 28, 31
creep-rupture properties, 36
diffusion in Zr, 39
microstrain, 152
solubility in molten K, 209
Iron (Armco)
welding, 168
Iron (irradiated)
C precipitation in, 221
damage, 159
Iron (white) (irradiated)
graphitization, 100
Iron alloys
impact properties, 91
U diffusion in, 153
Iron alloys (2541)
corrosion, 87
Iron coatings
failure of, on U, 175
Iron-nickel-plutonium alloys
transformation, 61
Iron oxide-lanthanum oxide-nickel oxide system
phase studies, 155
Iron oxide-nickel oxide system
phase studies, 155
Iron-plutonium alloys
transformation, 61
Iron-plutonium alloys (molten)
corrosive effects, 30
Iron-plutonium dioxide dispersions
preparation, 6
Iron-plutonium mononitride-uranium mononitride dispersions
preparation, 6
Iron-plutonium-uranium alloys
casting, 45
ignition, 62
Iron-silicon-uranium system (irradiated)
swelling, pressure effects on, 191
Iron-thorium alloys
eutectics, 183
Iron-uranium alloys
phase studies, 58
Iron-uranium dioxide dispersions
preparation, 6
Iron-uranium dioxide dispersions (2541 alloy-clad)
preparation, 125
Iron-uranium mononitride dispersions
preparation, 6
Iron-uranium rods
rolling, 45
Iron uranium silicide
crystal structure, 129-30
Iron-yttrium alloys
U diffusion in, 153
Iron-zirconium alloys
transformation kinetics, 150
Iron-zirconium diboride system
oxidation, 25

J

Joining (explosive), 109-12

K

Kovar
tensile properties, Cs effects on, 211
welding, laser, 228-29

L

Lanthanum beryllide
thermal dissociation, Be vaporization during, 80
Lanthanum oxide-nickel oxide system
phase studies, 155
Laser interferometry testing, 116-17
Laser welding
uses, 229
Lead (molten)
corrosive effects, 89, 146, 211-12
Lead-thorium alloys (molten)
corrosive effects, 89
Lead-uranium alloys (molten)
corrosive effects, 89
Level indicators
ultrasonic, 231
Lithium (molten)
corrosive effects, 89-90, 146, 211-12
Lithium bromide-lithium hydride system
phase studies, 201
Lithium chloride-lithium hydride system
phase studies, 201
Lithium halides
spectroscopy, 40
Lithium hydride
bonding, pressure, 107
Lithium hydride-lithium iodide system
phase studies, 201
Lithium hydride-sodium chloride system
phase studies, 201
Lithium hydride systems
phase studies, 201
Lithium-magnesium alloys
development, 163
Lithium-nickel-palladium alloys
use for brazing, 230-31
Lithium-silver alloys (irradiated)
He diffusion in, 15
Lucalox
corrosion, 211

M

Magnesium
Pu diffusion in, 97, 123
Magnesium (irradiated)
corrosion and mechanical properties, 30
Magnesium alloys
Pu diffusion in, 123
welding, explosive, 231
Magnesium coatings
failure of, on U, 175
Magnesium-neodymium alloys
mechanical properties, 35
Magnesium-niobium alloys
hardness and phase studies, 35
Magnesium oxide
compatibility with UO_2, 189
hot isostatic pressing, 227
mechanical behavior, 219
Magnesium oxide (irradiated)
expansion, 220
Magnesium oxide coatings
development, 67
Magnesium oxide-plutonium dioxide system
phase studies, 63
Magnesium oxide powder
bonding, pressure, 106
Magnesium oxide single crystals
mechanical behavior and explosion effects on structure, 219
Magnesium oxide-zirconium dioxide system
destabilization and high-temperature properties, 155
Magnesium-vanadium alloys
hardness and phase studies, 35
MAR-M-200
properties, 34
MAR-M-302
properties, 34
MAR-M-322
properties, 34
Marble
crushing, electrohydraulic, 41
Martensite (Zr)
tempering, 215-16
Mercury
corrosive effects, 30, 210-12
Metal borides
use in control rods, 25
Metal coatings
preparation on ceramics, 99-100, 166-67
Metal coatings (refractory)
electrodeposition, 228
Metal oxide coatings
for graphite, 166
Metal oxides
electrodeposition, 108
Metal oxides (rare earth)
use in control rods, 25
Metal powders
bonding pressure, 106
Metal whiskers
production on Cu, 108
Metallic fuels
Geneva Conference papers, 52-53
Metals
bonding, pressure, 47, 164
casting, graphite mold for reactive-, 106
compatibility with U carbides, 11
eddy current diffusion in, 49
electroplating with oxides, 108
forming, explosive, 167
H permeation through, 153
iodide refining, 47
joining to ceramics, 106
plating of, 109
reactions with gases, 14
thickness change detection, 171-72
Metals (bcc) (irradiated)
electrical resistivity, annealing effects on, 159
Metals (irradiated)
mechanical properties, 100
Metals (molten)
corrosive effects, 29, 91, 211-12
diffusion coefficients, 212
Metals (rare earth)
effects on Zr, 97
electrodeposition, 165
properties, 97
Metals (refractory)
behavior, 218
bonding, pressure, 164
coatings of, 48, 209
corrosion, 88-89
enthalpy, 218
metallurgy, 94-97
properties, 218
tensile properties, Cs effects on, 211
thermal expansion, 218
Ti carbide deposition on, 48

welding, 167-68
Metals (refractory) (inorganic-coated)
technology, 228
Metals (refractory)(silicide-coated)
behavior, 166
preparation, 109
Metals (transition)
interactions with C, 97
pack boronizing of, 48
Mobile Low Power Plant No. 1
fuel development, 125
Moderator materials, 18-23, 74-81, 135-38, 196-201
Geneva Conference papers, 55-56
Molybdenum
bibliography, 96-97
brazing, 48, 168, 170, 229
chemical plating using, 109
coatings for, 209
compatibility with UO_2, 189
corrosion, 89-90, 211
creep-rupture properties, 156
dislocation structures, 36
ductile-brittle transition, 217
ductility, B effects on, 152
electrodeposition, 228
flow, strain-rate dependence of, 213
fracture, 95, 214
grain refinement, B effects on, 152
hardness, 96
internal friction, 36
mechanical properties, 218
microstrain, 152
notch-tensile properties, 213-14
oxidation, 29, 88, 218
O gettering effects on Fe solubility in molten K, 209
pack boronizing of, 48
plastic strain, 148
reaction with water, 31-32
self-diffusion in, 218-19
solute diffusion in, 218-19
stored energy release from cold-worked, 101
strength, 96
stress-rupture properties, 91
tensile-ductility transition, 92-93, 213
tensile properties, 213-14
tensile properties, Cs effects on, 211
thermal expansion, 96
thermal properties, 218
use for brazing, 229
vapor deposition, 166
vapor pressure, 37
welding, 167, 229
yield point, 217
yielding, strain-rate dependence of, 213
Molybdenum (irradiated)
creep-rupture properties, 156-57, 159
defects, 148
dislocation loops, 221-22
ductility, 159
properties, 159-60
slip lines, 221
stored-energy release, 101
structure, 159-60
Molybdenum (phosphide-coated)
oxidation, 144
Molybdenum (Re-coated)
preparation, 228
Molybdenum (silicide-coated)
oxidation, 88
Molybdenum alloys
bibliography, 96-97
coatings for, 48
development, 96
microstructure, 36
tensile properties, 36
Molybdenum alloys (coated)
preparation, 109
Molybdenum alloys (Pt-clad)
oxidation, 89
Molybdenum alloys (Pt-Rh alloy-clad)
oxidation, 89
Molybdenum alloys (slurry-coated)
preparation, 144
Molybdenum coatings
failure of, on U, 175
Molybdenum couples
heat treatment, 47
Molybdenum-molybdenum disilicide system
interdiffusion, 39
Molybdenum-nickel alloys
properties, 149
Molybdenum-niobium alloys
oxidation, 143, 208
Molybdenum-niobium-tantalum-tungsten alloys
yield point return, 151
Molybdenum-niobium-titanium alloys
elasticity and shear modulus, 94
Molybdenum-niobium-titanium-vanadium alloys
elasticity and shear modulus, 94
Molybdenum-niobium-uranium alloys
stress cracking, 177-78
transformation, 59-60
Molybdenum-niobium-vanadium-zirconium alloys
(see B-66)
Molybdenum-osmium-tungsten alloys
phase studies, 37
Molybdenum oxide films
preparation of thin, 41
Molybdenum-palladium-rhenium alloys
use for brazing, 229
Molybdenum-plutonium dioxide-uranium dioxide dispersions
properties, 7
Molybdenum-plutonium-uranium alloys
casting, 45
compressive properties, 3-4
ignition, 3
properties, 121
tensile properties, 3
thermal expansion, 3
Molybdenum-rhenium alloys
dislocation structures, 36
internal friction, 36
mechanical properties, 91
precipitation in, sigma-phase, 152
stress-rupture properties, 91
twinning, 95
Molybdenum-rhenium-tungsten alloy tubing
preparation, 163
Molybdenum-rhenium tungsten alloys
ductility, 163
fabrication, 106
melting, 106
properties, 95
stress-rupture properties, 91
Molybdenum-rhenium-tungsten alloys (Mo-clad)
fabrication, 106
Molybdenum silicide
oxidation, 88-89
Molybdenum single crystals
crystallography, 151-52
deformation, 94-95, 217
dislocation loops in quenched, 152
self-diffusion in, 219
structure, fine, 217
Molybdenum-tantalum alloy single crystals
cleavage and electrical transport, 217
Molybdenum-tantalum-tungsten alloys
fabrication, 225
Molybdenum-thorium alloys
hot hardness, 183
Molybdenum-titanium alloys
bonding, pressure, 47, 164
corrosion, 90
local order, 150-51
notch-tensile properties, 213-14
tensile properties, 213-14
Molybdenum-titanium-uranium alloys
stress cracking, 178
Molybdenum-titanium-vanadium alloys
elasticity and shear modulus, 94
Molybdenum-titanium-zirconium alloys (see also TZM)
phase studies, 37
Molybdenum tubing
properties, 37
Molybdenum-tungsten alloys
casting, centrifugal, 46
corrosion, 146
local order, 150-51
Molybdenum-uranium alloys
corrosion, 60
deformation, 58
electroplating Ni on, 165-66
fabrication, 105
mechanical properties, 178
properties, 120
stress cracking, 177-78
transformation, 59-60
Molybdenum-uranium alloys (irradiated)
corrosion, 178
damage, 120-21
phase studies, 121
swelling, 130
Molybdenum-uranium dioxide cermet
fabrication, 125
Molybdenum-uranium-zirconium alloys
corrosion, 60
transformation, 59-60
Molybdenum-vanadium alloys
use for brazing, 229
Molybdenum-zirconium alloys
internal friction, 36
transformation kinetics, 150

N

NaK
corrosive effects, 146-47, 211
Neodymium oxide
hardness and melting point, 25
Neptunium (irradiated)
electrical resistivity, 191
Neutron-image intensification
use in nondestructive testing, 171-72
Nickel
compatibility with Eu oxides, 84
corrosion, 28, 207, 211
creep-rupture properties, 36
deposition on Al alloy (6061), 48
deposition on Be, 166
diffusion in graphite, 39
electrodeposition, 108, 165-66
electroforming, 107
O gettering effects on Fe solubility in molten K, 209
reaction with UN, 130
solubility in molten K, 209
welding, laser, 228-29
Nickel alloys
corrosion, 86-87
hot isostatic pressing, 226
tensile properties, Cs effects on, 211
Nickel alloys (200)
creep-rupture properties, 36
Nickel alloys (270)
creep-rupture properties, 36
Nickel alloys (MAR-M-200)
properties, 34
Nickel alloys (TD)
bonding, diffusion, 168

corrosion, 28
joining, 113, 230
recrystallization, 149
Nickel coatings
properties on Nb-Zr alloy, 166
scaling, 227-28
Nickel foils
bonding to Mo-Ti alloys and W pressure, 47
Nickel-nickel systems
surface diffusion, 154
Nickel-niobium alloys
electrodeposition, 107-8
Nickel-plutonium alloys
transformation, 61
Nickel-silver systems
surface diffusion, 154
Nickel solid solutions
self-diffusion, 97
Nickel-tantalum alloys
electrodeposition, 107-8
recrystallization, 218
Nickel-thorium alloys
eutectics, 183
Nickel-tin-zirconium alloys
hardening, 215
martensite stability in, 215-16
mechanical properties, 215
thermal stability, 215
Nickel-titanium alloys
electrodeposition, 107-8
Nickel-titanium-zirconium alloys
corrosion and hardening, 215
Nickel tubing (PyW-coated)
development, 109
Nickel-tungsten alloys
creep properties, 147
properties, 149
self-diffusion, 97
Nickel-uranium alloys (Al-clad)
ultrasonic testing, 231
Nickel-zirconium alloys
corrosion and hardening, 215
Nickel-zirconium diboride system
oxidation, 25
Nicrobraze
corrosion, 28
Niobium
bibliography, 96-97
compatibility with irradiated C-Pu-U system, 4
contamination in vacuum systems, 150
corrosion, 31, 89-90, 212
creep-rupture properties, 92
deformation, plastic, 91-92
diffusion in, 98
electrodeposition, 108, 228
hardness, 96
heat content, 150
hot isostatic pressing, 226
internal friction, 216
mechanical properties, 216, 218
metallurgy, 151
nitridation, 143-44
oxidation, 143-44, 208, 218
O contamination in vacuum, 38
O gettering effects on Fe solubility in molten K, 209
pack boronizing of, 48
phase transformation, 38
plastic strain, 148
self-diffusion, 39, 219
solubility in molten K, 209
strain aging effects, 216
strength, 96
stress-corrosion cracking, 210
tensile properties, Cs effects on, 211
thermal expansion, 96
thermal properties, 218
use in high-temperature alloys, steel, and superalloys, 151
vapor deposition, 47, 228
Niobium (coated)
preparation, 109, 209
Niobium (irradiated)
defects, 148
Niobium (Ir-coated)
feasibility, 209
Niobium (phosphide-coated)
oxidation, 144
Niobium-95
diffusion in Ta and Zr, 98
Niobium alloys
(see also AS-30, B-66, C-129 Y, Cb-752, D-43 and FS-85)
bibliography, 96-97
corrosion, 29
creep properties, 151
development, 96, 151
oxidation, 208
Re effects on faulting, 151
welding, 112-13
Niobium alloys (Cr-Si-Ti-coated)
feasibility, 209
Niobium alloys (coated)
oxidation, 144
preparation, 109
Niobium alloys
(see D-43 and FS-85)
Niobium alloys (Pt-clad)
oxidation, 89
Niobium alloys (Pt-Rh alloy-clad)
oxidation, 89
Niobium alloys (slurry-coated)
preparation, 144
Niobium alloys (V-modified disilicide-coated)
feasibility, 209
Niobium beryllide
oxidation resistance, 21
Niobium carbide
effect on ferrite grain growth in mild steel, 151
interaction with W, 96
precipitation in austenitic steel, 151
Niobium carbide-tungsten system
phase studies, 96
Niobium diboride
emissivity and thermal conductivity, 84
Niobium foils
bonding to Mo-Ti alloys and W pressure, 47
Niobium hydride
structure, 22
Niobium monocarbide
thermal expansion and thermodynamic properties, 40
Niobium monocarbide-uranium monocarbide system
deformation, 190
Niobium-niobium-titanium alloy couples
interdiffusion in, 219
Niobium-nitrogen system
phase studies, 151
Niobium oxide-tungsten oxide system
phase studies, 41
Niobium oxides
structure, 208
Niobium-palladium alloys
phase studies, 37-38
use for brazing, 229
Niobium-platinum alloys
phase studies, 37-38
Niobium-plutonium dioxide-uranium dioxide dispersions
properties, 7
Niobium-plutonium-uranium alloys
properties, 121
Niobium powder
bonding, pressure, 106
Niobium-rhenium alloys
transition temperature, 151
Niobium-rhodium alloys
phase studies, 37-38, 216
Niobium-ruthenium alloys
phase studies, 37, 151
properties, 38
Niobium-silicon system coatings
for refractories, 209
Niobium single crystals
annealing, 39, 150
yield strength, 216
Niobium-tantalum alloys
welding, 150
Niobium-tantalum-tungsten alloys
corrosion, 210
Niobium-tantalum-vanadium alloys
coatings for, 48
use in brazing, 113
Niobium-thorium alloys
hot hardness, 183
Niobium-tin alloys
crystallography and phase studies, 97
Niobium-titanium alloys
local order, 150-51
strength, 151
Niobium-titanium oxide
crystal structure, 220
Niobium-titanium-vanadium alloys
coatings for, 48
corrosion, 29
elasticity, 94
shear modulus, 94
use for brazing, 150
Niobium-titanium-vanadium alloys (silicide-coated)
oxidation, 144
Niobium tubing (Be-clad)
fabrication, 20
Niobium-tungsten alloys
corrosion, 146
mechanical properties, 148
oxidation, 143
Niobium-tungsten-zirconium alloys
coatings for, 48
Niobium-uranium alloys
corrosion, 60
lattice parameters, 176-77
phase studies, 120, 177
transformation, 59-60
Niobium-uranium-zirconium alloys
corrosion, 60
properties, 2
transformation, 60
Niobium-vanadium alloys
deformation, 96
use for brazing, 229
Niobium-zirconium alloys
brittleness, H effects on, 214
compatibility with UC, 11
contamination in vacuum systems, 150
corrosion, 30-31, 90, 210-11
electrical resistivity, 150
emittance, total hemispherical, 150
hardness, 94
H solubility in, 137
oxidation, 206
stress-corrosion cracking, 210
welds, thermoelectric testing of, 232
Niobium-zirconium alloys (irradiated)
strength of hydrided, 81
Niobium-zirconium alloys (Mo-coated)
preparation, 109
Niobium-zirconium alloys (Ni-coated)
properties, 166
scaling, 227-28
Nitrides
preparation of ultrahigh-purity, 154
Nitrides (Group 4a, 5a, and 6a)
properties and purification, 41

Nitrides (refractory)
constitution, 68
entropies, 40
properties, 68
Nondestructive testing, 48-49, 115-17, 171-72, 231-32
Geneva Conference papers, 54-55
Nuclear poisons, 24-25, 83-85, 139-41, 204-5

O

Oak Ridge Research Reactor
water chemistry of pressurized-water loop, 207
Organic Moderated Reactor Experiment
corrosion of SS-clad fuel, 28
Oxide particles (PyC-coated)(irradiated)
properties, 7
Oxides
preparation of ultrahigh-purity, 154
use in control rods, 25
vibratory compaction, 107
Oxides (refractory)
entropies, 40
Oxygen-plutonium system
phase studies, 5, 124
Oxygen-plutonium system (self-irradiated)
damage, 5
Oxygen-samarium-tungsten system
phase studies, 143
Oxygen-tantalum-titanium-zirconium system
phase studies, 38
Oxygen-titanium-tungsten system
phase studies, 143
Oxygen-tungsten system
phase studies, 143

P

Palladium-tantalum alloys
phase studies, 37-38
Palladium-tungsten alloys
phase studies, 37
Palladium-uranium alloys
phase studies, 2-3, 60-61
Particles
compaction, 227
Phosphide coatings
oxidation, 144
Piezoelectrics
hot isostatic pressing, 227
Piping
rupture in water-cooled reactors, 148-49
Plating
by vapor deposition, 47
electro-, 107-8
Platinum
oxidation, 89
Platinum-plutonium alloys
phase studies, 122
Platinum-rhodium alloys
oxidation, 89
Platinum-tantalum alloys
phase studies, 37-38
Platinum-tungsten alloys
interdiffusion, 39
Platinum-zirconium alloys
H pickup, 206
Plutonium
crystallography, 122
deformation, 123
diffusion in Mg, 97, 123
diffusion in Mg alloys, 123
fracture, 61
phase transformation, 3, 61, 122
physical metallurgy, 122
self-diffusion, 123, 179
solubility in U_2Ti, 179
Plutonium (irradiated)
electrical resistivity, annealing effects on, 191
Plutonium (molten)
W solubility in and vapor pressure, 179
Plutonium alloys
melting points, 122
phase studies, 178-79
phase transformation, 61, 122
Plutonium arsinide
properties, 63
Plutonium boride
preparation, 124
Plutonium carbide
constitution, 68
preparation by sol-gel process, 11
properties, 68
Plutonium carbide-uranium carbide system
compatibility with SS (316L), 124
thermal conductivity, 11
Plutonium compounds
physical properties, 63
solubility, 63
use as fuel, potential, 63
Plutonium dioxide
preparation by sol-gel process, 11
reaction with PuN, 5, 63
reaction with SS(304), 63
thermal expansion, 4
thermal reduction, stabilization against, 183
Plutonium dioxide-stainless steel dispersions
density, 125
fabrication, 184
Plutonium dioxide-stainless steel dispersions (irradiated)
stability, 184
Plutonium dioxide-stainless steel (304) dispersions
preparation, 183
Plutonium dioxide-stainless steel (304) dispersions (irradiated), 183
Plutonium dioxide-thorium dioxide system
stability in H, 123
Plutonium dioxide-tungsten-uranium dioxide dispersions
properties, 7
Plutonium dioxide-uranium dioxide dispersions
properties, 7
Plutonium dioxide-uranium dioxide mixtures (irradiated)
solid-solution formation, 183
Plutonium dioxide-uranium dioxide powder (Zy-clad)
vibrational compaction, 227
Plutonium dioxide-uranium dioxide rods
preparation, 165
Plutonium dioxide-uranium dioxide rods (Zy-2-canned)
preparation, 164-65
Plutonium dioxide-uranium dioxide-stainless steel (316L) dispersions
preparation and properties, 184
Plutonium dioxide-uranium dioxide system
electrical resistivity, 63
phase studies, 124
sintering, 63
Plutonium dioxide-uranium dioxide-zirconium dispersions
properties, 7
Plutonium monoboride
preparation, 124
Plutonium monocarbide
preparation, 183
properties, 4
Plutonium monocarbide-plutonium mononitride system
preparation and properties, 5
Plutonium monocarbide-plutonium monoxide system
preparation, 124
Plutonium monocarbide powder
sintering, 4
Plutonium monocarbide-uranium monocarbide pellets
preparation, 4
Plutonium monocarbide-uranium monocarbide system
preparation, 123, 183
Plutonium mononitride
melting point, 69
preparation, 123
reaction with PuO_2, 5, 63
reactions, chemical, 63
solid solubility with ThN, TiN, and ZrN, 5
stability, 63
volatility, 5
Plutonium mononitride (irradiated)
conversion to powder, 5
Plutonium mononitride powder
sintering, 183
Plutonium mononitride systems
reactions, chemical, 63
Plutonium mononitride-uranium mononitride system
volatility, 5
Plutonium mononitride-zirconium mononitride system
preparation, 183
Plutonium monophosphide
lattice parameters, 124
Plutonium monophosphide powder
preparation, 124
Plutonium monosulfide
lattice parameters and thermal expansion, 124
Plutonium monosulfide powder
preparation, 124
Plutonium monoxide
preparation, 63, 124
Plutonium monoxide-uranium monoxide system
preparation, 63, 183
Plutonium nitride
constitution, 68
fabrication, 63
preparation, 63
properties, 41, 68
purification, 41
Plutonium nitride-uranium nitride system
preparation, 123
Plutonium nitride-uranium nitride system (irradiated)
reaction with SS(304), 63
Plutonium oxide
electrodeposition, 108
properties, thermodynamic, 63
Plutonium oxide-uranium oxide couples
interdiffusion, 5
Plutonium phosphide
properties, 63
Plutonium-plutonium mononitride system
phase studies, 5
Plutonium-scandium alloys
phase studies, 3, 123, 178
Plutonium sesquioxide
compositional range, 183
phase studies, 63
Plutonium sesquioxide-uranium dioxide system
phase studies, 63
Plutonium silicide
properties, 63
Plutonium-silicon system

phase studies, 123
Plutonium single crystals
preparation, 61
Plutonium suboxides
thermal conductivity, 183
Plutonium-thorium alloys
electrical resistivity, 5
phase studies, 63-64
thermal expansion, 5
Plutonium-thorium-uranium alloys
phase studies, 63-64
Plutonium-titanium-uranium alloys
casting, 45
phase studies, 121-22, 179
properties, 121-22
strength, compressive, 180
Plutonium trialuminide
polymorphic transformations, 183
Plutonium-uranium alloys
ignition, 3
Plutonium-uranium-fissium alloys (jacketed)(irradiated)
damage, 180
Plutonium-uranium-fizzium alloys
compatibility with cladding materials, 4
compatibility with Ti-V alloy, 62
creep, compressive, 62
transformation, 62
Plutonium-uranium-vanadium alloys
casting, 45
Plutonium-uranium-zirconium alloys
properties, 121-22
Poisons (nuclear), 24-25, 83-85, 139-41, 204-5
Porcelains
heat transfer, effects of high-rate, 99
Potassium (molten)
corrosive effects, 90-91, 211-12
metal solubility in, 209
Potassium fluoride (irradiated)
Ar diffusion in, 15
Potassium-sodium alloys
(see NaK)
Praseodymium
electrodeposition, 165
Pyrolytic carbon
(see Carbon (pyrolytic) and Graphite (pyrolytic))
Pyrolytic tungsten
vapor deposition, 108
Pyrolytic tungsten coatings
development, 109
Pyrolytic zirconium monocarbide
properties, 99

R

Radium
diffusion in graphite, 39
Rare-earth borides
use in control rods, 25
Rare-earth cermets
review, 219-20
Rare-earth oxides
use in control rods, 25
Rare earths
effects on Zr, 97
electrodeposition, 165
properties, 97
Reactor components
joining, 171
Reactors (water-cooled)
pipe rupture, 148-49
Refractories
(see also Alloys (refractory) and Metals (refractory))
coating of, 48, 209
corrosion, 146
crushing, electrohydraulic, 41
handbook, 39
thermal properties, 218
Ti carbide deposition on, 48
Refractories (metal-coated)
preparation, 108-9
Refractory borides
entropies and heats of formation, 40
Refractory carbides
constitution, 68
entropies, 40
heats of formation, 40
properties, 68
Refractory metal alloys
contamination in vacuum, 38-39
Refractory nitrides
constitution, 68
entropies, 40
properties, 68
Refractory oxides
entropies, 40
René
brazing, 113
Rene 41
welding, 229, 231
Rhenium
bibliography, 96-97
corrosion, 146
electrical resistivity, 150
electrodeposition, 228
emittance, total hemispherical, 150
hot isostatic pressing, 226
mechanical properties, 218
oxidation, 218
stress-rupture properties, 91
thermal properties, 218
Rhenium alloys
bibliography, 96-97
Rhenium powder
bonding, pressure, 106
Rhenium-ruthenium-tungsten alloys
use for brazing, 229
Rhenium-tantalum alloys
fracture, 151
Rhenium-thorium dicarbide system
phase studies, 129
Rhenium-thorium dioxide-tungsten system
tensile properties, 214
Rhenium-tungsten alloy tubing
fabrication, 106
preparation, 163
Rhenium-tungsten alloys
brazing, 229
corrosion, 146
creep, 214
creep-rupture properties, 156
drawing, 225
ductility, 163
extrusion, 46, 225
mechanical properties, 148
melting, 106
oxidation, 29
preparation, 46, 105-6
properties, 37
sleeve production, 225
stress-rupture properties, 91
tensile properties, 214
vapor deposition, 47, 108, 166
Rhenium-tungsten alloys (irradiated)
creep-rupture properties, 156-57
ductility, 157
Rhenium-tungsten tubing
extrusion, 46
Rhodium-tantalum alloys
phase studies, 37-38
Rhodium-tungsten alloys
interdiffusion, 39
use for brazing, 229
Ruthenium
corrosion, 211-12
Ruthenium-tungsten alloys
use for brazing, 229
Ruthenium-uranium alloys
phase studies, 177

S

Samarium oxide
hardness and melting point, 25
Samarium-tungsten alloys
oxidation, 143
Santowax OM
corrosive effects, 30
Sapphire
corrosion of synthetic, 211
Shippingport Pressurized Water Reactor
blanket fuel rod corrosion, 27
Silicide coatings
behavior on refractory metals, 166
formation, 48
repair, 48
Silicides
oxidation, 88-89
Silicon
corrosion, 30
Silicon carbide
crushing, electrohydraulic, 41
Silicon coatings
for refractories, 209
Silicon dioxide (irradiated)
expansion, 220
Silicon dioxide whiskers
preparation, 108
Silicon monocarbide
compatibility with UO_2, 189
Silicon monocarbide (irradiated)
expansion, 220
Silicon nitride crystals
preparation, 108
Silicon-titanium system coatings
for refractories, 209
Silicon-uranium rods
rolling, 45
Silicon-uranium system
hot hardness, 58-59
microstructure, 58-59
phase studies, 58
Silver
diffusion in graphite, 39
Silver (molten)
corrosive effects, 146, 211-12
Silver-silver systems
surface diffusion, 154
Silver-thorium alloys
eutectics, 183
Sodium
effects on mechanical properties of SS(316), 209-10
effects on mechanical properties of steel (Cr-Mg), 210
Sodium (molten)
corrosive effects, 29-31, 90, 145, 210-12
Sodium alloys
(see NaK)
Sodium-cooled reactors
materials for, 31
Stainless steel
boronizing, 228
carburization, 90
compatibility with Eu oxides, 84
compatibility with Pu-Ti-U alloys, 121
compatibility with U carbides, 11
compatibility with UO_2, 189
corrosion, 27-28, 30-31, 86-87, 147, 207
corrosion products, 87
corrosion resistance, B effects on, 24
electroplating on, 165
fabrication, manual of, 149
fatigue detection using ultrasonics, 232
joining, 171

mechanical properties, B effects on, 24
metallurgical stability, 36
oxidation, 87
properties, manual of, 149
reaction with UC, 69
reaction with UN, 130
stress-corrosion cracking, 87
tensile properties, Cs effects on, 211
weight loss in vacuum systems, 150
Stainless steel (17-4 PH)
corrosion, 28, 211
Stainless steel (17-7 PH)
corrosion, 211
Stainless steel (18-8)
corrosion, 27
Stainless steel (18-10)
corrosion, 207
Stainless steel (302)
tensile properties, Cs effects on, 211
Stainless steel (304)
compatibility with B_4C, 205
corrosion, 31, 143, 207
creep, 212-13
creep-rupture properties, 36
reaction with PuO_2, 63
stress-corrosion, 28, 143
thermal-stress fatigue, 212
welding, 168
Stainless steel (304) (irradiated)
corrosion, 30, 87, 143
mechanical properties, 30
properties, 155
reaction with PuN-UN system, 63
tensile properties, 100
Stainless steel (304L)
thermal-stress fatigue, 212
ultrasonic testing, 171
welding to Al alloy (6061), 115
Stainless steel (304L) tubing
eddy-current testing, 232
Stainless steel (310) (irradiated)
corrosion, 143
Stainless steel (316)
compatibility with C-Pu-U system, 4
corrosion, 145-47, 210-11
creep properties, 150
mechanical properties, 145, 209-10
welding, 230
Stainless steel (316L)
compatibility with Pu carbide-U carbide system, 124
Stainless steel (321)
welding, laser, 229
Stainless steel (347)
corrosion, 146-47
Stainless steel (347)(irradiated)
corrosion, 30
mechanical properties, 30, 33
Stainless steel (347)-uranium dioxide dispersions (SS(347)-clad)
fabrication, 6
Stainless steel (347)-uranium dioxide dispersions (SS(347)-clad) (irradiated)
damage, 65
Stainless steel (347)-uranium dioxide (sol-gel) dispersions
fabrication and structure, 65
Stainless steel (348)
corrosion products, 87
Stainless steel (348) (irradiated)
corrosion, 143
properties, 155
Stainless steel (403)
thermal-stress fatigue, 212
Stainless steel (430)
compatibility with B_4C, 205
Stainless steel (440C)
welding, laser, 229
Stainless steel (4340)
ultrasonic testing, 171
Stainless steel (A-286)(irradiated)
mechanical properties, 33
Stainless steel (AM-350)
corrosion, 211
Stainless steel (austenitic)
corrosion, 28
thermal-stress fatigue, 212
Stainless steel (austenitic) (irradiated)
ductility, 155
stress-rupture properties, heat treatment effects on, 221
Stainless steel (irradiated)
properties, 87, 221
Stainless steel (martensitic)
thermal-stress fatigue, 212
Stainless steel plates
ultrasonic testing of thin, 49
Stainless steel-plutonium dioxide-uranium dioxide dispersions
properties, 7
Stainless steel tubing (Be-clad)
fabrication, 20
Stainless steel-uranium dioxide dispersions
fabrication, 65
preparation, 125
structure, 65
thermal cycling, 125
Stainless steel-uranium dioxide dispersions (irradiated)
properties, 65
Stainless steel-uranium dioxide dispersions (SS-clad)
roll bonding, 46-47
Steel
boronizing, 228
corrosion, 27
embrittlement by plastic fatigue, 213
Nb use in, 151
tempering effects, 149
welding to Al alloys, 115
Steel (1151)
welding, laser, 229
Steel (4130)
compatibility with B_4C, 205
Steel (4130)(irradiated)
corrosion and mechanical properties, 30
Steel (A-212)
ultrasonic testing, 171
Steel (A-302B)
thermal-stress fatigue, 212
Steel (A-302B) (irradiated)
ductile-brittle transition temperature, 220
fatigue, 33
stability, stress effects on, 220-21
transition temperature, 100
Steel (A-387D)
thermal-stress fatigue, 212
Steel (alloy)
embrittlement, 35-36
Steel (Al-Cr-Mo)
corrosion, 28
Steel (AMM02, grade S)(irradiated)
mechanical properties, 33
Steel (APS 10M4)
corrosion, 28
Steel (austenitic)
corrosion, 30
Nb carbide precipitation in, 151
Steel (carbon)
boronizing, 228
corrosion, 27-28
Steel (carbon)(irradiated)
corrosion, 30
damage recovery, 220
mechanical properties, 30, 220
transition temperature, 33
wear resistance, 221
Steel (Cr)
boronizing, 228
Steel (Cr-Mg)
mechanical properties, Na effects on, 210
Steel (Cr-Mo)
corrosion, 29-30, 145
mechanical properties, 145
oxidation, 88
Steel (Cr-Mo-Ti)
corrosion, 210
Steel (Croloy 2 1/4)
corrosion, 145
thermal-stress fatigue, 212
Steel (Croloy 9M)
corrosion, 146-47
Steel (DFOV 4S, grade V) (irradiated)
mechanical properties, 33
Steel (ferritic)
corrosion, 30
Steel (ferritic) (irradiated)
damage recovery, 220
ductile-brittle transition temperature, 220
mechanical properties, 220
toughness, 100
Steel (high-strength)
welding, 170-71
Steel (irradiated)
embrittlement measurement, 220
Steel (low-alloy)
corrosion, 27
Steel (low-alloy)(irradiated)
transition temperature, 33
Steel (low-carbon)
corrosion, 210-11
Steel (low-carbon)(irradiated)
annealing effects and mechanical properties, 220
Steel (Mn-Mo)(irradiated)
mechanical properties, 33
Steel (maraging)
welding, 168, 171
Steel (mild)
corrosion, 29
explosive drilling and welding, 231
ferrite grain growth in, 151
Steel (mild)(irradiated)
annealing effects and mechanical properties, 220
Steel (Mo)(irradiated)
embrittlement, 33
Steel (refractory-metal-coated)
preparation, 228
Steel piping
rupture in water-cooled reactors, 148-49
Structural materials, 27-41, 86-100, 142-60, 206-22
Geneva Conference papers, 55
summary for FARET, 147
Sulfur-uranium system
phase studies, 190
Superalloys
hot isostatic pressing, 226
Nb use in, 151
weight loss in vacuum systems, 150
welding, 230
Systems for Nuclear Auxiliary Power
nondestructive determination of ^{235}U in fuel, 49

T

T-111
bonding, diffusion, 168
corrosion, 146
electrical resistivity, 150
emittance, total hemispherical, 150
stress-rupture properties, 93
welding, 112, 150, 168
T-111 (Al-Sn-coated)

preparation, 144
Tantalum
bibliography, 96-97
boronizing, 48
brazing, 113, 229
brazing alloys for, 168, 170
compatibility with UO_2, 189
corrosion, 30, 89-90, 145-46
diffusion in, 98
electrodeposition, 108, 228
flow stress, 96
hardness, 96
hot isostatic pressing, 226
mechanical properties, 218
^{95}Nb diffusion in, 98
oxidation, 208, 218
O gettering effects on Fe solubility in molten K, 209
preferred orientation, 216
reactions with CO_2 and CO, 208
solubility in molten K, 209
solubility in molten Sn, 145
strength, 96
stress-rupture properties, 93
tensile properties, Cs effects on, 211
thermal expansion, 96
thermal properties, 218
use for brazing, 229-30
vapor deposition, 47
Tantalum (carbide-coated)
corrosion, 179
Tantalum (Ir-coated)
feasibility, 209
Tantalum (phosphide-coated)
oxidation, 144
Tantalum alloys
(see also T-111)
bibliography, 96-97
development, 96
fabrication, 225
oxidation, 208
Re effects on faulting, 151
Tantalum alloys (carbide-coated)
corrosion, 179
Tantalum alloys (Cr-Si-Ti-coated)
feasibility, 209
Tantalum alloys (coated)
preparation, 109
Tantalum alloys (slurry-coated)
preparation, 144
Tantalum alloys (V-modified disilicide-coated)
feasibility, 209
Tantalum carbide
bonding, pressure, 106
Tantalum foils
bonding to Mo-Ti alloys and W pressure, 47
Tantalum monocarbide
thermal expansion, 40
Tantalum monocarbide-tungsten single crystals
tensile properties, 214
Tantalum monocarbide-zirconium monocarbide system
thermal expansion, 40
Tantalum powder
bonding, pressure, 106
Tantalum-titanium-vanadium alloys
use in brazing, 113, 150
Tantalum-tungsten alloy single crystals
tensile properties, 214
Tantalum-tungsten alloys
bonding, pressure, 164
brazing, 48, 229
coatings for, 48
corrosion, 30, 146, 210
fabrication, 225
mechanical properties, 148
stress-rupture properties, 91
tensile properties, 214
welding, 167-68
Tantalum-tungsten alloys (Al-Sn-coated)
preparation, 144
Tantalum-tungsten alloys (V-modified disilicide-coated)
preparation, 144-45
Tantalum-tungsten-zirconium alloys
fabrication, 225
phase studies, 37
TD
(see Nickel alloys (TD))
Technetium-tungsten alloys
preparation, 226
Television
use of x-ray-sensitive, for position determination, 49
Tellurium (molten)
corrosive effects, 212
Testing (nondestructive), 48-49, 115-17 171-72, 231-32
Geneva Conference papers, 54-55
Third International Conference on the Peaceful Uses of Atomic Energy
materials information presented, 52-56
Thorium
diffusion in graphite, 39, 186-87
hot hardness, 183
vapor deposition, 108
welding, use of Zr in, 5
Thorium alloys
corrosion, 184
eutectics, 183
hot hardness, 183
Thorium aluminide
properties, 124
Thorium beryllide
properties, 124
Thorium beryllide-uranium beryllide system
properties, 124
Thorium carbide
constitution and properties, 68
Thorium carbide-uranium carbide particles (PyC-coated)
compatibility with water vapor, 187
Thorium ceramics
preparation of ultrahigh-purity, 154
Thorium dicarbide
electrical resistivity, 129
preparation by sol-gel process, 11-12
properties, 124
Thorium dicarbide spheres
preparation and properties, 189
Thorium dicarbide-uranium dicarbide particles (PyC-coated) (irradiated)
behavior, 7, 67, 127
stability, 185
Thorium dicarbide-uranium dicarbide system
phase studies, 68-69
properties, 124, 190
Thorium dioxide
bonding to W, pressure, 47
preparation by sol-gel process, 11-12
Thorium dioxide (irradiated)
Xe diffusion in, 15
Thorium dioxide microspheres (PyC-coated)
interactions, 12
Thorium dioxide particles (PyC-coated)
compatibility, 8
Thorium dioxide spheroids
preparation, 189
Thorium dioxide-tungsten system
density, 46
extrusion, 46
preparation, 46
tensile properties, 214
Thorium dioxide-uranium dioxide microspheres (PyC-coated)
interactions, 12
Thorium dioxide-uranium dioxide particles (PyC-coated)(irradiated)
behavior, 7, 67
stability, 185
Thorium dioxide-uranium dioxide pellets
fabrication, 68
Thorium dioxide-uranium dioxide powder
sintering, 10
vibratory compaction, 10, 107
Thorium dioxide-uranium dioxide system
preparation by sol-gel process, 12
Thorium dioxide-uranium dioxide system (irradiated)
fission-gas release, stress effects on, 192
Thorium monocarbide
properties, 124
Thorium monocarbide-uranium monocarbide system
properties, 124
Thorium mononitride
melting point, 69
preparation by sol-gel process, 12
solid solubility with PuN, 5
Thorium monophosphide-uranium monophosphide system
properties, 129
Thorium monosilicide
properties, 124
Thorium monosilicide-uranium monosilicide system
properties, 124
Thorium nitrate
electrodeposition, 165
Thorium nitride
constitution, 68
properties, 68
purification, 41
Thorium oxide
electrodeposition, 108
Thorium sesquisilicide
properties, 124
Thorium sesquisilicide-uranium sesquisilicide system
properties, 124
Thorium tetraboride
properties, 124
Thorium tetraboride-uranium tetraboride system
properties, 124
Thorium-thorium dioxide-zirconium system
tensile strength, hot, 63
Thorium-titanium alloys
hot hardness, 183
Thorium-uranium alloys
corrosion, 184
hot hardness, 183
Thorium-uranium alloys (Zy-2-clad)
brazing, use of Be-Zy-2 alloy in, 5-6
Thorium-uranium-zirconium alloys
corrosion, 184
Thorium-uranium-zirconium alloys (Zy-2-clad)
coextrusion, 5
Thorium-vanadium alloys
hot hardness, 183
Thorium-yttrium alloys
corrosion, 184
hot hardness, 183
Thorium-zirconium alloys
melting and casting, 5
phase studies, 64
Tin
corrosion, 31
Tin (molten)
corrosive effects, 89, 212
Ta solubility in, 145

Tin-uranium alloys (molten)
corrosive effects, 89
Tin-vanadium-zirconium alloys, 215
Titanium
bonding, pressure, 164
boronizing, 48
brazing using, 48
casting, graphite mold for, 106
compatibility with Pu-Ti-U alloys, 121
corrosion, 90
diffusion in, 154
electrodeposition, 108
tensile properties, Cs effects on, 211
vapor deposition, 166
welding, laser, 229
Titanium alloys
(see also B120VCA)
tensile properties, Cs effects on, 211
Titanium carbide
deposition on refractory metals, 48
Titanium ceramics
preparation of ultrahigh-purity, 154
Titanium diboride
emissivity and thermal conductivity, 84
Titanium dioxide
vapor deposition, 47-48
Titanium films
formation on ceramics, 166-67
Titanium foils
bonding to Mo-Ti alloys and W pressure, 47
Titanium mononitride
hydriding, 201
solid solubility with PuN, 5
Titanium mononitride-uranium mononitride system
phase studies, 11, 130
Titanium-tungsten alloys
oxidation, 143
Titanium-uranium intermetallic compounds
Pu solubility in, 179
strength, compressive, 180
Titanium-vanadium alloys
compatibility with Pu-Ti-U alloys, 121
compatibility with Pu-U-Fz alloys, 4, 62
consolidation, 225-26
corrosion, 30
fabrication, 225-26
preparation, 46
use in brazing, 48
Titanium-vanadium-zirconium alloys
hardening, 215
Transition metal borides
use in control rods, 25
Transition metals
pack boronizing of, 48
Tungsten
bibliography, 96-97
bonding, pressure, 47, 164
boronizing, 48
brazing, 229
compatibility with UO_2, 189
corrosion, 146, 211
creep, 214
drawing, 46
ductile-brittle transition, 217
ductility, 95
electrodeposition, 228
electroplating on, 165
extrusion, 46, 225
fabrication, 105
grain growth, 204
hardness, 96
hot isostatic pressing, 226
interaction with Nb carbide, 96
mechanical properties, 37, 218
oxidation, 29, 88, 143, 208, 218
solubility in molten Pu, 179
strength, 96
tensile properties, 214
tensile properties, Cs effects on, 211
tensile strength, 95
thermal expansion, 96
thermal properties, 218
vapor deposition, 47-48, 109, 166
welding, 168
yield-point return, 95-96
Tungsten (irradiated)
mechanical properties, 156-57
Tungsten (phosphide-coated)
oxidation, 144
Tungsten (pyrolytic)
vapor deposition, 108
Tungsten (Re-coated)
preparation, 228
Tungsten (silicide-coated)
oxidation, 88
Tungsten (Si carbide-coated)
oxidation, 109
Tungsten (Si-W-coated)
corrosion and preparation, 144
Tungsten (Si-W, Ti, Zr-coated)
corrosion and preparation, 144
Tungsten alloys
bibliography, 96-97
development, 96
ductility, 37
mechanical properties, 148
oxidation, 208
Tungsten carbide
bonding, pressure, 106
corrosion, 211
Tungsten coatings
for graphite, 166
uses, 166
Tungsten coatings (pyrolytic)
development, 109
Tungsten couples
heat treatment, 47
Tungsten powder
bonding, pressure, 106
Tungsten silicide
corrosion, 89
Tungsten single crystals
Re diffusion in, 219
self-diffusion in, 219
tensile properties, 214
Tungsten systems
strength, 37
Tungsten tubing
fabrication, 105-6
Tungsten-uranium dioxide dispersions
fabrication, preparation and tensile properties, 6
TZM
bonding, diffusion, 168
brazing, 48
coatings for, 209
contamination in vacuum systems, 150
corrosion, 89-91, 146
creep, 214
extrusion, 163
O contamination in vacuum, 38
welding, 167

U

Ultrasonic testing
(see Nondestructive testing)
Uranium, 119
analysis, X-ray, 119
annealing effects, 1, 175-76
casting, 163-64
chemical properties, 176
corrosion, 71, 175-76
creep, activation energy for, 1
diffusion in, 154
diffusion in graphite, 39
diffusion in Fe alloys, 153
ductile-brittle transition, 175-76
ductility, annealing effects on, 1
fracture, annealing effects on, 1
grain size effects, 57
grain size ultrasonic measurement, 48-49
hot hardness, 120
H content, 1
intermetallic compound precipitation in adjusted, 177
loading rate effects, 57
nitriding, 189
oxidation, 13
physical metallurgy, 175-76
physicochemical properties, 176
plastic deformation effects, 57
polygonization, 175-76
production, 176
reaction with steam, 13-14
stacking faults, 175-76
tensile properties, 57
texture, quench-induced, 175
thickness change detection, 171-72
transition temperature, 57
welding, 113, 168
Uranium (Al-clad)
bonding, 226
Uranium (ferrous metal-clad)
roll bonding, 47
Uranium (irradiated)
behavior, 57
defects, annealing effects on, 191
dislocation loops, 131
electrical resistivity, 191
growth, anisotropic, 57
Kr diffusion, 131
mass transport by fission fragments, 14
swelling, 14-15, 119, 130-31, 175, 191
tensile creep ductility, 175
U ejection, 190-91
Xe diffusion, 131
Uranium (metal-coated)
failure, 175
Uranium (Nb-coated)
preparation, 228
Uranium (UAl_3-coated)
oxidation, 175
Uranium-233 (irradiated)
electrical resistivity, 191
Uranium-235
nondestructive determination in fuels, 49
Uranium alloys, 119
cracking, tempering effects on, 164
development by SLIS technique, 176
mechanical properties, 120
particle size in, 176
Uranium alloys (ferrous metal-clad)
roll bonding, 47
Uranium alloys (irradiated)
growth, 57
swelling, 130
Uranium beryllide-uranium monocarbide system
phase studies, 68
Uranium billets
hole broaching and scalping, 45
Uranium carbide powder
preparation, 130
sintering, 70
Uranium carbides
compatibility with cladding materials, 11
constitution, 68
creep, 11
data manual, 127
melting, 70
preparation by sol-gel process, 11
properties, 68
technology, 10
Uranium ceramics
data manual, 127
Uranium compounds

chemical and physicochemical properties, 176
Uranium dicarbide
precipitation in UC single crystals, 129
thermal conductivity, 69
Uranium dicarbide (irradiated)
fission product release, 131
Uranium dicarbide particles (PyC-coated) (irradiated)
behavior, 7, 67, 127
stability, 185
Uranium dicarbide-uranium dioxide system
phase studies, 129
Uranium dioxide
B_4C addition to fuel, 204
compatibility with reactor materials, 189
crushing of sintered, electrohydraulic, 41
density of sintered, oxide addition effects on, 68
grain growth, 67
preparation of granular, 10
reaction with Al, 9-10
thermal conductivity, 127, 189
thermal conductivity of sintered, 67
thermochemical deposition, 68
vapor deposition, 228
vapor pressure, 128
Uranium dioxide (irradiated)
damage in thin layers, 132
fission-product behavior in, 127-28, 131-32
fission-product release, 187-89, 192-93
melting point, 67, 132
refabrication, 129
swelling, 14
U formation in, 9
Xe diffusion in, 15
Uranium dioxide (SS-clad)
bonding, roll, 226
fabrication, 10
vibratory compaction, 107
Uranium dioxide (Zy-2-clad)
fabrication, 10
vibratory compaction, 107
Uranium dioxide (Zy-2-clad)(irradiated)
reaction with water, 13
Uranium dioxide disks
fabrication, 10
Uranium dioxide particles
impaction, 68
preparation of spheroidal, 128-29
Uranium dioxide particles (Al_2O_3-coated)
preparation and structure, 126
Uranium dioxide particles (BeO-coated)
preparation, 185
Uranium dioxide particles (PyC-coated)
compatibility, 8
size, 126
Uranium dioxide particles (PyC-coated) (irradiated)
properties, 7, 67, 126, 185-86
Uranium dioxide pellets
fabrication with controlled B content, 187
N diffusion in, 67
preparation, 129
Uranium dioxide pellets (Cr-Ni alloy-coated)
preparation, 65, 67
Uranium dioxide powder
bonding, pressure, 106
compaction, vibratory, 67-68, 129
He solubility in, 9
production, 129
sintering, 187
Uranium dioxide single crystals
preparation, 187
thermal expansion, 9
Uranium dioxide single crystals (irradiated)
bubble diffusion in, 192
damage, 192
fission-gas release, 9
rare-gas release, 192
Xe diffusion in, 15
Uranium dioxide-zirconium diboride pellets
fabrication, 84
interactions, 85
properties, 84-85
Uranium dioxide-zirconium dioxide system
fabrication, phase studies, and physical properties, 10
Uranium dioxide-zirconium hydride powder compaction, 68
Uranium hydride-zirconium hydride system
bibliography, 21
Uranium hydride-zirconium hydride system (irradiated)
fission product release, 22-23
Uranium monocarbide
C diffusion in, 190
casting, 70
compatibility with 3Z1, Nb-Zr alloys, and SS(304), 11
fabrication, 69
hot hardness, 190
preparation, 12-13
properties, 69
reaction with SS, 69
thermal conductivity, 69
Uranium monocarbide (irradiated)
behavior, 69-70
damage, 70
fission-gas release, 190
Xe diffusion in, 15
^{133}Xe release, 11, 130
Uranium monocarbide (SS(304)-clad) (irradiated)
damage, 11
Uranium monocarbide powder
preparation, 130
sintering, 70, 189
Xe release, 71
Uranium monocarbide single crystals
UC_2 precipitation in, 129
Uranium monocarbide single crystals (irradiated)
rare-gas release, 192
Uranium monocarbide-uranium mononitride system (irradiated)
^{133}Xe release, 130
Uranium monocarbide-uranium mononitride-uranium oxide system
phase studies, 68
Uranium monocarbide-zirconium monocarbide system
mechanical properties, 129
Uranium mononitride
decomposition pressure, 11
melting point, 69
preparation, 12, 189
preparation of cast, 71
properties, 130
properties of cast, 71
reactions with metals and alloys, 130
structure, 71
volatility, 5
Uranium mononitride (irradiated)
^{133}Xe release, 130
Uranium mononitride particles (PyC-coated)
temperature range, 126
Uranium mononitride powder
sintering, 70-71, 189
Uranium mononitride-zirconium mononitride system
phase studies, 11, 130
Uranium nitrate
electrodeposition, 165
Uranium nitride
constitution, 68
data manual, 127
properties, 41, 68
purification, 41
Uranium ores
processing, 176
Uranium oxides
data manual, 127
electrodeposition, 108
hot isostatic pressing, 227
optical properties, 189
preparation by sol-gel process, 11
Uranium powder
sintering, 119
Uranium rods
rolling, 45
Uranium sesquicarbide
thermal expansion, 11
Uranium silicide
data manual, 127
Uranium single crystals (irradiated)
elongation, 71
Uranium systems (irradiated)
swelling, 130
Uranium trialuminide coatings
oxidation of, on U, 175
Uranium tubing
extrusion, Dynapak, 105
Uranium-uranium monocarbide dispersions
production, 184
Uranium-zirconium alloys
phase transformation, 2
Uranium-zirconium alloys (irradiated)
annealing effects and swelling, 59
Uranium-zirconium hydride system (SS-clad)
fabrication, 107

V

Vanadium
chemical plating using, 109
corrosion, 90
diffusion in, 98
electrodeposition, 228
mechanical properties, 218
oxidation, 218
strain aging, N effects on, 152
thermal properties, 218
transition temperature, N effects on, 152-53
Vanadium alloys
corrosion, 29
Vanadium-zirconium alloys
corrosion and hardening, 215
Vasco Jet X-2
welding, 170-71

W

Water-cooled reactors
pipe rupture, 148-49
Welding, 112-15, 171
uses of explosive, 231
uses of laser, 229
Welds
ultrasonic testing, 116
Wood's metal
eddy-current diffusion in, 49

X

X7039-T6
welding, 114-15
X-ray imaging testing, 116

Y

Ytterbium ceramics
preparation of ultrahigh-purity, 154
Yttrium
corrosion, 89
Yttrium beryllide
thermal dissociation, Be vaporization during, 80
Yttrium ceramics
preparation of ultrahigh-purity, 154
Yttrium deuteride
thermodynamic properties, 81
Yttrium hydride
dissociation pressure and heat of formation, 22
Yttrium oxide
tensile properties, Cs effects on, 211
Yttrium-zirconium dioxide system
oxidation, 206

Z

Zinc (molten)
corrosive effects, 89
Zircaloy
corrosion, 86, 206
electroplating with Cu, 108
H absorption, 206
welding to Hf, 24-25
welding to Inconel 600, explosive, 109-12
Zircaloy (hydrided)
tensile properties, 137
Zircaloy (irradiated)
oxide on, dissolution of, 142
Zircaloy-2
annealing, 93
brittleness, H effects on, 214-15
corrosion, 27-28, 86, 148
creep, 215
creep-rupture properties, 148
electroplating Cu on, 165
fracture, 34-35
heat treatment, 93
hydrides in, directional precipitation of, 93
hydriding, 86, 90, 201
H effects on, 21
H pickup, 206
H supercharging, 27
hydrogenation, 142
oxidation, 90, 142
particle-strengthening using Y_2O_3, 149-50
stress relaxation, 93
stress rupture, 215
tensile properties, 156
texture, 93
thermal-stress fatigue, 212
Zircaloy-2 (hydrided)
fracture, 137
Zircaloy-2 (irradiated)
burst properties, 101
corrosion, 27, 142
strength of hydrided, 81
tensile properties, 101, 156
Zircaloy-2 powder
corrosion, 142
Zircaloy-2 tubing
stress during vibratory compaction, 227
Zircaloy-2 tubing (irradiated)
mechanical properties, 33-34
Zircaloy-4
annealing, 93
bending-fatigue strength, 215
strengthening, 93-94
Zircaloy-4 (irradiated)
burst properties, 101
hydriding, 142
tensile properties, 101
Zirconium
bonding, pressure, 164, 227
compatibility with Pu-Ti-U alloys, 121
compatibility with UO_2, 189
corrosion, 31, 90
crystal structure, 97
diffusion in, 98, 154
dispersion-strengthening, 150
electrodeposition, 228
H pickup, 206
H solubility in, 80
Fe diffusion in, 39
mechanical properties, 97, 215
^{95}Nb diffusion in beta, 98
oxidation, 97, 206
O gettering effects on Fe solubility in molten K, 209
properties, 80
properties, rare earth effects on, 97
reaction with UN, 130
self-diffusion, 97-98
use in welding Th, 5
^{95}Zr diffusion in beta, 98
Zirconium (ferrous metal-clad)
roll bonding, 47
Zirconium (irradiated)
He diffusion in and release, 218
Zirconium-95
diffusion in beta Zr, 98
Zirconium alloys
brittleness, H effects on, 214-15
corrosion, 86, 142, 215
hardening, 215
hydrogenation, 142
oxidation, 142
Zirconium alloys (3Z1)
compatibility with UC, 11
Zirconium alloys (ferrous metal-clad)
roll bonding, 47
Zirconium alloys (irradiated)
oxidation, 142-43
Zirconium beryllide
oxidation resistance, 21
Zirconium boride
preparation, 40
Zirconium carbide
fluorination, oxidation, and preparation, 46
Zirconium ceramics
preparation of ultrahigh-purity, 154
Zirconium coatings
failure of, on U, 175
Zirconium crystals
H effects on shear stress, 149
Zirconium diboride
electrical resistivity, 84
emissivity, 84
fluorination, 40
oxidation, 25, 40, 84
production, 84
thermal conductivity, 84
Zirconium diboride powder
sintering, 84
Zirconium dioxide
defect structure, 40
electrical conductivity, 98-99
oxidation, 206
O diffusion in, 40
properties, 155
Zirconium dioxide (CaO-stabilized)
high-temperature properties, 155
Zirconium dioxide (irradiated)
expansion, 220
Zirconium dioxide (MgO-stabilized)
destabilization, 155
Zirconium dioxide coatings
development, 67
Zirconium dioxide powder
hot pressing, 99
O adsorption, 98
preparation of ultrahigh-purity, 154
Zirconium halides
electron diffraction, equilibria, and heats of formation, 40
Zirconium hydride
bibliography, 21
bonding, pressure, 107
neutron interactions, 22
preparation, 22
properties, 80-81
Zirconium martensite
tempering, 215-16
Zirconium monocarbide
heat of formation, 99
oxidation, 25
thermal expansion, 40
Zirconium monocarbide (pyrolytic)
properties, 99
Zirconium mononitride
solid solubility with PuN, 5
Zirconium oxide
hot hardness and tensile properties, 27

LEGAL NOTICE

This journal was prepared under the sponsorship of the U. S. Atomic Energy Commission. Neither the United States, nor the Commission, nor any person acting on behalf of the Commission:

A. Makes any warranty or representation, expressed or implied, with respect to the accuracy, completeness, or usefulness of the information contained in this journal, or that the use of any information, apparatus, method, or process disclosed in this journal may not infringe privately owned rights; or

B. Assumes any liabilities with respect to the use of, or for damages resulting from the use of any information, apparatus, method, or process disclosed in this journal.

As used in the above, "person acting on behalf of the Commission" includes any employee or contractor of the Commission, or employee of such contractor, to the extent that such employee or contractor of the Commission, or employee of such contractor prepares, disseminates, or provides access to, any information pursuant to his employment or contract with the Commission, or his employment with such contractor.

NUCLEAR SCIENCE ABSTRACTS

The U. S. Atomic Energy Commission, Division of Technical Information, publishes *Nuclear Science Abstracts (NSA)*, a semimonthly journal containing abstracts of the literature of nuclear science and engineering.

NSA covers (1) research reports of the U. S. Atomic Energy Commission and its contractors; (2) research reports of government agencies, universities, and industrial research organizations on a world-wide basis; and (3) translations, patents, books, and articles appearing in technical and scientific journals.

Complete indexes covering subject, author, source, and report number are included in each issue. These are cumulated quarterly, semiannually, and annually providing a detailed and convenient key to the literature.

Availability of *NSA*

SALE *NSA* is available on subscription from the Superintendent of Documents, U. S. Government Printing Office, Washington, D. C., 20402, at $30.00 per year for the semimonthly abstract issues and $22.00 per year for the four cumulated-index issues. Subscriptions are postpaid within the United States, Canada, Mexico, and all Central and South American countries, except Argentina, Brazil, British and French Guiana, Surinam, and British Honduras. Subscribers in these Central and South American countries, and in all other countries throughout the world, should remit $37.00 per year for subscriptions to semimonthly abstract issues and $25.00 per year for the four cumulated-index issues.

EXCHANGE *NSA* is also available on an exchange basis to universities, research institutions, industrial firms, and publishers of scientific information. Inquiries should be directed to the Division of Technical Information Extension, U. S. Atomic Energy Commission, P. O. Box 62, Oak Ridge, Tennessee, 37831.

TECHNICAL PROGRESS REVIEWS may be purchased from Superintendent of Documents, U. S. Government Printing Office, Washington, D. C., 20402. *Isotopes and Radiation Technology* at $2.00 per year for each subscription or $0.55 per issue; the other four journals at $2.50 per year and $0.70 per issue. The use of the coupon below will facilitate the handling of your order.

POSTAGE AND REMITTANCE: Postpaid within the United States, Canada, Mexico, and all Central and South American countries except as hereinafter noted. Add $0.50 per year or $0.15 per single issue for the *Isotopes and Radiation Technology* journal and $0.75 per year or $0.20 per single issue for the other four journals for postage to all other countries, including Argentina, Brazil, British and French Guiana, Surinam, and British Honduras. Payment should be by check, money order, or document coupons and MUST accompany order. Remittances from foreign countries should be made by international money order or draft on an American bank, payable to the Superintendent of Documents, or by UNESCO book coupons.

order form

SUPERINTENDENT OF DOCUMENTS
U. S. GOVERNMENT PRINTING OFFICE
WASHINGTON, D. C., 20402

Enclosed:
document coupons ☐ check ☐ money order ☐

Charge to Superintendent of Documents No. _____

Please send a one-year subscription to

☐ NUCLEAR SAFETY

☐ POWER REACTOR TECHNOLOGY

☐ REACTOR FUEL PROCESSING

☐ REACTOR MATERIALS

(Each subscription $2.50 per year; $0.70 per issue.)

☐ ISOTOPES AND RADIATION TECHNOLOGY

(Each subscription $2.00 a year; $0.55 per issue.)

SUPERINTENDENT OF DOCUMENTS
U. S. GOVERNMENT PRINTING OFFICE
WASHINGTON, D. C., 20402

(Print clearly)

_____
Name

_____
Street

_____
City, State, ZIP Code